EVOLUTION OF ELECTRICAL CONDUCTIVITY, HARDNESS AND STRENGTH DURING AGE HARDENING OF AA7010

MANUEL ANTONIO SALAZAR - GUAPURICHE

Ph.D. 2009

Evolution of Electrical Conductivity, Hardness and Strength during Age Hardening of AA7010

Thesis submitted in accordance with the requirements of the

University of Liverpool for the Degree of Doctor of Philosophy

by

Manuel Antonio Salazar - Guapuriche

January 2009

Materials Science and Engineering

Department of Engineering, Faculty of Engineering

ABSTRACT

Localised overheating in aircraft structural components made from AA 7010 can occur during machining, causing a decrease in electrical conductivity (EC), hardness (Hv) and strength. When overheating is detected by non-destructive testing with electrical conductivity and hardness is slightly outside the material specification, the affected components are scrapped. If data correlating EC and Hv with strength were available, the severity of overheating could be assessed and the component could be repaired. It is also commonly observed that the EC and Hv change notably from the outside surface towards the centre of the plate, even when no overheating is present. This suggests property inhomogeneity through the plate thickness. However, little information is available in the public domain on the property correlation and property inhomogeneity in thick products of AA7010.

This investigation studied the evolution of properties with age hardening for AA 7010 and correlated EC, Hv, strength and ductility for a range of age hardening conditions. The property homogeneity through the plate thickness of AA 7010, perpendicular and parallel to the rolling direction, was also assessed. The effect of quenching rate on the properties, specifically the evolution of EC, Hv and strength with artificial age hardening, was assessed for seven different quench delays.

The tensile strength (UTS) and 0.2% proof strength (PS) have a good linear correlation with hardness, regardless of the test piece thermal history. The PS gives a lower regression correlation coefficient than UTS, but the accuracy of its prediction can be improved by combining Hv and EC, especially for any EC values above 35.9% IACS. The EC, Hv and strength show inhomogeneity across the plate thickness, both in the directions perpendicular and parallel to the rolling direction. The inhomogeneity is inherent from segregation of alloying elements during casting, with the segregation of Zr and Ti at the plate centre resulting in high EC and low Hv. The gradient of quench rate from the surface to the centre of the plate, after the solution heat treatment, is not the main contributor to the inhomogeneity. The EC, Hv and strength are sensitive to the changes of heat treatment conditions such as quench delays, ageing temperature and time. The variations of properties are a direct result of the formation of various precipitates and the continuous changes in their sizes and volume fractions. The combination of EC and Hv tests is found to be a reliable quality indicator to assess the ageing process of AA 7010 and can be used in non-destructive assessment of property homogeneity of thick products. From the network of EC - Hv curves obtained under a wide range of age conditions, an unknown thermal condition for AA 7010 can be estimated for any EC and Hv values. For test pieces smaller than 11×11 mm^2, quench delays shorter than 198 seconds, followed by standard artificial ageing, can produce satisfactory properties. Longer quench delays result in mechanical properties below the material specification. This is because high temperature heterogeneous precipitation of the equilibrium phases during quenching depletes the solid solution of alloying elements available for subsequent age hardening.

CONTENTS

Acknowledgements

The author is indebted to Dr Yuyuan Zhao, my supervisor, and Dr Peter Fox, my advisor, from the University of Liverpool, for the many valuable discussions and guidance throughout the course of this exploratory investigation and thesis compilation. In particular, I am indebted to Dr Zhao for consistently motivating me in times of need and for his patience and understanding shown with the nature of my part time PhD studies. This achievement would not have been possible without his excellent supervision and invaluable support.

I am grateful to Airbus UK Quality Division, Mr Alan White VP CoE Wing & Pylons and National Quality, for financing this investigation. I would like to express my gratitude also to Mr Mark Fowles and Mr John Hope, my immediate bosses from Airbus UK Materials Laboratory, for allowing me the use of available facilities within the Materials Laboratory.

Last but not least, thanks to my wife Julie (the PhD widow) and my daughters Amie, Rosie and Annie for their patience and understanding when I was absent from home during many evenings and long weekends.

Statement of Originality and Publications

This thesis is submitted for the degree of Doctor of Philosophy in the Faculty of Engineering at the University of Liverpool. The research project reported herein was carried out, unless otherwise stated, by the author at Airbus UK Materials Laboratory – Broughton between January 2001 and January 2009.

No part of this thesis has been submitted in support of an application for a degree or qualification of this or any other university or educational establishment. However, some parts of this thesis have been published in the following papers:

(1) M.A. Salazar-Guapuriche, Y. Y. Zhao, A. Pitman and A. Greene, "Correlation of Strength with Hardness and Electrical Conductivity", **Material Science Forum**, **519-521**(2006), 853-858.

(2) M.A. Salazar-Guapuriche, Y. Y. Zhao, A. Pitman and A. Greene, "Variations of Properties across Billet Thickness for Al alloy 7010", **Transactions of Nonferrous Metals Society of China**, **15**(2005), 1258-1263.

(3) M.A. Salazar-Guapuriche and Y. Y. Zhao, "Effect of quench delay on properties of AA 7010 and the prediction of strength and thermal history", (to be submitted).

Note: As an outcome of the learning from the PhD studies, I was awarded the qualification of NDT Level 3 in material evaluation by Electrical Conductivity and Hardness (Ref: ANS MO6012402). The Head of NDT & Testing Technology, Airbus UK awarded this in August 2006.

Manuel Antonio Salazar - Guapuriche

January 2009

List of Tables

Chapter 3

Chapter 4

Chapter 5

List of Figures

Chapter 2

Chapter 3

Chapter 4

Chapter 5

Chapter 1

Introduction

1.1 Overheating during machining operation

Aluminium alloy (AA) 7010 in the T7651 temper condition is one of the main structural aluminium alloys used in the aircraft industry, because of its high strength coupled with good fracture toughness and high resistance to stress corrosion cracking, particularly in thick sections (Reynolds 1976, Military Handbook 5G 1994). This aluminium alloy is extensively used in the manufacture of structural aircraft components; a significant number of these components are machined on a daily basis from this alloy. During the machining operation, overheating can be induced by an inadvertent temperature increase at the cutter-metal interface. The temperature increase can be the result of several factors: inadvertent use of blunt / damaged cutters, lack of lubrication at the interface between the cutter and the material being machined, excessive removal of material in one cut, or a combination of these.

Generally, overheating on heat treatable high strength aluminium alloys manifests itself by a decrease in its electrical conductivity and hardness values. The extent of decreasing electrical conductivity and hardness values depends on the attained temperature during machining and the exposure time at this temperature. The higher the amount of heat generated at the machining interface, the greater the number of age hardening precipitates that are likely to re-dissolve back into the solid solution.

For the aluminium alloy under investigation, AA 7010, the temperature required to re-dissolve most of the strengthening alloying elements, such as Zn, Cu and Mg, back into the solid solution is approximately 473°C (Airbus UK 2003).

1.2 Inspection for overheating

To guarantee freedom from unacceptable localised overheating on main aircraft structural components made of aluminium alloys, the machined components are normally non-destructively tested (NDT) by using chromic acid anodising treatment and visual examination. Generally, this inspection method is also used to detect any possible surface braking discontinuities and indications of corrosion (Airbus UK 2008).

When visual examination of the anodised surface indicates a possibility of overheating, the component is assessed by electrical conductivity and hardness measurements. The electrical conductivity and hardness results are then compared with the values of the non-affected areas of the components and with the values of the material specification to determine whether or not the affected area has been over-heated to conditions outside the material specification requirements.

Although the presence of localised overheating on aluminium alloys, generated during the machining operation, can be detected and analysed by the above NDT inspection methods, the degree of its severity in terms of its effect on the properties, such as tensile strength, is not well established.

1.3 Effect of overheating on properties

In the aircraft industry it has been observed that when AA 7010-T7651 is exposed to slight overheating, there are decreases in electrical conductivity and hardness, associated with a loss of strength. This suggests that some of the strengthening alloying elements precipitated in a coherent or semi coherent manner within the matrix, during standard heat treatment, have re-dissolved back into the solid solution. This is supported by the fact that alloying additions in solid solution depress the electrical conductivity to a greater extent than when out of solution (Morris *et al.*1984). When the coherent precipitates re-dissolve back into the solid solution, the associated strain hardening effect also disappears, lowering the strength.

Previous investigations on overheating showed that the electrical conductivity and hardness for AA 7010-T7651 decrease significantly when it is exposed to excessive heating or high temperatures (Brown and Heaton 1984). Other alloys in the 7000 series, for example AA 7150-T651 and 7075, have also shown similar decreases in hardness and conductivity (Jolley 1992).

Historical data at Airbus UK shows that, during machining of components from AA 7010-T7651, the failure of the cutting edge of the machine tool (for example a blunt cutter edge) causes overheating of the components in localised areas. The effect of this overheating could decrease the electrical conductivity up to 7% IACS (International Annealed Copper Standard) in the worst cases. This was accompanied by a significant loss of hardness when compared to adjacent non-overheated areas. Even a small

decrease in electrical conductivity of 0.5% IACS was found to decrease the hardness values below the material specification requirement. In both cases, the components were scrapped due to the loss of hardness or strength.

1.4 Property homogeneity through the plate thickness

The AA 7010 plates used for structural parts are manufactured from a cast slab by rolling. They are then solution heat-treated, control stretched and artificially aged to peak strength, followed by slight over ageing. When these plates are machined, it is commonly observed that, even when overheating is not detected by chromic acid anodising, the electrical conductivity and hardness change notably from the outside surface towards the centre of the plate, indicating a lack of property homogeneity through the plate thickness. The quenching-rate gradient in the solution heat treatment was reported to be a major factor leading to the property differences in thick sections (Staley *et al.* 1984). However, the other factors inherent from the manufacturing route can also contribute to the inhomogeneity.

1.5 Measurements of electrical conductivity and hardness

It is well documented that electrical conductivity and hardness of heat treatable aluminium alloys vary with changes in chemical concentrations of certain alloying elements within the solid solution. Due to accuracy and fast response, hardness and electrical conductivity measurements have been used extensively to study the age hardening process and the associated precipitation mechanisms in many heat treatable aluminium alloys. Rosen *et al.* (1982) reported that electrical conductivity and hardness

responded in a complementary manner to the varying microstructure that forms in different stages of the ageing process in AA 2024. Rosen (1989) also used the eddy current method to study the changes in the mechanical properties during the age hardening process in AA 2024 and evaluated quantitatively the extent of removal of the minor constituents Cu and Mg from the solid solution. Brasche *et al.* (1989) and Koch and Kolijn (1979) studied the correlations of electrical conductivity and hardness with strength, fracture toughness and stress corrosion cracking for AA 7075 and AA 2090, respectively.

In practice, the suppliers of raw materials commonly use electrical conductivity and hardness to monitor the quality consistency during the manufacturing and heat treatment of the aluminium alloy products. The aircraft industry also uses the above NDT methods to assess the indications of overheating initially detected by chromic acid anodising, which may be induced during the machining operations.

1.6 Reasons for investigation

In the aircraft industry, when indications of overheating on localised areas have been detected by chromic acid tests and the assessment by electrical conductivity and hardness reveals values outside the materials specification requirement, the standard practice is to scrap the affected aircraft components. If data correlating the electrical conductivity and hardness with mechanical properties were available for the machined aluminium alloy, the structure design engineers could assess the severity and consider a possible repair for the affected area, especially when the values of electrical conductivity

and hardness are slightly outside the specification requirements and the affected area is unlikely to be significantly stressed during the life span of the aircraft. However, there is lack of correlation data in the public domain. For this reason, the prediction of the tensile and proof strength for aluminium alloys with known values of hardness and conductivity would be of significant interest to the structure design engineers. This thesis intends to address this shortfall for AA 7010.

Electrical conductivity and hardness can vary with plate thickness, without the presence of over heating. This suggests a lack of property homogeneity through the plate thickness. The factors influencing the property homogeneity may also, to some degree, affect the correlation between hardness and strength. However, very little information is available to explain property inhomogeneity on thick aluminium alloy products. This thesis aims to identify the main factors influencing the property inhomogeneity through the plate thickness of AA 7010.

Quenching is one of the most critical steps in the manufacture of high strength aluminium alloys. Following the quenching operation, the maximum strength attained upon artificial ageing largely depends on the amount of alloying elements retained within the solid solution, or on the initial amount of quench-induced precipitates developed during the quenching operation. Heterogeneous formation of quench-induced precipitates can occur when there is a slow or sluggish cooling during quenching (Godard 2002). The formation of the coarse or heterogeneous precipitates could have an adverse effect on the hardness and strength of the final product. This investigation

attempts to determine the effect of quenching rate on the properties of AA 7010, including electrical conductivity, hardness, ultimate tensile strength (UTS) and 0.2 % proof strength (PS).

1.7 Objectives

The main objectives of the present investigation are:

a) To investigate the evolution of properties with age hardening for AA 7010 and to correlate hardness, electrical conductivity, strength and ductility for the full range of age hardening conditions (natural ageing, artificial ageing and over ageing). It is envisaged that the data generated could be used to determine non-destructively the mechanical properties of a suspected area of an affected component. The knowledge could aid the assessment of possible repairs of certain aircraft components, which otherwise would be considered not acceptable and wasted.

b) To assess the homogeneity of properties through the plate thickness of AA 7010 and to identify the main contributors to the inhomogeneity. This would help to identify whether an area is affected by machining or the property values are inherent of the manufacturing route.

c) To study the effect of quenching rate on the properties of AA 7010. Specifically the evolution of electrical conductivity, hardness and strength with artificial age hardening will be assessed for seven different quench delays. By correlating electrical conductivity

with hardness, an unknown ageing condition of a suspected component could be predicted from known values of hardness and electrical conductivity. The study will also show the range of acceptable ageing conditions.

The findings and the acquired knowledge of this study would be of particular practical benefits to the following departments of Airbus UK:

a) for the Machining Department to assess whether an area has genuine over heating.
b) for the Structural Design Engineering Department to assess the possibility of repairing an affected area based on the NDT values.
c) for the Materials Laboratory to understand the combined effects of property inhomogeneity of the plate and overheating on the materials properties, especially at the plate centre.

1.8 Outline of thesis

Chapter 2 of the thesis reviews the literature related to the studies performed in this project. This literature review will consider the following topics: a brief outline of the features influencing the cast structure; the thermo-mechanical processes employed to manufacture aluminium plates from cast ingots; the heat treatment processes necessary to generate the required mechanical properties; the metallurgical principles governing the hardening / strengthening mechanisms; the diffusion of the alloying elements; precipitation hardening; and the effect of alloying elements on electrical conductivity of aluminium, both in and out of solution.

Chapter 3 investigates the evolution of electrical conductivity, hardness, UTS, PS and ductility with varying age hardening conditions for AA 7010. The main objectives are to determine non-destructively the strength of the alloy from values of electrical conductivity and hardness and to evaluate the age hardening characteristics of the alloy to consider its practical uses.

Chapter 4 presents the assessment of property homogeneity through the plate thickness of AA 7010. Electrical conductivity, hardness and tensile strength were assessed through the thickness of the plate perpendicular and parallel to the rolling direction under the as received and a series of re-treated conditions, including re-solution heat treatment, quench, natural age hardening and artificial age hardening. The main objectives are to identify the main contributors of the inhomogeneity and to establish whether the inhomogeneity is due to the effect of machining or inherent of the previous manufacturing route.

Chapter 5 reports the study on the effect of varying quenching rate on the properties of AA 7010. For different quench delays following solution treatment, electrical conductivity, hardness and strength are assessed after artificial age hardening. The main objective is to create a network of EC / Hv curves from which the thermal history of the material can be estimated using values of electrical conductivity and hardness.

Chapter 6 compiles the main conclusions derived from the data presented and discussed in Chapters 3, 4 and 5. It also outlines recommendations for future work and the main benefits to the sponsor of this exploratory work.

Chapter 2

Literature review

AA 7010 is manufactured by re-melting primary aluminium, alloying to the specific chemical composition and casting to an ingot, which is then subjected to subsequent shaping processes. The ingot is homogenised, hot rolled, solution heat-treated, stretched and finally artificially age hardened. The mechanical and physical properties of the resultant plate are dependent upon the operating parameters employed during each stage of the whole process.

Since the main objectives of the thesis are to correlate the mechanical properties of AA 7010 with electrical conductivity and hardness, and to assess the property homogeneity through the plate thickness, this review will consider the literature in the following areas: a brief outline of some aspects of solidification and the thermal processes employed in manufacturing the aluminium plates from the cast ingots; the heat treatment processes necessary to generate the required mechanical properties; the metallurgical principles governing the hardening / strengthening mechanisms, with some emphasis on how the alloying elements diffuse, precipitate and harden the aluminium alloy matrix; and the effect of alloying elements on electrical conductivity of aluminium, both in and out of solution.

2.1 Thermal-mechanical manufacturing processes of aluminium

2.1.1 Solidification

The solidification of metals has been extensively studied by many researchers and is well documented in literature. The following is a brief review of the fabrication and

structure of ingot castings, which are likely to influence the mechanical properties of the aluminium alloy under investigation.

2.1.1.1 Factors influencing crystal size and shape

In both ingots and castings a small uniform grain size is generally desirable, as poor mechanical properties are often associated with coarse structure. The shape and size of the grains depend mainly on the number and distribution of nuclei and the direction and rate of crystal growth. These factors are influenced in practice by (a) the thermal conductivity of mould material, (b) the casting temperature, (c) the mass of liquid metal and (d) the composition of the alloy (Rollason 1973).

a) Thermal conductivity of mould material

The higher the thermal conductivity of the casting mould material, the faster the heat dissipation and therefore the smaller the grain size of the metal solidified. It is a well-known fact that the rate at which a molten metal is cooled when it reaches its freezing point affects the size of the crystals formed. Rapid cooling leads to a high degree of under cooling being attained. The onset of crystallization results in the formation of a large number of effective nuclei with a heterogeneous distribution. Consequently small equi-axed crystals result. This condition arises when metal is cast from just above its freezing temperature into a chilled mould or by adding inoculants to increase the number of nucleating sites (Rollason 1973).

On the other hand, uniform slow cooling, which leads to small degree of undercooling, promotes the formation of relatively few nuclei at the onset of solidification. These nuclei are fairly evenly distributed and their growth is roughly

the same along various crystal axes. The result is a coarse structure of equi-axed grains, of about the same size but differing in orientation. This condition is found frequently in sand castings in which there is slow heat dissipation (Rollason 1973).

b) Casting temperature

When molten metal at a temperature well above its freezing point is cast into a metal mold, the portion in contact with the cold surface will be almost instantly cooled below its freezing point, while the metal at the centre will be little affected. A high number of seed crystals are therefore formed only on the outer layer of the cast metal. Growth takes place in all directions but contact is soon made with adjacent crystals, with the result that very small equi-axed chilled crystals are formed. If the casting temperature is very high these chilled crystals may re-melt. Quite often the inner layer of the chilled crystals, which have a favourable growth axis, continue to grow in the opposite direction to the heat extraction. This occurs because the chance of crystal growth is greater than the tendency to form fresh nuclei. Side growth is prevented by collision with neighbouring crystals, hence long thing columnar crystals are formed, which, if the initial temperature of the metal is high enough, may reach the center (Rollason 1973). On the other hand, with a lower casting temperature, the centre portion of the ingot may be cooled sufficiently to crystallize from a large number of nuclei before the columnar grains reach the centre. Such an ingot will consist of an outer shell of columnar crystals with a core of equi-axed grains, and generally possesses good rolling and mechanical properties (Rollason 1973).

However, although the ingots should be cast at as low temperature as possible in order to get good working properties, it is just as important that the metal should be sufficiently fluid to prevent semi-solid skins forming on the surface as the metal level rises in the mould (Rollason 1973).

c) Mass of liquid metal

In a large ingot the crystal size may vary considerably from the outside surface to the centre. This is due to the variation in the temperature gradient, which exists as the ingot solidifies and heat is transferred from the metal to the mould. When metal first makes contact with the cold mold, the chilling effect, which results in the formation of equi-axed crystal at the surface of the ingot, tends to be reduced due to mold warming up. This in turn retards the formation of nuclei as solidification proceeds. As a consequence, the crystals towards the centre of the ingot will be larger (Higgins 1983). In an intermediate position the rate of cooling is favourable to the formation of elongated columnar crystals. Therefore, in large cast ingots it is expected to distinguish three separate zones in the crystal structure (Higgins 1983).

d) Composition of the alloy

The solidified grain size is not only dependent on the above factors but is also influenced by the purity of the alloy (Riggs *et al.* 1984). Generally the purer the metal the larger the grains formed. Since a small and uniform grain size is generally desirable, small additions of titanium are often made to most sand and permanent mould castings of aluminium alloys. The objective of this is to refine the primary aluminium grain structure. Boron in an amount of a few dozen of PPM is frequently added together with titanium to improve the degree of grain refinement and to

increase retention of refinement during repeated re-melting. Zirconium is also a grain refiner, but larger quantities are needed to achieve the same effect as titanium diborate (Riggs *et al.* 1984). For AA 7010, 0.032% of Ti and 0.12% of Zr where added to the alloy.

2.1.1.2 Solidification of aluminium alloy ingots

Once chemical analysis of the molten metal shows that the alloying elements are within the specified concentrations, the aluminium alloy is cast into large ingots. From the molten stage, all commercial solidification processes involve some non-equilibrium effects. In real casting processes, the extent of deviation from equilibrium conditions has a significant effect on the actual microstructure observed. For example in a large solidified ingot, the as-cast microstructure is cored dendritic with a solute content increasing progressively from the centre to the edge. This cored structure also has inter-dendritic distribution of second phase particles or eutectics.

Non-equilibrium solidification produces non-uniform distribution of the solute because, during solidification, the first part to freeze has a solute concentration lower than the alloy composition. As the temperature drops below the liquidus temperature, the solid forming at the freezing interface is higher in solute concentration than the previously one frozen. To maintain a solute balance, additional solute is present in the liquid as a consequence of coring (Dunn *et al.*. 1984).

During solidification of the AA 7010, it is expected that, as well as the solidification of dendrites with low-melting point alloying element and the associated inter dendritic eutectic, dendrites of high melting point inter-metallic compounds are also formed (Dunn *et al.* 1984). The latter are formed by a peritectic reaction taking place between elements such as Ti and Zr with aluminium. At the start of solidification, dendrites containing peritectic inter-metallic compounds segregate in a manner opposite to the dendrite formation of the low-melting point alloying element. In this case, the first portion of the dendrite to be formed is richer in Zr and Ti than the subsequently solidified portions (Dunn *et al.* 1984). Consequently, the content of Zr and Ti in the dendrites is a higher at the centre and diminishes progressively towards the edges. These dendrites, which are formed during the early stages of solidification, tend to break away and are transported towards the centre of the ingot by the liquid metal flow, induced by convection. This leads to higher concentration of Zr and Ti at the centre of the ingot. The presence of Al_3Zr inter-metallic compounds at the centre of the ingot lowers the concentrations of strengthening alloying elements of the solid solution. At high temperature Al_3Zr inter-metallic compounds or dispersoids will aid the formation of equilibrium precipitates by facilitating precipitation sites to the diffusing alloying elements (Godard *et al.* 2002).

2.1.1.3 Casting defects

From the preceding section it is apparent that most metals when solidified consist of many crystals or grains. In an industrial scale these crystals are never perfect in atomic scale. The most important crystal imperfections are vacancies, interstitials and dislocations. Vacancies are simply empty atom sites and they can move within

the lattice structure and therefore play an important part in aiding the homogenisation of the cast core structure by diffusion at high temperature. This will be briefly reviewed in section 2.4.3.

As well as the cored microstructure produced by the non-equilibrium solidification of large ingots, other inherent casting features are minor segregation, major segregation and inverse segregation.

Minor segregation. The dendrites, which form first in solidification are almost pure metal. This means that the impurities become progressively more concentrated in the remaining liquid. Hence the metal that freezes last at the crystal boundaries contains the remaining impurities, which were dissolved in the original molten metal (Higgins 1983).

Major segregation. As the columnar crystals begin to grow inwards, they progressively push in front of them some of the impurities. In this way there is a tendency for many of the impurities to become concentrated in the central pipe (Higgins 1983).

Inverse segregation. With very large ingots the temperature gradient may decrease towards the end of the solidification process. Therefore it is common for a band of metal, which acquires highly level of impurities just in front of the advancing columnar crystals, to solidify last. Hence this band of impure metal has a much lower freezing point than the relative pure metal at the centre. Since the temperature gradient is slight, this metal at the centre may begin to solidify in the form of equi-

axed crystals, so that the impure molten metal is trapped in an intermediate position. This impure metal therefore solidifies last and causes inverse- segregation (Higgins 1983).

During the homogenising process of large ingots, these regions of major segregation are expected to be totally dispersed in order to yield uniformity of property through the thickness of the products. However, variations of chemical composition of alloying elements in a single plate have been reported, typically due to segregation carried forward from the original ingot (Rummel and Arbegast 1981). According to Morris (1984), the variations in chemical composition can result in variations in electrical conductivity values within the plate.

2.1.2 Homogenisation

Prior to homogenisation the ingots are frequently surface scalped to remove dross and dirt inclusions at the surface. Cored structures are most common in as cast metals. From the previous discussion of the origin of the cored structure, it is apparent that the last solid formed along the grain boundaries and in the interdendritic spaces is very rich in the lower-melting- point metals. Depending on the properties of these lower-melting-point metals, the grain boundaries may act as planes of weakness. Because of the relatively low ductility of the inter-dendritic or intergranular second phase particles, the non-uniform cast structure of aluminium alloys generally has inferior workability (Staley *et al.* 1984). The cast structure can also result in serious non-uniformity in mechanical and physical properties. Therefore, for most applications, cored structure is objectionable (Avner 1974).

The preferred industrial method to achieve homogenisation of composition of the cored structure is by diffusion in the solid state (Avner 1974). Most metals have a slow diffusion rate at room temperature. However, when the alloy is reheated to a temperature below the solidus, diffusion will be more rapid and homogenisation will occur in relatively shorter time (Avner 1974).

Rapid solidification, because it deviates more from equilibrium, produces relatively smaller dendrites with high level of micro segregation across the dendrite walls. On the other hand, coarse dendrites have smaller initial composition differences across the thickness than fine dendrites, however they take a longer time for homogenisation because of the greater distance through which the solute atoms have to diffuse in the coarse structure (Avner 1974).

Using electron microprobe analysis of unidirectional solidified castings, for Al-2.5% Mg alloy, Staley *et al.* (1984) reported that the degree of micro segregation was greater in the coarser, more slowly solidified structure, and that the approach to uniform solute distribution during heating at 425°C was more rapid for the finer structure Therefore, homogenisation of ingots containing smaller dendrites will be much quicker than in ingots with larger dendrites.

2.1.2.1 Homogenising temperature

From examination of the phase diagram it can be seen that the ingot homogenisation temperature range can be selected anywhere between the solvus

and solidus temperatures (Dunn *et al.* 1984). However, to avoid the possibility of non-equilibrium melting, the upper limit of the temperature range should be below the eutectic temperature and the holding time should be of sufficient duration to produce complete diffusion of the elements comprised in the eutectic (Dunn *et al.* 1984). Generally cast ingots are preheated to a homogenising temperature of approximately 425°C and heat treated for sufficient time, prior to the hot rolling (Staley *et al.* 1984).

2.1.2.2 Purpose of homogenising

The homogenising operation is only one step towards providing maximum workability by dissolving the intermetallic phases rejected inter- dendritically during solidification. Because most of the solute is in solid solution after this heat treatment, further softening and improvement in workability can be obtained by slow cooling, in order to re-precipitate and coalesce the solute in an intradendritic distribution of fairly large particles (Stalet *et al.* 1984). After homogenisation or redistribution of solute elements is accomplished, a higher rate of workability and improve surface appearance of the product can be obtained by extending the homogenisation periods.

Secondary effects of homogenisation are also achieved by precipitation of additional transition elements, such as Zr and Ti, from solid solution and by aiding the completion of delayed peritectic transformation that could not be fully formed during solidification. Aluminium alloy ingots containing peritectic intermetallic compounds are designed to induce precipitation, resulting in the formation of particles of equilibrium phases during homogenisation; AA 7010 under investigation falls in this category. The high temperature precipitates, which are frequently called dispersoids,

occur within the original dendrites, with a distribution essentially the same as that established during solidification; this is thought to be because the diffusion rates are too slow in the solid state to permit any substantial redistribution (Stalet *et al.* 1984).

2.1.3 Hot rolling

Aluminium alloy cast ingots after homogenising are hot rolled to improve their mechanical properties. This is because the inherent characteristics of a cast metal, in particularly coarse grains and segregation of impurities, are such that its mechanical properties are always inferior to those of a wrought product (Higgins 1983).

Aluminium plates are manufactured from cast ingots by hot rolling. Commercially, the initial reduction is carried out with the material at an elevated temperature, which is above the re-crystallisation temperature and the final reductions are done at lower temperatures because of better surface finish (Avner 1974). Hot rolling can be defined therefore as an operation where the material is worked above its re-crystallisation temperature and where a simultaneous occurrence of deformation and recovery processes takes place. The amount of deformation is large enough to break down the original coarse grains and also to prevent grain growth from critical amounts of strain (Avner 1974).

The effects of hot working are:

a) refinement of crystal structure;

b) elimination of the orientated cast structure;

c) promotion of material uniformity by facilitating diffusion of alloying constituents and breaking up brittle films of hard constituents or impurities;

d) improvement of mechanical properties, especially elongation. However, some properties will be different in different directions.

e) welding up cracks and unoxidised blowholes (Rollason 1973).

2.1.3.1 Effect of hot rolling finishing temperature

The finishing temperature in hot working will determine the grain size that is available for further cold working. Higher temperatures are used initially to promote uniformity in the material, and the resulting large grains allow more econo mical reduction during the early working operation. As the material cools and working continues, the grain size will decrease, becoming very fine just above the recrystallisation temperature (Avner 1974).

If work is completed while the object is at a temperature higher than that necessary for recrystallisation, grain growth occurs during the undisturbed cooling. The finishing temperature should, therefore, be just above the recrystallisation temperature, resulting in the production of fine crystals. A typical hot working temperature for aluminium is 350 to 450°C (Rollason 1973).

Rapid cooling after working at elevated temperature may avoid recrystallisation and thereby preserve the previously formed sub grain structure. When this occurs, the

subsequent room temperature strength of the hot work aluminium is a function of sub grain size (Riggs *et al.* 1984).

2.1.4 Rolling effect on anisotropy and texture

During rolling operations, the rolls exert a squeeze for a short interval and are used extensively on the shaping of plates. On plates the rolls elongate the metal in one direction only, except for slight side spread. Plates or sheets are frequently rolled in two directions at right angles (Rollason 1973). Cross-rolled practice employed on AA 7010 thick products reduces the difference in longitudinal / long transverse yield strength ratios through the thickness and tend to increase the longitudinal / short transverse yield strength ratios (Chakrabarti *et al.*1996). For these reasons the properties of wrought aluminium and its alloys, as in most materials, are never completely uniform in all directions, some degree of anisotropy is always present. The exact nature of this anisotropy depends upon both alloy composition and the thermo-mechanical processes employed during manufacturing, which can change the crystal orientation biases, leading to texture development and anisotropy (Gottsteins *et al.* 2007).

2.1.4.1 Anisotropy

Anisotropy is exhibited when a material shows different property values when measured in different directions. The cause of anisotropic behaviour is the crystallographic preferred orientation (texture) of the grain in a polycrystal (Krol *et al.* 1995). Many properties of single crystals such as yield strength, ductility, and conductivity depend on the crystallographic orientation, i.e. they are anisotropic. As

a consequence of this, polycrystalline samples can only behave macroscopically isotropically when they are randomly distributed and consist of a great number of grains (Krol *et al.* 1995).

2.1.4.2 Texture

In most polycrystalline materials the crystal directions of the individual grains are not randomly (statistically) distributed in space. They show certain preferred orientations with respect to the geometrical directions of the sample. This feature is called (crystallographic) texture (Krol *et al.*1995). During metal plastic deformation there is a tendency for certain crystallographic planes and directions to orientate themselves parallel to the rolling plane and rolling direction. Thus in a rolled sheet certain preferred orientations or textures develop. Hot rolled aluminium alloys generally exhibit a range of preferred orientations from {110}<112> to {112}<111>, together with a large spread of orientation depending on the deformation variables (Martin 1998).

The yield strength of the metal in the direction of mechanical working may be greater or less than that in the transverse direction, depending on the type of preferred orientation that is produced during deformation (Chakraborty 2000).

Crystallographic textures should not be mixed up with mechanical fibrin that occurs on worked alloys due to manufacturing processes. Mechanical fibrin normally consists of elongated grains, banding of small grains, alignment of intermetallic inclusions and preferential precipitation, all of which can produce differences in

mechanical properties in different directions (Martin 1998). This effect can also be as important as crystallographic textures (Krol *et al.*1995).

2.1.4.3 Types of crystallographic textures

2.1.4.3.1 Rolling texture

During the hot rolling of aluminium cast ingots deformation texture develops. Cast aluminium tends to have a random distribution of grain orientations, except in large aluminium rich casting, where columnar grains are formed (Krol *et al.* 1995). The random nature of the cast structure is rapidly lost during hot or cold rolling. This fabrication process replaces the random nature of the cast by crystallographic textures, in which considerable numbers of deformed grains assume, or approach, certain orientations. Such textures occur because deformation, or slip, in aluminium is confined to certain crystallographic planes and directions (Riggs *et al.* 1984).

2.1.4.3.2 Recrystallisation texture

Preferred orientation developed during working is usually referred to as a deformation texture, while preferred orientation present when a heavily worked metal is recrystallised is called recrystallisation texture (Rollason 1973). The new crystal formed frequently develops in orientations that are different from the principal components of the deformation texture. However, if the heavily worked metal is recovered instead of recrystallised, no significant change in preferred orientation or texture of the deformed metal will take place (Riggs *et al.* 1984).

However, Engler *et al.* (1996) reported for rolled plate AA 7010 that recrystallisation takes place after hot rolling and during solution treatment with almost no change in

texture. This was explained by the balancing effect of randomisation of the texture during recrystallisation and texture sharpening within the recovered matrix region. Morere *et al.* (1996) also reported for AA 7010 that, the cooling condition after deformation and the heating rate for the solution treatment seem to have little or no effect on the final microstructure.

Although the final texture and grain size of recrystallised components is mainly dependent on the type of fabrication, degree of cold work and annealing conditions, it also depends on alloy composition and distribution and size of intermetallic phases (Krol *et al.*1995). In the as deformed microstructure for thick rolled plate AA 7010 recrystallisation is inhibited by the presence of dispersoids, mainly Al_3Zr, which when present in the specimens can strongly suppress the deformation of textures by acting as barriers to the rotation of the aluminium grains (Engler *et al.*1996).

2.1.4.4 Through thickness anisotropy

The influence of the production stages (casting and their subsequent thermo-mechanical processes) on the through thickness anisotropy of properties of AA 7010 has also been researched for some time. Investigation on the effect of hot rolling and solution treatment parameters on this alloy showed that deformation temperature has a strong influence on the microstructure after solution treatment. Electron back scattering diffraction measurements showed a deformation temperature dependence of the orientation distribution of the recrystallised grains (Morere *et al.* 1996).

Through thickness anisotropy of longitudinal yield strength on thick rolled plates of 7000 series aluminium alloys often occurs. This has been attributed to a gradient

effect through the thickness of chemical composition, quench path and crystallographic texture. The results of recent research on AA 7050 - T74 plate indicated that, anisotropy induced by an interaction of precipitates with crystallographic texture also plays a role (Chakrabarti *et al.*1996) and Bate *et al.* (1981).

The through thickness mechanical property anisotropy for AA 7010 rolled plate has been simulated (Solas *et al.* 1996). Using an elastoplastic self-consistent simulation model, it was shown that the variation of macroscopic yield stress is mainly a crystallographic texture effect. The yield stress profile calculated with elongated grains and rolling texture was compared with the experimental results. A difference of 40 MPa between experimental yield stress and the one predicted by the model was explained as been a product of poor fit in the elastic plastic transition domain

2.2 Strengthening of aluminium alloys

Aluminium alloys are classified according to whether they are heat treatable or not. One or more of the following strengthening mechanisms increases the strength of non-heat treatable aluminium alloys: grain size hardening, solute hardening and work / strain hardening. Heat treatable aluminium alloys are strengthened by the precipitation hardening mechanism. The strength of aluminium alloys is increased by the above mechanisms because they provide barriers to the movements of dislocations.

2.2.1 Non heat treatable aluminium alloys

2.2.1.1 Grain size hardening

By reducing the grain size of a wrought aluminium product its strength is increased. The yield strength (σ_y) - grain size (d) relationship is expressed by the well-known Hall - Petch equation:

$$\sigma_y = \sigma_o + kd^{-1/2} \qquad (2.1)$$

where σ_o is the intrinsic yield strength and k is a constant for a given material. The dependence of the yield strength on the grain size, up to a few percent of plastic deformation, can be explained by the fact that for a given amount of plastic deformation the dislocation density generated by the grain boundaries, decreases with increasing grain size (Martin 1998).

2.2.1.2 Solute hardening

By adding a small amount of alloying elements, the solute atoms replace the aluminium ones, causing the crystal lattice to distort and a local increase in the crystal lattice energy. Dislocations passing through such a region will experience the increase of energy, and hence additional work must be done to move them. In this way alloying elements, such as Mg, Mn and Cu can impede the mobility of dislocations, thereby strengthening the material. For successful strengthening, alloy additions must satisfy two main criteria: a high room temperature solid solubility and a misfit to create local compressive or tensile strains.

2.2.1.3 Work or strain hardening

Strain hardening, or work hardening, generally involves cold working at ambient temperatures, at which the multiplication of dislocations occurs at a faster rate than they are annihilated by dynamic recovery. The increase of dislocation density leads to the formation of dense dislocation tangles, which can obstruct the movements of other dislocations. When the strain field surrounding a dislocation in the aluminium lattice is sufficiently large to inhibit the passage of other dislocations gliding on the intercepting slip plates, a stress must be applied in addition to the lattice friction stress in order for dislocations to intersect. In this manner, the aluminium alloys are strengthened

2.2.2 Heat treatable aluminium alloys

Precipitation age hardening is the most important strengthening mechanism of heat treatable aluminium alloys. The age hardening mechanism which operates in a given aluminium alloy will depend on several factors, such as the type of particles precipitated (e.g. whether GP zone, intermediate precipitate or stable phase), the magnitude of the strain and testing temperature.

It is generally agreed that an increase in hardness is synonymous with an increased difficulty of moving dislocations. A dislocation must either cut through the precipitate particles in its path, or move between them. In either case, it has been shown that a stress increase is needed to move the dislocations through a lattice containing precipitate particles (Reed – Hill 1991). The actual cause of strength increase is the obstruction to slip or dislocation movements set up by a critical dispersion of fine particles sometimes with coherent stress fields around them

(Rollason 1973, Polmear 1995). Small and finely dispersed precipitates can significantly increase the strength of aluminium alloys.

The obstacles to the motion of dislocations in precipitation-hardening alloys may be either the strains around GP zones, or the zones / precipitates themselves, or both. Clearly, if it is the zones / precipitates themselves, it will be necessary for the moving dislocations either to cut through them or to go around them. In the early stages of ageing, i.e. before over ageing, the coherent GP zones are cut by dislocations moving through the matrix and hence both internal strain hardening and chemical hardening will be important (e.g. in alloys such as Al – Cu). In alloys such as Al – Zn, however, the GP zones possess no strain field, therefore the flow stress would be entirely governed by the chemical hardening effect (Smallman 1970). When the precipitates are incoherent with the matrix, over ageing has occurred. In this case the flow stress is predominantly governed by the dispersion mechanism.

Three mechanisms have been suggested as the cause of precipitation hardening (Smallman 1970), these are: (1) internal strain hardening, (2) chemical hardening, i.e. when the dislocation cuts through the precipitate and (3) dispersion hardening, i.e. when the dislocation goes around or over the precipitate.

2.2.2.1 Internal strain hardening

The contribution of coherency strain hardening to the overall yield strength depends on the number and spacing of the zones or precipitates, and also on the degree of strain produced by them. As the GP zones nucleate and grow, there is an increase in the level of coherency strain hardening (Marshall *et al.* 2007). For strains around GP

zones, it has been shown that the maximum hindrance to the dislocation motion, i.e. maximum coherency strain hardening, is to be expected when the spacing between the particles is equal to the limiting radius of curvature of moving dislocation lines, i.e. about 50 atomic spacings or 10 nm (Polmear 1995). At this stage the dominant precipitate in most alloys is the coherent GP zone. High-resolution transmission electron microscopy has revealed that these zones are, in fact, sheared by moving dislocations (Polmear 1995). The individual GP zone has only a small effect in impeding the gliding dislocations, however, the large increase in yield strength caused by the zones may arise because of their high volume fraction (Polmear 1995).

The internal strain-hardened mechanism, originally suggested by Mott and Nabarro (Smallman 1970), is based on the knowledge that the precipitation of particles having a slight misfit in the matrix gives rise to internal stress fields, which hinder the movement of gliding dislocations. For the dislocations to pass through the regions of internal stress the applied shear stress must be at least equal to the average internal stress, and it has been shown that for spherical particles this is given by:

$$\tau = 2\,\mu\varepsilon c \qquad (2.2)$$

where μ is the shear modulus, ε is the misfit of the particle and c is the atomic concentration of solute.

2.2.2.2 Chemical hardening

When a dislocation actually passes through a GP zone, an increase in the number of solvent-solute bonds in the near-neighbours occurs across the slip plane. This tends

to reverse the process of clustering and, hence additional work must be done by the applied stress to bring this about. The magnitude of the work is controlled by factors such as relative atomic sizes of atoms involved and the difference in stacking - fault energy between the matrix and the precipitate (Polmear 1995, Smallman 1970). This process, known as chemical hardening, provides a short-range interaction between dislocations and precipitates and involves bonds at the surface and inside the precipitate; therefore it makes an additional contribution to the overall strengthening of the alloy. As the number and size of coherent precipitates increases, the role of chemical hardening becomes greater. However, as the precipitate reach a certain size, coherency starts to break down (Marshall *et al.* 2007).

Once the GP zones are cut, dislocations continue to pass through the particles on the active slip planes and work hardening is comparatively small. Deformation tends to become localized on only a few active slip planes so that some intense bands develop which allows dislocations to pile up at grain boundaries. The development of this may be deleterious with respect to mechanical properties such as ductility, toughness, fatigue and stress corrosion (Polmear 1995).

2.2.2.3 Dispersion hardening

At higher ageing times or temperatures, the precipitates become incoherent with the matrix and dislocations are no longer able to cut trough them. In this case, dispersion hardening becomes the predominant mechanism. Therefore the dislocations by-pass the precipitate by either bowing, climbing or cross slip (Marshall *et al.* 2007). The transition between chemical and dispersion hardening is rarely abrupt; the two mechanisms can operate within the same alloy.

Assuming that the dislocation by-passes the precipitates by the so called Orowan bowing mechanism, then the yield stress is the stress necessary to expand a loop of dislocation between the precipitates, and is inversely proportional to the particle separation. This stress has been expressed (Smallman 1970) as follows:

$$\tau = 2\alpha\mu B/L \qquad (2.3)$$

where $\alpha = 1/2$, μ is the shear modulus, B is Burgers vector and L is the separation of the precipitates. This process will be important in the later stages of precipitation when the precipitate becomes incoherent and the internal lattice strains disappear. A moving dislocation is then able to bypasses the obstacles, as shown in Fig. 2.1b, by moving in the clean pieces of crystal between the precipitated particles. Clearly, the flow stress will decrease as the distance between the obstacles increases, so this effect can account for the over-aged condition, which occurs in these alloys. However, even when the dispersion of the precipitate is coarse, a greater applied stress is necessary to force a dislocation past the obstacles than would be the case if the obstruction were not there.

2.3 Aluminium alloys heat treatments

There are only two principal methods for increasing the strength and hardness of aluminium alloys, these being cold working and heat treatment. The cold work method employed on non-heat treatable aluminium alloys was described in section 2.2.1. The heat treatment method is performed on heat treatable aluminium alloys to obtain a variation in mechanical properties by promoting precipitation hardening.

The heat treatment method is only effective in increasing the strength, when the equilibrium phase diagram of a particular aluminium alloy shows the solid solubility of one or more alloying elements decreasing with decreasing temperature. This effect is one of the fundamental characteristics that provide the basis for a substantial increase in hardness and strength, when the aluminium alloy is solution heat-treated, quenched and subsequently precipitation hardened (Staley *et al.*1984).
The main alloying elements of AA 7010 are zinc (6.3%), magnesium (2.24%) and copper (1.7%). The binary equilibrium diagrams for the Al –Zn, Al-Mg and Al-Cu systems, all exhibit the features of decreasing solubility with decreased temperature.

Fig. 2.2 shows an equilibrium phase diagram for the Al-Zn system, where the maximum solubility of Zn in Al at approximately 275°C is 31.6% and the concentration shows an appreciable decrease to approximately 5.6% at 125°C (Avner 1974). At room temperature the solubility of Zn in aluminium is much less than this. It has been demonstrated by researchers and wrought aluminium manufactures that optimum mechanical properties for heat treatable aluminium alloys are usually obtained when a suitable heat treatment cycle is employed. Fig. 2.2 illustrates this cycle, which consists of solution heat-treatment, quenching and precipitation treatment. The hardening mechanisms governing the precipitation hardening processes were briefly reviewed in section 2.2.2. For now the practice of these heat treatment process stages is considered.

2.3.1 Solution heat-treatment

Solution heat-treatment is the first of the two treatment stages prior to the precipitation hardening of aluminium alloys. For AA 7010, this treatment is best

explained by using as reference the Al-Zn binary system, Fig. 2.2. The solution heat-treatment consists of heating the aluminium alloy to a temperature above the solvus line or solvus temperature and holding at that temperature until a homogeneous solid solution α phase is produced. This operation dissolves the inter-metallic compounds precipitated and helps to further reduce any segregation present in the original alloy (Askeland 1992). Position 1 of Fig. 2.2 indicates the approximate solutionising temperature (473°C) for AA 7010.

The main purpose of solution treatment is to put the maximum practical amount of hardening solutes such as Zinc, Magnesium and Copper into the α aluminium solid solution matrix. From Fig. 2.2 it can be seen that, after quenching the matrix will consist of super saturated solid solution α. When precipitation takes place the structure is expected to be β in a α matrix.

Solution treatment temperature

The maximum practical level of solute elements in the matrix can be achieved by solution treating the aluminium alloys between the solvus and the solidus temperatures. However, in industrial practice it would be inadvisable to quote such a large permissible temperature range. This is because an error leading to the use of a temperature just below the solidus temperature would cause melting of the alloy to begin. The use of a temperature below the solvus line on the other hand would mean that a considerable amount of intermetallics had not been absorbed in to the solution (Higgins 1970).

The AA 7010, like most commercial alloys, is more complex in composition than the simple binary Al-Zn alloy under consideration. This means that the available temperature range between complete solution of the precipitated phase and the commencement of fusion is much smaller.

For some alloys, the temperature at which the maximum amount is soluble also corresponds to a eutectic temperature. Consequently, solution treatment temperatures must be limited to a safe level below the maximum to avoid any possibilities of overheating and partial melting of non-equilibrium eutectic precipitates (Staley *et al.* 1984). Therefore, the permissible temperature range of solution treatment is usually of the order of 10 to 20°C.

In accordance with Airbus UK (2003), the solution heat-treatment temperature range for AA 7010 is 465 to 485°C. In practical terms the upper limit of the solutionising temperature will be set with regards to grain growth, surface effects and economy of operation.

Some alloys of the 7000 series, such as AA 7075 and AA 7050, which should allow a much wider temperature range for selection of the solution treatment temperature, based on the equilibrium solvus and solidus temperatures, can exhibit incipient melting at temperatures much below the latter under certain circumstances. AA 7075 has two soluble phases $MgZn_2$ and Al_2CuMg. The latter phase is very slow to dissolve. Local concentrations of this phase can produce non-equilibrium melting

between 485 and 490°C if brought to this or higher temperature too rapidly (Staley *et al.* 1984). This makes accurate pyrometric control of the process a necessity.

Heat treatment time

The time required for solution heat treatment depends on the type of product, alloy, casting or fabrication procedure used and its thickness because they influence the pre-existing microstructure. Sand castings are usually held at the solution treatment temperature for 12 hours; permanent mould castings, because of the finer structure, may only require 8 hours (Staley *et al.* 1984). Thick section wrought products are generally heated longer. Once the product is at temperature, the rate of dissolution is the same for a given size of intermetalic particle, regardless of section thickness. The main consideration is the coarseness of the microstructure and the diffusion distance required to bring about a satisfactory degree of homogeneity. Thin products such as sheet may require only a few minutes. The time specified for treatment should be measured from the moment when the coldest part of the charge reaches the minimum treatment temperature. The time to heat up to solution treatment temperature cannot be too rapid, because soluble phases containing magnesium have the tendency to leave behind micro-voids when they dissolve, especially when the particles are large and the heating rate is very rapid (Staley *et al.* 1984).

2.3.2 Quenching

The quenching process is a continuation of the solution treatment, and it is in many ways the most critical step in the sequence of the heat treatment cycle. The maximum strength attained upon natural or artificial ageing depends on the quantity of alloying

elements retained within the solid solution after the quenching operation. The objective of quenching is to preserve the homogeneous solid solution formed at the solution heat treatment temperature, by rapidly cooling to some lower temperature, usually near to room temperature. Quenching not only retains solute atoms in solution but also maintains a certain minimum number of vacant lattice sites. This assists in promoting the low temperature diffusion required for zone formation (Staley *et al.* 1984). Fast quenching will produce a supersaturated solid solution, where the atoms of alloying elements do not have sufficient time to diffuse to potential nucleation sites and permit the formation of the second phase. After quenching the AA 7010 microstructure is expected to consist of a super-saturated alpha phase (α), containing excess of Zn, Mg, and Cu.

In general, the highest strength attainable and the best combination of strength and toughness are those associated with the most rapid quenching rates. Resistance to corrosion and stress corrosion cracking are other characteristics that are generally improved by maximum speed of quenching. Some of the alloys used in artificial ageing, in particular the copper free 7000 alloys, are exceptions to this rule (Staley *et al.* 1984).

The maximum attainable quench rate decreases as the thickness of the product increases. Because of these effects, much work has been done over the years to understand and predict how quenching conditions and product form influence properties (Staley *et al.* 1984).

When the solution treatment process is complete the charge must be quenched as quickly as possible. Rapid transfer of the charge to the quenching tank is essential, since any delay will allow precipitation of phases to take place during the relative slow cooling. Precipitation of phases due to delays in quenching will lead to poor mechanical properties and a lower resistance to corrosion. This is because the solute atoms that precipitate either on grain boundaries, dispersoids, particles or vacancies are irretrievably lost and are not available to contribute to subsequent strengthening.

2.3.3 Age hardening heat treatment

While some alloys are required to harden naturally at room temperature, it is also necessary to treat others at higher temperatures in order to obtain in them their optimum properties.

After solution treatment and quenching the aluminium alloy is very soft or ductile. Two hours after this treatment some aluminium alloys, at room temperature, will start their natural ageing process. Storing the quenched charge at a lower temperature than room temperature, however, considerably retards precipitation hardening. Refrigeration equipment is employed for this purpose. A refrigerator at -14°C can prevent the natural precipitation age hardening of aluminium alloys for up to 150 hours (Airbus UK 2004b).

The relationship between time and temperature of precipitation treatment and the mechanical properties obtained for many aluminium alloys has been investigated by many researchers. Generally the higher the temperature used, the shorter is the time

necessary to produce optimal mechanical properties. During artificial ageing, if the optimum time is exceeded for any given temperature, the properties begin to deteriorate due to over ageing or the precipitation of non-coherent particles (Higgins 1983). The time and temperature of precipitation treatment differ with the composition of the alloy, and must be controlled accurately to give optimum results.

Artificial ageing treatment

Artificial precipitation treatment must always be planned in order to accommodate materials of various thickness. Thin sections tend to heat up more quickly than thick sections, so if a high-temperature and short time treatment was employed, variations in properties between thick and thin sections would be inevitable. Therefore, it is general practice to perform precipitation treatments at relative low temperatures for corresponding long times. This minimises differences in properties due to the time lag in reaching treatment temperatures of heavy sections with respect to thin sections (Higgins 1970). The precipitation age hardening process is discussed in more details in section 2.5.

Over ageing treatment

Over-ageing is the condition where softening results from prolonged ageing. In some age-hardening alloys, over-ageing appears simultaneously with the loss of coherency by the precipitate. Therefore during precipitation treatment, heating should not be continued after the maximum properties are obtained. Otherwise the over-ageing process in the material begins and softening of the alloy occurs. The higher the recipitation temperature used, the sooner the maximum properties are attained, and

the sooner over-ageing takes place (Higgins 1970). However, in the case of AA 7010, slight over-ageing is some times desired in the material to improve other properties such as toughness, stress corrosion cracking and corrosion. This occurs at the expense of a slight loss of strength.

Reversion

Reversion, a commonly observed phenomenon in precipitation hardening, occurs when an alloy hardened by ageing at low temperature is temporarily softened by subsequently heating to a higher ageing temperature. The alloy becomes harder again on prolonged heating (Smallman 1970). The reversion occurs because some of the nuclei or zones precipitated at the low temperatures are very small and unstable when raised to the higher ageing temperature. Consequently they re-dissolve and the alloy becomes softer; the temperature above which the nuclei or zones dissolve is known as the solvus temperature. A typical phase diagram showing different solvus lines for its precipitate variant are shown in Fig. 2.3. On prolonged ageing at the higher temperature larger nuclei, characteristic of that temperature, are formed and the alloy again hardens. Clearly, the reversion process is reversible, provided re-hardening at the higher ageing temperature is allowed to occur (Smallman 1970)

2.4 Diffusion

Diffusion is the movement of atoms within a material. Atoms move in an orderly fashion to eliminate concentration differences and produce a homogeneous, uniform composition (Askeland 1990). Diffusion in metals is very complex but of great practical and theoretical importance in the manufacture and thermal treatments of

wrought aluminium alloys.

2.4.1 Diffusion mechanisms

Many investigators have extensively studied diffusion mechanisms and their influencing factors. This has been well documented through the years. The interstitial, interchange and vacancy mechanisms have been reported as possible mechanisms to explain the diffusion in substitution solid solutions (Reed-Hill 1973). Based on the motion of individual atoms, the vacancy mechanism is the predominant mechanism to explaining diffusion in substitution solid solutions.

It is well documented that the crystal structure of industrial metals is never perfect. Defects such as vacancies, dislocations and interstices are a normal feature of a crystal structure. These crystal imperfections facilitate the movement of adjoining atoms (Higgins 1983).

Fig. 2.4 illustrates a vacancy defect in the lattice. Fig. 2.5 illustrates the motion or diffusion of a single atom by the vacancy-solute mechanism. The associated pair of vacant site and solute atom can migrate easily through the crystal in stages as indicated in Fig. 2.5 (a)-(f) (Higgins 1993).

2.4.2 Diffusion in aluminium

It is well documented that diffusing of the solute atoms through the aluminium matrix can only take place by the vacancy mechanism, because atoms of comparable size with the aluminium atoms cannot migrate in the close packed fcc lattice (Bergner *et al.* 1995). The amount, distribution and type of vacancy complexes

present in the aluminium matrix determine the migration of the atoms. The vacancies could exist in two forms: those in thermodynamic equilibrium at the ageing temperature and the excess of vacancies. The latter occurs when the alloy is quenched fairly quickly from higher temperatures to room temperature (Bergner *et al.* 1995, Federighi and Cotterill 1965).

Analysis of diffusion rate data for several elements in aluminium, produced by many authors, gave reliable proof that diffusion of non-transition elements, such as Zn, Mg, Cu etc., in aluminium is predominantly by the single vacancy mechanism (Staley *et al.*1984, Bergner *et al.* 1995).

2.4.3 Factors influencing diffusion

The rate of diffusion of one metal in another is dependent on the diffusion coefficient. A mathematical expression for the diffusion coefficient D has been written (Reed-Hill 1973) as:

$$D = D_o \, e^{-Q/RT} \qquad (2.4)$$

where D_o is the pre-exponential factor, Q is the activation energy, R is the gas constant and T is the temperature.

Whereas the diffusion coefficient mainly depends on temperature and the activation energy, as shown in equation (2.4), other variables such as solute concentration, excess vacancy and time also influence the diffusion rate. All above factors are briefly described bellow.

Temperature

The dependence of the diffusion coefficient on temperature T can be seen from equations (2.4). When the temperature of the material increases, the diffusion coefficient and the flux of atoms increase as well (Askeland 1990). The diffusion coefficient can double for every 20°C rise in temperature (Avner 1974).

The temperature is the most important variable for diffusion. This is because all atoms are constantly vibrating on their equilibrium positions in the lattice, and the amplitude of vibration increases with increasing temperature or thermal energy. At high temperatures, the thermal energy supplied to the diffusing atoms permits the atoms to overcome the activation energy barrier and more easily move to another lattice site. At low temperatures, often below 0.4 times the absolute melting temperature of the material, diffusion is very slow (Askeland 1990). Therefore in aluminium thermal treatments, prolonged annealing is always necessary to remove casting coring completely. Precipitation age hardening will take several hours depending on the temperature selected. The time for solution treatment would be much shorter because of the higher temperature.

Activation energy

From equation (2.4) it can also be seen that the rate of diffusion is dependent on the activation energy Q of the atoms. The activation energy is the energy required to move an atom from its lattice position to another location in the lattice. Atoms normally overcome this energy barrier when heat is supplied to the material. A small activation energy Q increases the diffusion coefficient and flux, since less energy is required to overcome the smaller activation energy barrier (Askeland 1990).

Activation energies are usually lower for atoms diffusing through open crystal structures than through close-packed crystal structures.

Solute concentration

It is well documented that the rate of diffusion is dependent on the concentration gradient of the solute atoms within the solvent metal (Reed-Hill 1973). The general tendency would be for the solute atoms to diffuse away from regions of high concentration towards regions of low concentration (Higgins 1993). Diffusion will ultimately cease when a uniform distribution of solute atoms has been achieved. An alloy has the lowest free energy when it is in a homogeneous condition (Avner 1974). The driving force for diffusion is the reduction in strain energy. When solute atoms move away from regions of high concentration the overall distortion of the crystal is reduced (Higgins 1993).

Vacancies

The rate of diffusion depends to some extent on the number of vacant sites. The diffusion rate is greater in a rapidly cooled alloy than in the same alloy slowly cooled. The reason for this is the presence of excess vacancies retained by the fast cooling. Increasing the speed of quenching from solutionising temperatures will increase the number of vacancies available for diffusion (Federighi and Cotterill 1965).

In aluminium alloys the excess vacancy concentration has been reported to enhance the diffusion rate at room temperature (Kelly and Nickelson 1963). The excess vacancies play a significant role in the formation of GP zones at low temperatures

(Staley *et al.* 1984). Vacancy migration has lower activation energy when compared with the other mechanisms (Avner 1974).

Time

Diffusion requires time. If a large number of atoms must diffuse to produce uniform structure, long times may be required, even at high temperatures. Times for thermal treatments may be reduced by using higher temperatures or by making the diffusion distances as small as possible (Askeland 1990).

2.5 Precipitation hardening

During precipitation in a solid solution, the changes in properties, mechanical in particular, in a material are more significant than those produced during quenching. For example, the tensile strength of duralumin (4.0% Cu, with Mg, Si and Mn) may be raised from 210 to 410 MPa (Smallman 1970). Other properties, such as hardness and electrical conductivity, also change during precipitation. All these properties are dependent on the structural distribution of the fine precipitate phases formed. Age hardened alloys usually exhibit softening as their finely dispersed precipitates coarsen.

Heat treatable aluminium alloys (2000, 6000 and 7000 series) are thermally treated to increase the strength. The strengthening effect depends on the nature, type and volume fraction of the precipitates formed. Artificial age hardening is designed to produce a uniform dispersion of a fine, hard and coherent precipitate in the softer, more ductile matrix (Askeland 1990). How these precipitates strengthen the alloy by inhibiting dislocation mobility was reviewed in section 2.2.2. The three thermal

treatments required for precipitation hardening (solution treatment, quenching and age hardening) were reviewed in section 2.3. Basic aspects for the development of the microstructure during precipitation hardening are reviewed in this section, with emphasis on the microstructures developed and their effect on strength.

2.5.1 Basic requirements for precipitation hardening

The basic requirements for an alloy to have the ability to respond to age hardening during heat treatment are (Askeland 1990):

a) The phase diagram must display a decreasing solid solubility with decreasing temperature.
b) The alloy must be quenchable, i.e, the speed of quenching for the alloy must be rapid enough to suppress the formation of the second phase.
c) The matrix should be soft and relatively ductile and the precipitate, an inter-metallic compound in most age hardenable alloys, should be hard.
d) The precipitate that forms must be coherent with the matrix structure in order to develop the maximum strength and hardness. Furthermore, its size, shape and distribution must be able to be controlled.

An alloy, which meets the above criteria, in the solutionised and freshly quenched condition, is in a super saturated condition and therefore unstable. The precipitation of the excess solute constituents can generally be controlled at will by the ageing heat treatment to give an increase in strength and hardness. This ageing treatment can occur at any temperature below the solvus temperature, even at room temperature. On many aluminium alloys (including AA 7010), in the quenched condition, age

hardening takes place to a great extent spontaneously at room temperature, although heating to high temperatures accelerates the rate of ageing.

The rate of ageing increases markedly with increasing temperature while the peak hardness decreases, as shown in Fig. 2.6 (Smallman 1970). Two-stage hardening takes place at low ageing temperatures and is associated with high maximum hardness. Single-stage hardening occurs at higher ageing temperatures.

2.5.2 Homogeneous nucleation

A precipitate particle can be nucleated either homogeneously or heterogeneously. Homogeneous nucleation involves the spontaneous formation of nuclei, i.e., the solute atoms cluster in the lattice of the matrix and start a second-phase particle (Reed – Hill 1991). This type of nucleation occurs with difficulty, while heterogeneous nucleation is normally easier.

However, homogeneous nucleation of GP zones will occur spontaneously provided a critical vacancy concentration exists. At low temperatures (below 100°C) the critical nucleus size for a GP zone may be so small that the incubation time for a nucleus effectively vanishes. This would account for the rapid growth rates of the GP zones at these temperatures (Reed-Hill 1991). GP zones may also form by the spinoidal transformation, for which there is no barrier for nucleation of coherent second phase particles with a uniform and homogeneous distribution (Martin 1998).

The principal difficulty in the formation of nuclei homogeneously is that a surface is created when a second-phase particle is nucleated. Since the free energy depends on

the area and volume of the particle, assuming a spherical particle, the expression for the free energy change has previously been written as (Reed-Hill 1973):

$$\Delta F = - A_1 r^3 + A_2 r^2 \qquad (2.5)$$

where A_1 is equal to $4\pi\Delta g/3v_1$ (Δg is the volume free energy difference per atom and v_1 is the volume per atom), A_2 is equal to $4\pi\gamma$ (where γ is the is the surface free energy between the precipitate and the alpha phase) and r is the particle radius. Fig. 2.7 is a plot of equation (2.5). At small radii, the surface free energy A_2r^2 is larger than the volume free energy A_1r^3, leading to a positive total free energy (Reed-Hill 1973).

The situation changes, however, as the radius grows in size. With large radii the free energy becomes negative. There is a critical radius r_o. Below this value a particle lowers its free energy by decreasing its size, so that particles with radii smaller than the critical radius r_o tend to dissolve and go back in solution. On the other hand, particles with radii larger than r_o undergo a decrease in free energy with increasing radius. For this reason they are stable and continue to grow (Reed-Hill 1973).

In many alloys, the precipitation-hardening phenomenon is complicated because nucleation occurs both homogeneously and heterogeneously. Since heterogeneous nucleation is easier, precipitation tends to occur more rapidly at lattice defect locations. This introduces a time lag between the ageing responses in areas undergoing heterogeneous and homogeneous nucleation, hence over-ageing frequently occurs at the grain boundaries long before precipitation in the matrix has

had a chance to develop fully.

2.5.3 Coherency of precipitate and matrix

An important factor in the interaction between precipitate particles and dislocations is the presence of stress fields surrounding the particles. This is especially true when the precipitate particle is coherent with the matrix, as illustrated in Fig. 2.8.
The coherent or semi-coherent precipitates by nature will strain the lattice. The degree of strain depends on the type of precipitate. Discs cause least strain, needles intermediate and spheres most strains. The type of dispersion depends on the degree of super-saturation of the matrix.

Over-ageing is the condition where softening results from prolonged ageing. In some age-hardening alloys, over-ageing appears simultaneously with the loss of coherency by the precipitate. In any case, it is connected with the continued growth of precipitate particles. Growth will continue as long as the metal is maintained at a fixed temperature. This does not mean that all particles continue to grow, because this is impossible once the solute has attained an equilibrium concentration. It just means that certain particles (the larger ones) continue to grow, while others (the smaller ones) disappear (Reed-Hill 1991).

2.5.4 Precipitate structures in aluminium alloys

In virtually all age-hardening systems the initial precipitate is not the same structure as the equilibrium phase (Smallman 1970). Instead, an ageing sequence is followed: saturated solution → GP zones → intermediate precipitates → equilibrium precipitates. This sequence occurs because the equilibrium phase is incoherent with

the matrix, whereas the transition precipitates are either fully coherent or at least partially coherent. Due to surface energy and strain energy factors, the precipitation process follows the above sequence, in order to have the lowest free energy in all stages of precipitation.

For the incoherent type of precipitate, the nuclei must exceed a certain minimum size before they can form a new phase. To avoid such a slow mode of precipitation, a coherent type of precipitate is formed instead (i.e. GP zones), for which the size effect is relatively unimportant (Smallman 1970). The condition for coherence usually requires the precipitate to strain its equilibrium lattice to fit that of the matrix, or to adopt a meta-stable lattice. In spite of both a higher volumetric free energy and higher strain energy, the transition structure is more stable in the early stages of precipitation because of its lower surface energy (Smallman 1970).

Upon solution heat treatment of aluminium alloys, all soluble alloying elements dissolve into solid solution. Following the quenching operation, the maximum strength attained upon artificial ageing largely depends on the amount of alloying elements retained within the solid solution. Controlled precipitation of the solute elements at low artificial ageing temperatures promotes the formation of the homogeneous age hardening precipitates in 7000 series aluminium alloys (Staley *et al.* 1984).

Although AA 7010 has low quench sensitivity, heterogeneous precipitation can occur during slow quench and the equilibrium precipitate η forms (Godard *et al.* 2002). The quench induced precipitates form mainly on zirconium containing dispersoids

(Deschamps and Brechét 1998, Godard *et al.* 2002). This results in a decrease of the solute available for the fine-scale precipitation and therefore a reduction in hardness and an increase in the electrical conductivity (Staley *et al.* 1984). Therefore, AA 7010 requires a rapid quench to prevent heterogeneous precipitation from occurring. Due to the importance of AA 7000 series for high strength structural components, the age hardening process in these alloys have been extensively studied (AMS Handbook 1991). According to Staley *et al.* (1984), from a super saturated solid solution, the general sequence of precipitation reactions for the AA 7000 series is:

$$\alpha \rightarrow \text{GP zone} \begin{cases} \rightarrow \eta' \rightarrow \eta \\ \rightarrow T' \rightarrow T \end{cases}$$

where α is the super saturated solid solution, η ($MgZn_2$) and T ($Mg_3Zn_3Al_2$) are equilibrium precipitates and η' and T' are the respective transition phases or variants of the η and T precipitates. The precipitation sequence depends on composition. Evidence exists for a transformation of α → GP zones → T' → T in alloys with lower Zinc – Magnesium ratios (Staley *et al.* 1984).

The η' and η phases have hexagonal plate like structure that grows preferentially in the {111} plane of the matrix and have been found to be of the composition closely approximate to $MgZn_2$ (Bigot et al. 1976). The T' and T are cubic phases with a chemical composition close to $Mg_3Zn_3Al_2$ (Godard *et al.* 2002)

For AA 7050, which is almost identical to AA 7010, the decomposition reaction from a super saturation solid solution was reported by Dixit *et al.* (2008) as:

$$\alpha \rightarrow \text{clusters} \rightarrow \text{GP zones} \rightarrow \eta' \rightarrow \eta$$

Most recently, using differential scanning calorimetry (DSC) and transmission electron microscopy (TEM) techniques, the above precipitation sequence was re-confirmed for AA 7050 (Buha *et al.* 2008). Therefore, the AA 7010 in this investigation is expected to have the same sequence of precipitation reactions as above during ageing.

The strength of the artificially aged AA 7010 will depend mainly on the nature, size and volume fraction of the precipitates. The clusters and the GP zones are fine and coherent precipitates formed at low temperatures or during the early stages of artificial ageing. At early stages of ageing, GP zones are the predominant precipitates (Buha *et al.* 2008). Due to their coherency with the matrix, the effect of these fine precipitates is to increase the strength of the alloy with increasing volume fraction.

The η' phase is larger than the GP zones and is the precursor of the equilibrium precipitate. This transition phase (η'), which often forms by transformation of GP zones, is also fine but is semi-coherent with the matrix because it has misfit dislocations along one interface at least (Staley 1992). The effect of the η' precipitate is also to increase the strength and has been associated with the peak strength in AA 7000 series. For example, the maximum hardness in AA 7075 arose mainly from the presence of the fine dispersion of the η' particles (Park and Ardell 1983). In AA 7050 –T76, the η' phase was also reported as the matrix strengthening precipitate (Staley 1992). In AA 7050 the η' precipitate is characteristic of the peak aged T6

microstructure along with smaller fractions of GP zones (Staley 1992, Buha *et al.* 2008).

For AA 7010, artificial ageing at low temperature (200 to 100°C) promotes the precipitation of fine-scale homogeneous precipitates, where the η' phase is the predominant one (Deschamps and Brechét 1998, Godard *et al.* 2002). The equilibrium precipitate (η), which is coarser than the transition phase η' and more widely spaced, is non-coherent with the matrix; therefore it does not strengthen the alloy. The equilibrium precipitate is normally formed in over ageing through transformation from the transition phase η' or formed heterogeneously at dispersoids and grain boundaries during cooling from solution treatment temperature.

During slow cooling of AA 7010 from solution treatment temperature, it was reported that, at lower temperature than typically 250°C, the solid solution decomposition promotes the precipitation of the η phase first, and then of the S and T phases (Godard *et al.* 2002). The S phase is orthorhombic with a chemical composition close to that of Al_2CuMg. It was also reported that homogeneous age hardening can occur when the temperature falls to the age hardening temperature range, leading to an increase in hardness at the surface of the material (Tanner and Robinson 2004). For Al-Zn alloys, it was reported that metal-stable transition phases precipitated and grown to various sizes at 200°C can decompose at room temperature ageing (Bartŭska *et al.* 1979).

2.7 Electrical conductivity

Precipitation of solute elements during age hardening of heat treatable aluminium alloys not only influences mechanical properties, as discussed in the preceding sections, but also affects other properties, such as electrical conductivity. These properties change considerably during the ageing process (Smallman 1970). By studying the progressive changes of electrical conductivity and hardness during precipitation hardening, one can learn more about the development of mechanical properties with ageing and probably predict non-destructively their expected values with some degree of accuracy.

During the last few decades, the aircraft industry has made necessary strides to guarantee the integrity of its aircraft structural components. This has been attained by improved methods of monitoring the quality of aluminium plates. Among the most common methods used is electrical conductivity, normally measured by the eddy current technique. This section reviews the factors affecting electrical conductivity and its contribution and limitations in the studies of age hardening of aluminium alloys.

2.7.1 Factors affecting electrical conductivity

Electrical conductivity is the measure of the material's ability to conduct electrical current and is the reciprocal of the electrical resistivity (Sigli *et al.* 2007). The unit of electrical conductivity is Siemens per meter (Sm^{-1}). A common alternative is to refer conductivities to an agreed standard with high purity annealed copper, which gives a high conductivity of 58 MSm^{-1} (mega Siemens per meter). This is referred to as 100% IACS (International Annealed Copper Standard) (Sigli *et al.* 2007). The

accepted value for the electrical conductivity of super purity aluminium (99.99%) is 64.94% IACS (Frank *et al.* 1984).

The electrical conductivity arises from the motion of electrons through the lattice. The electron wave scattering by any kind of irregularity in the lattice arrangement can result in decrease in electrical conductivity. These irregularities can arise from any disturbance to the periodicity of the lattice, due to temperature, alloying concentration, lattice deformation, nuclear irradiation, etc (Smallman 1985).

Electrical conductivity is one of the most sensitive properties of aluminium, being particularly responsive to changes in composition and thermal conditions (Milek and Welles 1969). The measurement of resistivity detects the overall disturbance in the crystal lattice. The total resistivity of a crystalline metallic specimen is the sum of the resistivity due to thermal agitation of the metal ions of the lattice and the resistivity due to impurities in the crystal (Matthiessen's law):

$$\rho = \rho_t + \rho_i \qquad (2.6)$$

where ρ is the total resistivity, ρ_t is the intrinsic thermal response of the pure metal and ρ_i is the contribution from impurities, solute and vacancies (Sigli *et al.* 2007).

According to Matthiessen's law, when the solid solution of an alloy undergoes precipitation, the solutes depleted from the matrix decreases the resistivity as precipitation progresses. However, equation (2.6) can only be used to estimate the

contribution of the matrix to the measured resistivity. It does not account for the effect of precipitates on the development of resistivity during ageing, which will be dealt with in section 2.7.2.

2.7.1.1 Temperature

The intrinsic resistivity of a metal, ρ_t, is influenced by temperature. When the temperature of a metal increases, the thermal energy causes the atoms to vibrate and scatter electrons. When the mobility of electrons is reduced, or the mean free path decreases, the resistivity increases (Askeland 1992). The change of resistivity, $\Delta\rho$, with temperature can be estimated by:

$$\Delta\rho = \rho_r (1 + a\Delta T) \qquad (2.7)$$

where ρ_r is the resistivity at room temperature (25°C), ΔT is the temperature difference between room and temperature of interest, and a is the temperature resistivity coefficient (Askeland 1992).

2.7.1.2 Alloying elements

All crystallographic features that disrupt the regularity of a metal lattice tend to increase its electrical resistivity. Solute atoms produce distortions in the lattice and therefore cause scattering of the electrons being conducted, leading to an increase in the electrical resistivity (Milek and Welles 1969). Therefore, all metallic additions to aluminium reduce its electrical conductivity. Strengthening alloying elements added to aluminium can have widely differing effects on electrical conductivity, depending upon whether they are in or out of solid solution (Morris *et al.* 1984). The non-

strengthening elements, such as vanadium, chromium, manganese and titanium, have a dramatic effect on conductivity with little or no contribution to strength (Rummel and Arbegast 1981).

The effect of the additions of two or more alloying elements on the resistivity of aluminium depends on the relationship of the elements. In general, if the elements individually go into solid solution in aluminium, their effects on the resistivity are additive. In the Al-Mg- Zn system, the effect of the combined presence of Mg and Zn on the resistivity of aluminium is approximately additive, even when Mg and Zn are present in the ratio to form $MgZn_2$ compound (Morris *et al.* 1984).

2.7.1.3 Lattice structure

Thermo mechanical processing techniques and strengthening mechanisms influence the structure of aluminium alloys, as reviewed in sections 2.1 and 2.2 respectively. The structure in turn affects the electrical conductivity. The conductivity of a defect free pure metal is determined by the electronic structure of the atoms. The defects in a metal have significant effect on the mobility of the electrons (Morris *et al.* 1984). The mobility is proportional to the average velocity of electrons, which is low if the electrons collide with imperfections in the lattice. The mean free path is the average distance between collisions; a long mean free path permits high mobility and therefore high electrical conductivity (Morris *et al.* 1984). A great number of defects reduces the mean free path of electrons and reduces their mobility. A purer material has a longer mean free path and therefore has a higher electrical conductivity.

2.7.1.4 Texture, strain hardening and grain size

The electrical conductivity is isotropic unless orientated dislocations are present. During the various types of deformation of cast ingots or semi-finished products, textures develop or the initial textures are altered. The electrical conductivity of metals with a texture or preferred orientation normally varies with direction, since the mean free path varies (Askeland 1992).

The effect of strain hardening on electrical conductivity of aluminium is small and generally less than that of alloying elements in solid solution or of the heat treatments used on many aluminium alloys (Milek and Welles 1969). The electrical conductivity of a conductor grade aluminium is decreased from a typical value of 63% IACS in the annealed condition to 62.5% IACS in the strain hardened H19 condition (Morris *et al.* 1984). The effect of grain size in commercial materials is also negligible (Morris *et al.* 1984). Strain hardening and grain size have less effect on electrical conductivity than alloying, because dislocations and grain boundaries are further apart than solid solution atoms, resulting in a longer mean free path for electrons (Sigli *et al.* 2007). The dislocation tangle network does not significantly affect the mean free path (Askeland 1992).

2.7.2 Effect of age hardening on electrical conductivity

Quenching an alloy after a solution heat-treatment generally results in the lowest electrical conductivity, because a large part of the alloying elements present are retained in solid solution. The electrical conductivity progressively changes during the age hardening of a freshly solution heat-treated aluminium alloy. This change is

induced by precipitation of solute alloying element atoms from the saturated solid solution, which disturbs the lattice periodicity.

In general, the contribution of the ageing phenomena to the electrical conductivity of aluminium has two distinct effects. Firstly, when a solid solution alloy undergoes precipitation, solutes are depleted from the matrix and hence the electrical resistivity decreases or the conductivity increases as precipitation progresses. Secondly, as precipitates form, they produce a scattering effect, which tend to reduce the electrical conductivity. Overall, the precipitation can either decrease or increase the electrical conductivity, depending on the ageing temperature and time.

2.7.2.1 Low temperature age hardening

In the early stages of age hardening, a large number of fine precipitates form and strain the lattice. This lattice strain can cause at least as much scattering as the original solute atoms from which the precipitates form (Sigli *et al.* 2007). This decreases the electrical conductivity during the initial stages of ageing at room temperature. The changes in electrical conductivity at low temperature age hardening have been a subject of interest for many researchers for several decades (Kelly and Nicholson 1963, Rossiter 1971, Hillel *et al.* 1975, Hillel and Rossiter 1981, Raeisinia *et al.* 2006). The general view is that the increase in resistivity in the early stages of ageing is attributed to GP zone formation and related phenomena.

From a solution heat-treated and freshly quenched aluminium alloy, on age hardening at room or low temperatures, the main disturbance of the lattice is the formation of the first forms of the transition precipitates (Polmear 1995).

The extremely small and uniformly distributed precipitates induce a short mean free path and increase the electron scattering effect. As a result, the electrical conductivity of the alloy is decreased (Polmear 1995).

2.7.2.2 High temperature age hardening

The nature, size, morphology and distribution of the precipitates in age hardening aluminium alloys, and their interaction with the matrix, vary with ageing temperature. Therefore, the effect of precipitates on electrical conductivity is complicated.

High temperature ageing has a different effect on electrical conductivity from that of low temperature ageing. In age hardening at high temperature, the electrical resistivity decreases as the average particle size become larger, less numerous and less coherent with the matrix. Because of the increased particle size at higher temperature of ageing, the mean free path for electrons is much greater than that at room temperature. As a consequence, the precipitate does not interfere with conductivity as much as the solid solution atoms or GP zones (Askeland 1992).

Larger precipitates occupy only a small fraction of the volume, therefore are rarely encountered by the average electron. It was reported that when heavy precipitates are formed along the grain boundaries in AA 2024, they did not affect the conductivity of the samples (Sundberg 1989). A similar observation was reported in AA 6111 that, at high ageing temperatures (350 -560°C), the effect of precipitates on the resistivity could be ignored (Raeisinia *et al.* 2006). The decrease of the precipitate contribution to the resistivity with increasing ageing temperature is directly related to

the decrease in density of the precipitates. The number density was reported to be inversely related to the precipitate spacing (Esmaeili *et al.* 2007). Very large precipitates and other second phases have little influence on conductivity.

2.7.3 Contributions of electrical conductivity in ageing study

In general, the electrical conductivity of aluminium alloys can provide some information on their chemical composition, changes in crystalline structure, mechanical properties as well as their response to temperature changes (Suhr and Güttinger 1993).

It is a well-known fact that, following solution heat-treatment of aluminium alloys, the maximum strength attained upon natural or artificial ageing depends on the amount of alloying elements retained within the solid solution after quenching. For this reason, manufacturers and consumers of heat treatable aluminium alloys commonly use electrical conductivity, due to its accuracy and fast response, to check the solution heat treatment homogeneity, the level of alloying elements within the solid solution post quenching, and subsequent monitoring of the ageing process (The Aluminium Association Inc. 1982). In this manner, electrical conductivity measurements are useful for in-process quality control.

In contrast to the precipitate characterisation methods, such as transmission electron microscopy (TEM) and differential scanning calorimetry (DSC), electrical resistivity measurement does not use sophisticated equipment or sample preparation methods. Instead it measures the property in the macroscopic scale very easily and quickly. At

the same time, it is sensitive to atomic scale changes such as clustering and vacancy-cluster interactions (Sato 2000).

Due to this sensitivity, electrical conductivity or resistivity has been used extensively for the assessments of the ageing phenomena of heat treatable aluminium alloys by many researches for several decades. It has proven to be very useful in giving information regarding the initial clustering reactions which occur during natural ageing or in the early stages of precipitation hardening (Panseri and Federighi 1966). Correlations between electrical conductivity and hardness have also been established for several aluminium alloys (2014, 2024, 6061 and 7075 alloys) of various ageing heat treatments (Hagemaier and Kleint 1964). Electrical conductivity was also used as a tool for verifying that AA 7000 series was in the T7 age hardened condition, which is an early stage of over ageing to provide good corrosion resistance (The Aluminium Association Inc. 1982). The values of electrical conductivity changes in a sheet of aluminium alloy D16, in the naturally aged condition, could be used to determine the depth of inter-crystalline corrosion (Naumov *et al.* 1976).

Electrical conductivity has been combined with a number of different analytical techniques to gain the required understanding of age hardening. By using electrical conductivity, hardness and microstructural analysis, it was shown that an appropriate short time heat treatment (retrogression treatment) of AA7150 can reduce the susceptibility to stress corrosion cracking, while maintaining the peak aged strength of the alloy (Matthew *et al.* 1994).

A model was established in terms of composition and heat treatment to determine the electrical resistivity of most commercial aluminium alloys (Olafson *et al.* 1996). Using Matthiessen's law and the calculated solubility (using thermo dynamical computer programs), the resistivity was predicted with a good accuracy (Olafson *et al.* 1996). Natan and Chihoski (1983) used electrical conductivity, hardness and TEM analysis to study the microstructural evolution of AA 2219 during ageing. They confirmed that hardness and electrical conductivity values were uniquely related to the microstructure. They also showed that, for a fast quenching, the precipitation sequence upon ageing was that as expected, i.e., supersaturated α phase - GP → θ" → θ'. This age hardening sequence led to an increase in hardness, until the transformation of θ" → θ' took place. However, by increasing the quenching time, primary θ' and θ phases (stable precipitates) can be precipitated as well as coarsening, leading to low hardness.

Non-destructive evaluation of electrical conductivity using the eddy current technique has been applied to steels for studying recovery during the initial ageing stage. A decrease in resistivity during the recovery of maraging steel M250 was attributed to the reduction in scattering of conductive electrons at point defects and vacancies (Tajkumar *et al.* 2007). Complemented with hardness, the eddy current method was found to be suitable to study the ageing and over ageing processes. This non-destructive evaluation method was considered to hold good promise for shop floor assessment of heat treatment adequacy for maraging steel M250 (Tajkumar *et al.* 2007). The eddy current technique has also been successfully used in studying porosity of porous metals (Ma and Peyton 2004).

In spite of the continued use of electrical resistivity measurements in recent years to gain better understanding on the precipitation phenomena and to quantify the microstructural evolution in aluminium alloys (Esmaeili *et al.* 2000a, Esmaeili *et al.* 2005, Raeisinia *et al.* 2006), the sensitivity of the technique is not capable of differentiating the changes in the structure, chemical and electronic nature of the precipitates, particularly during the early stage of decomposition (Panseri and Federighi 1966). Another limitation of the method is that it is difficult to assure the mechanical properties using electrical conductivity alone. The final decision on the acceptance of a heat treatment still depends on mechanical testing (The Aluminium Association Inc. 1982).

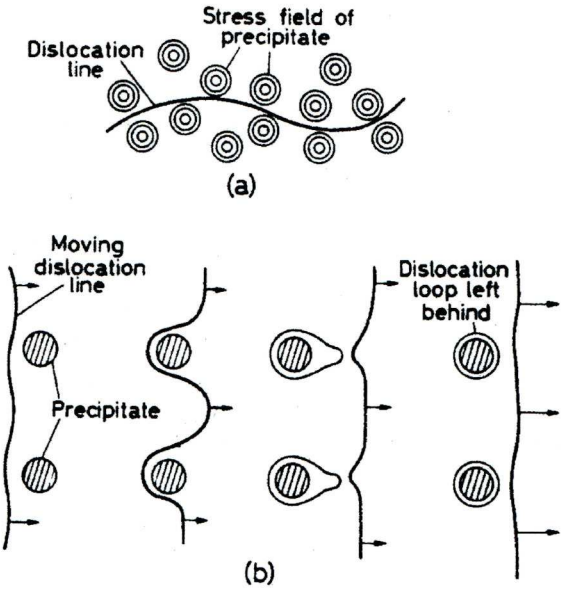

Fig. 2.1 Schematic representation of a dislocation (a) curling round the stress fields from precipitates and (b) passing between widely spaced precipitates (Smallman 1970)

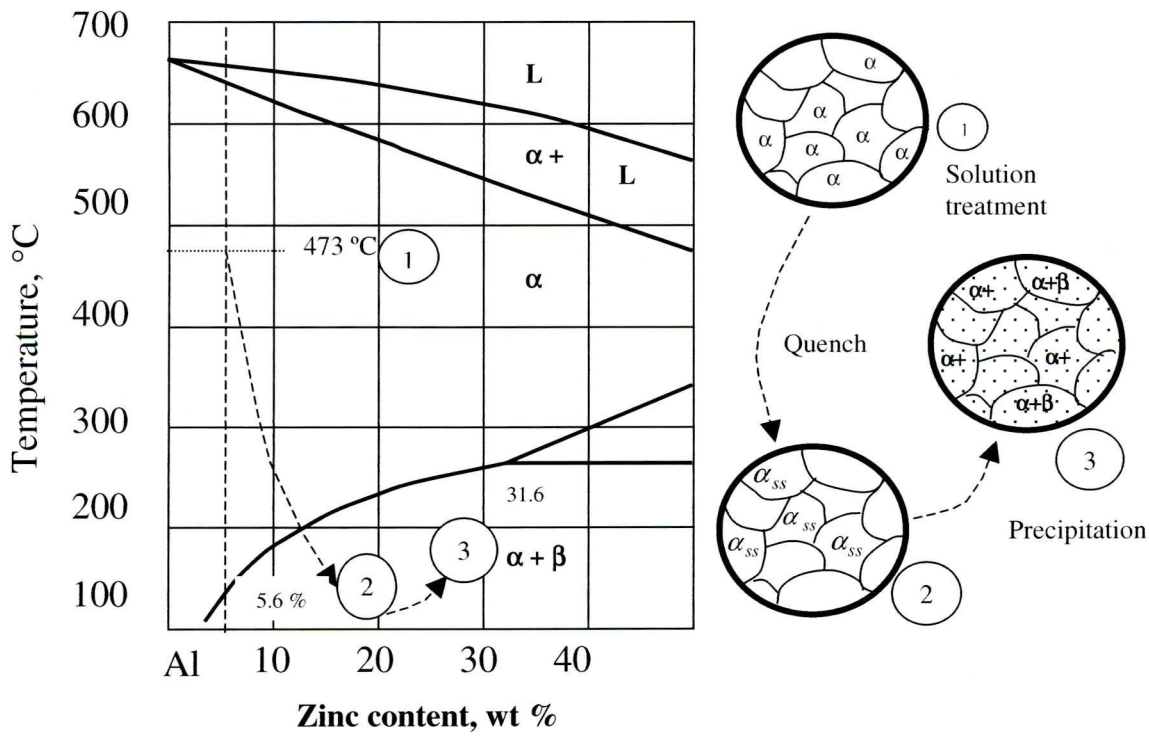

Fig. 2.2 Aluminium rich end of the phase diagram of the Al – Zn alloy system (Avner 1974)

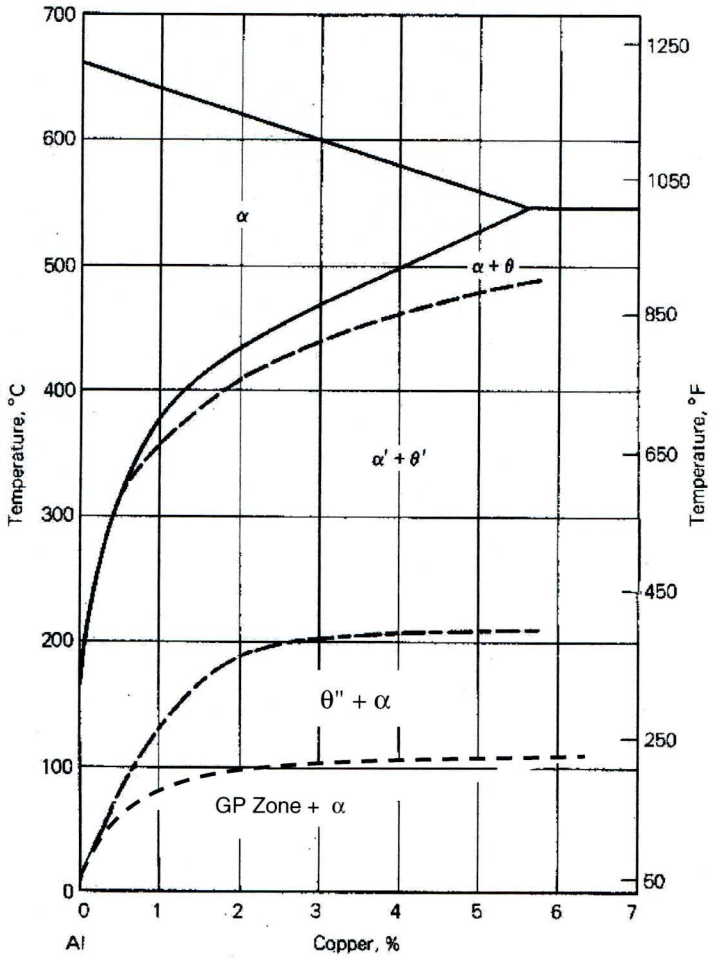

Fig. 2.3 Solubility curves for stable θ and meta-stable phases in Al-rich Al-Cu alloys (Dunn et al. 1984)

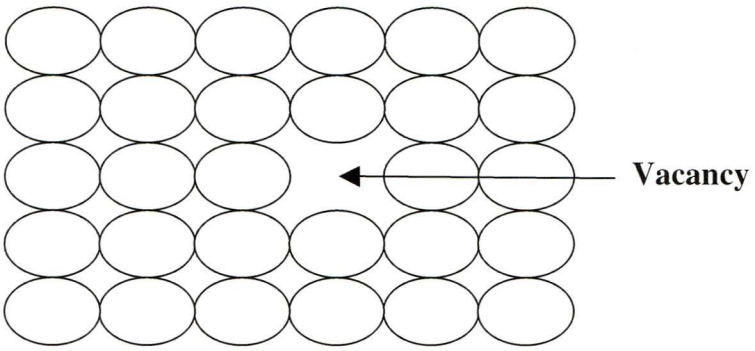

Fig. 2.4 Vacant site in a crystal lattice (Higgins 1993).

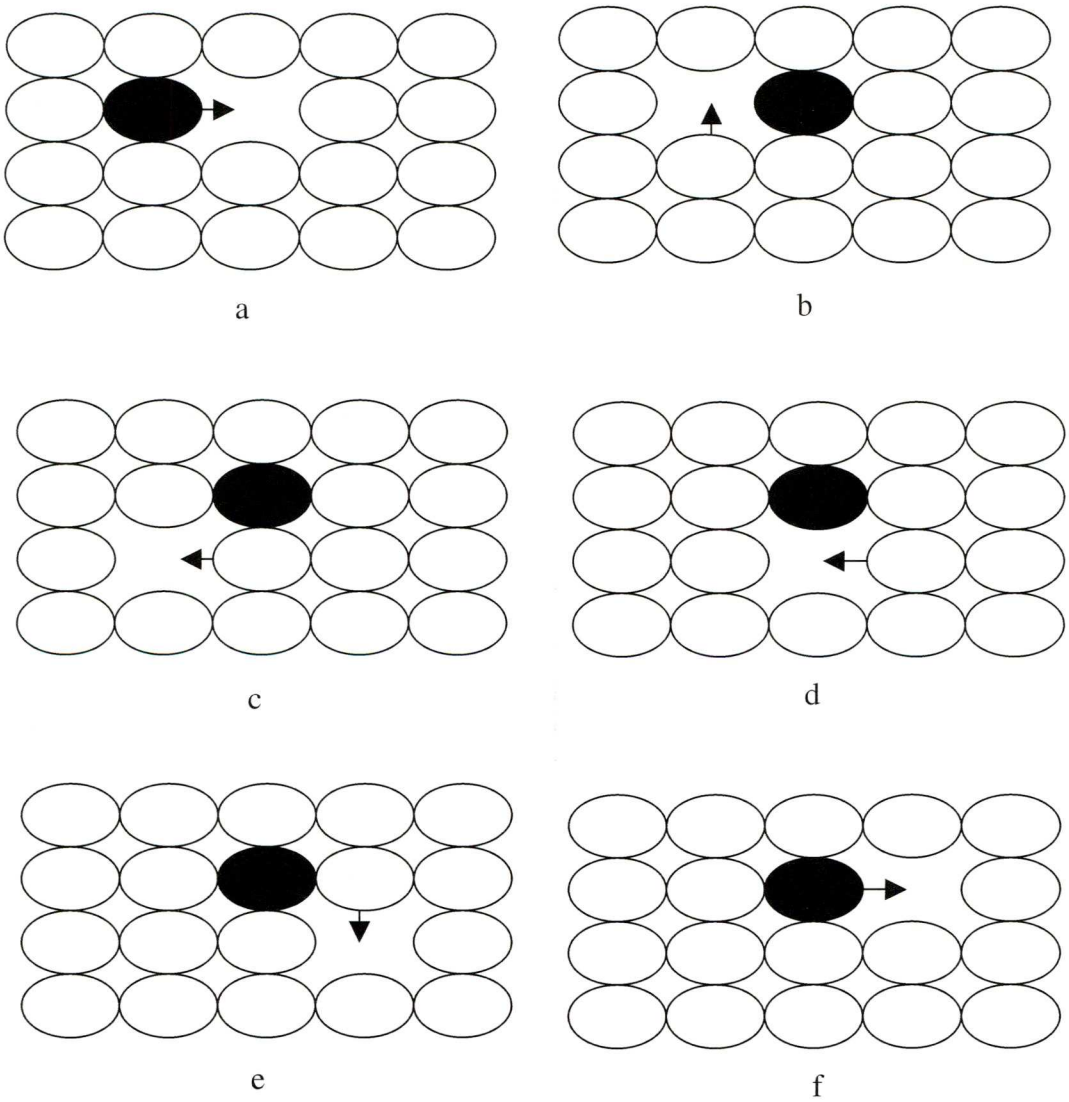

Fig. 2.5 The diffusion of a solute atom, which is associated with vacant sites (Higgins 1993).

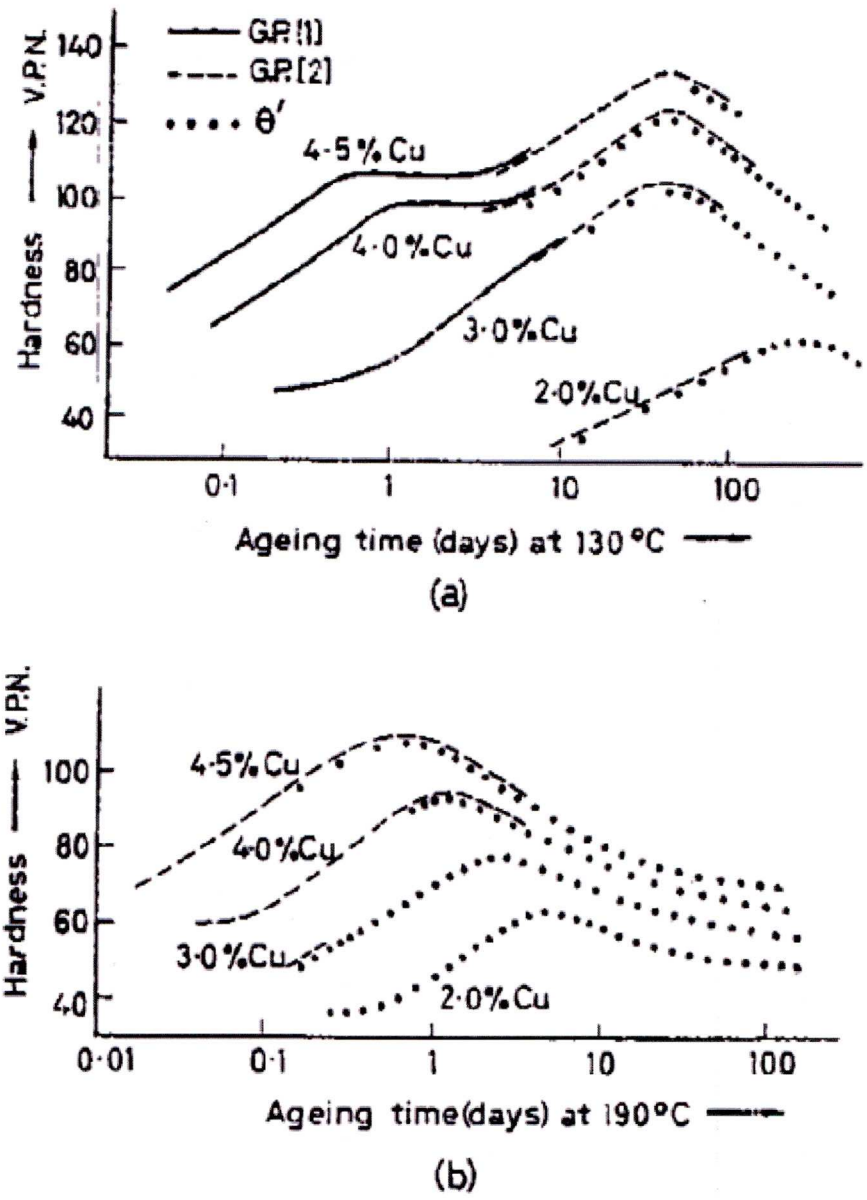

Fig. 2.6 Ageing of aluminium cupper alloys at
(a) 130°C and (b) 190°C (Smallman 1970)

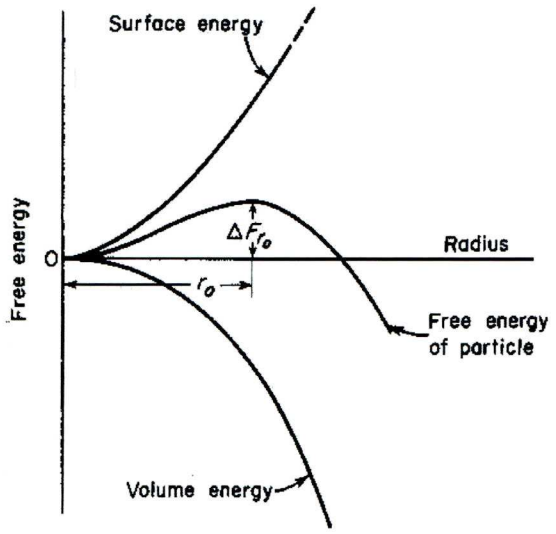

Fig. 2.7 Free energy of a precipitate as a function of its radius (Reed-Hill 1973)

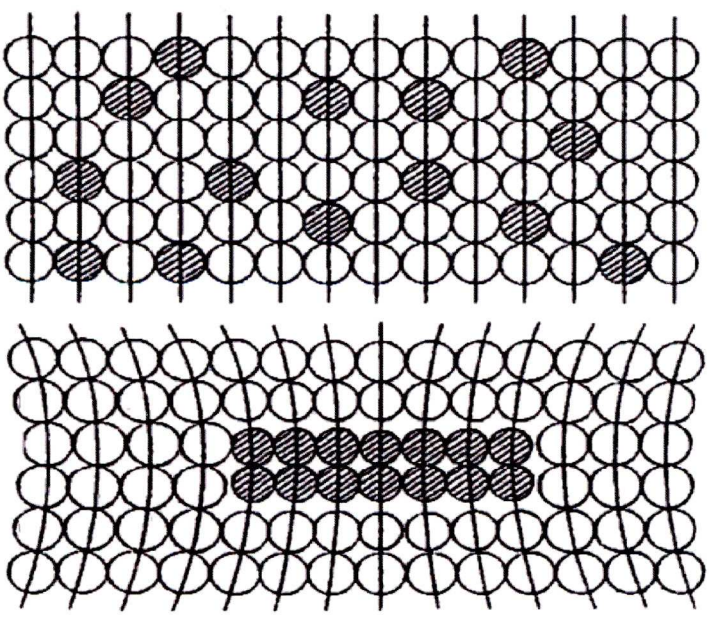

Fig. 2.8 Coherency. The upper figure represents a supersaturated solid solution of B atoms (dark circles) in a matrix of A atoms (light circles). The lower figure shows a coherent precipitate particle formed by the clustering of the B atoms (Reed-Hill 1973).

Chapter 3

Evolution and correlation of properties in age hardening of AA 7010

3.1 Introduction

The prediction of strength on many aluminium alloys has been researched for many years and by many investigators. More recently, the prediction of strength of aluminium alloys by modelling or by correlating it with measurements of hardness has been reported with exceptionally good results. For example, a quench factor analysis model has been applied successfully to predict the post-quench physical properties in aged aluminium alloys (Flynn and Robinson 2004). Furthermore, a model to predict the yield strength based mainly on micro-structural data, which could predict proof strength with an accuracy of 14 MPa, was reported (Starink and Wang 2003).

For Al-Cu-Mg alloys, an age hardening model was also developed to describe the evolution of strength and microstructure (Yan *et al.* 2004). The model was applied to fit and predict the yield strength data from the literature. The predictions were consistent with experiments for both natural and artificial ageing curves of AA 2024. Using an elasto-plastic self-consistent simulation model Solas (1996) showed that the yield stress calculated was in agreement with the experimental results. A difference of 40 MPa between the experimental and the predicted values was attributed to be a product of poor fit in the elastic-plastic transition domain.

Many other investigators have shown correlations of hardness with strength and of electrical conductivity with strength for many aluminium alloys, e.g., AA 7075 (Koch and Colijn 1979) and AA 2219 (Natan and Chihoski 1983). Undoubtedly the above modelling approaches to predict strength offer useful tools to assist in the improvement of ageing treatments of existing alloys or on the design of new alloys. The prediction of static strength for AA 7010 using non-destructive measurements of hardness and electrical conductivity becomes important when components made from this heat treatable aluminium alloy are inadvertently exposed to overheating. Earlier investigations showed that when AA 7010 is overheated from the T7651 temper condition, it exhibits decreases in electrical conductivity and hardness, indicating a loss of strength (Brown and Heaton 1984). At present, the prediction of strength from corresponding values of electrical conductivity and hardness is difficult due to lack of data available in the public domain.

The loss of strength indicated by lower electrical conductivity and hardness, after overheating or temperature increase, suggests that some of the strengthening alloying elements, initially precipitated by a controlled age hardening process, have been re-dissolved back into the solid solution. This suggestion is supported by the fact that alloying elements in solid solution depress the electrical conductivity to a greater extent than when they are out of solution (Morris *et al.*1984).

It is a well-known fact that the dissolution of coherent or semi coherent precipitates induces a loss of matrix strain and therefore a loss of strength. For the above reasons, the correlation of strength with hardness and electrical conductivity is essential to gain understanding of the degree of strength loss and thus to provide an accurate

assessment of the areas affected by overheating. The exploratory investigation in this thesis intends to address this shortfall and to gain an understanding of the metallurgical phenomena underlying the response of hardness and electrical conductivity to the age hardening process of AA 7010. It is envisaged that this data could be used to predict non-destructively the strength of AA 7010 and to obtain an approximation of the unknown thermal history of a given area of a component suspected of overheating.

The properties of hardness, electrical conductivity, UTS, PS and elongation of AA 7010 with different age hardening conditions were investigated in this chapter. The main aim is to determine non-destructively the strength of the alloy from values of electrical conductivity and hardness, and also to establish the approximate temper condition.

3.2 Experimental

3.2.1 Material

The investigation was carried out on AA 7010 - T7651 temper condition. The material was supplied by one of the aluminium suppliers to Airbus UK in the form of a plate. The chemical composition of the plate is listed in Table 3.1.

The plate was manufactured from a cast slab by rolling. The T7651 temper condition implies that the plate after rolling was solution heat treated (473 °C), control stretched between 1.5 to 3% (for stress relieving) and artificially aged to peak strength, followed by slight over ageing (120°C for 10 hrs and 172°C for 8 hrs) to improve fracture toughness and stress corrosion cracking properties.

In the T7651 temper condition, the alloy exhibits a high strength coupled with good fracture toughness and stress corrosion properties (Reynolds *et al.* 1976). In the civil aircraft industry, this aluminium alloy is mainly used for structural parts, such as spars and ribs of aircraft wings.

3.2.2 Test pieces

Flat dog-bone tensile test pieces (Fig. 3.1) were used in the investigation to correlate strength with non-destructive properties of electrical conductivity and hardness. The flat dog-bone tensile test pieces were machined to the dimensional requirements of British Standard BS 4A – 4 (196), with a width of 12.5 mm, a minimum parallel length of 71 mm, a gauge length of 50 mm, a minimum transition radius of 25 mm and a thickness of 3 mm.

Fig. 3.2 illustrates the plate under investigation and how it was cut to produce the required test pieces. The plate, which weighed 980 kg and was tapered along the length, had a length of 3403 mm, a width of 838 mm at its widest end and 482 mm at the other end, and a thickness of 157 mm. From this plate, a number of cross sectional or transverse slices (5.0 mm thick) were saw-cut as indicated in Fig. 3.2. Each of these 5 mm thick transverse slices was further cut into five strips and each strip represented a different depth across the plate thickness, with strip number 3 corresponding to the plate centre. Then each of the five strips was cut to make the dog-bone type test pieces as shown in Fig. 3.1.

3.2.3 Thermal treatment

3.2.3.1 Overview

The test pieces were all solution heat-treated and quenched using parameters recommended for AA 7010. The subsequent age hardening treatments were performed differently, in order to create a diversified range of ageing conditions. Solution heat treatment of the aluminium alloy, before the precipitation age hardening, was performed using a Caltherm electric air furnace. Fig. 3.3 shows the inside of the furnace with a typical setup of test piece distribution and thermocouple arrangement used to measure the temperatures and to calculate the ageing and quenching times.

The solution heat treatment operation consists of heating the alloy to a suitable temperature above the solvus, holding at that temperature long enough to allow alloying elements to enter into the solid solution, and then cooling rapidly enough to retain the elements in solution. After quenching, the alloy is in a supersaturated and unstable condition, which is the required pre-condition for precipitation age hardening (Avner 1974).

Precipitation age hardening was completed in two stages: the first stage was natural ageing at room temperature and the second stage was high temperature artificial ageing. Natural ageing in aluminium occurs due to spontaneous precipitation of alloying elements, such as Zn, Mg and Cu, from a supersaturated solid solution at room temperature, and no specific equipment was used on this ageing stage. Artificial age hardening was performed above room temperature using a Townson & Mercer electric air furnace. The arrangement of test pieces was similar to that shown

in Fig. 3.3.

Fig. 3.4 shows a schematic representation of the overall heat treatment procedure applied to the flat dog-bone test pieces. The applied treatments were solution heat treatment and quenching (stage A), natural ageing (stage B), artificial ageing (stage C) and over ageing (stage D).

3.2.3.2 Solution heat treatment and quenching

The solution heat treatment temperature and ageing time were chosen to be consistent with the requirements of AA 7010 (Airbus UK 2003). The solution heat treatment was performed at 473°C for 50 minutes as shown in Fig. 3.4, stage A. The test pieces were quenched in water at room temperature. To guarantee the required minimum ageing time the temperature of the test pieces was monitored with attached thermocouples as illustrated in Fig. 3.3. The ageing time started to be counted only when the temperature of test pieces attained 473°C. The quenching rate was calculated to be approximately 95°C / s. After quenching, all test pieces were immediately refrigerated at a temperature of −18°C to retard the onset of natural ageing.

3.2.3.3 Natural ageing

Some of the test pieces, which were already solution heat-treated, quenched and frozen, were taken from the freezer and allowed to be age hardened at room temperature. The test pieces were naturally age hardened at different time intervals before they were subjected to hardness, electrical conductivity and mechanical

testing.

For test pieces with natural age hardened condition, the testing was performed immediately after room temperature ageing. The ageing times ranged from 0.25 hrs to 16 days; a total number of 27 test pieces were treated in this manner. The remaining test pieces were all natural aged beyond the 16 days for conditioning at room temperature for future artificial age hardening.

3.2.3.4 Artificial age hardening

The remaining natural age hardened test pieces were artificially aged as indicated in Fig. 3.4, stage C. In a full cycle, the temperature was first increased to 120°C for 10 hours, and then increased to 172°C for 8 hours. In this investigation, the test pieces were artificially age hardened at different time intervals. At 120°C 22 test pieces were removed from the furnace at different times ranging from 8 minutes to 10 hours. At 172°C, a further 22 test pieces were removed from the furnace at different time intervals, ranging from 10 minutes to 8 hours.

3.2.3.5 Over ageing

Over ageing is a condition that develops during artificial ageing when the age hardening time and / or temperature exceed the parameters required to obtain the maximum peak strength. At a fixed ageing temperature, when the maximum strength has been attained, further artificial ageing will induce a decreased strength. This loss in strength is attributable to an over ageing effect.

As shown in Fig. 3.4, stage D, the over ageing conditions were obtained by prolonging the artificial ageing time up to 100 hours, at 172°C. During the over ageing stage, the remaining test pieces were removed from the furnace at various time intervals, ranging from 9 to 100 hours. A total of 28 test pieces were over aged under this condition.

3.2.4 Electrical conductivity testing

The electrical conductivity measurement is based on the eddy current method, which works on the electromagnetic induction principle. It involves the measurement of change in coil impedance in the same exciter coil placed over a material. The coil impedance changes when the exciter coil is placed on different materials, due to the change in electrical resistivity and magnetic permeability of the material over which the coil is placed.

The electrical conductivity measurements were carried out using a Forster SIGMATEST Ec 2.068 electrical conductivity meter. These measurements were performed in compliance with the Airbus UK process specifications (Airbus UK 2005).

All the test pieces were polished for electrical conductivity measurements prior to the heat treatments. The measurements were performed after completion of each individual precipitation age hardening treatment. On flat dog-bone tensile test pieces, the electrical conductivity measurements were performed immediately before hardness and tensile tests. The locations of measurements were on the centre of the parallel length, one side only.

In order to minimise any possible errors during the electrical conductivity measurements, the following actions were taken (Suhr and Guttinger 1993):

a) The electrical conductivity measurements were carried out at ambient temperatures. Because the change in ambient temperature influences the probe response and therefore the conductivity of the material being tested, the instrument was frequently re-calibrated against copper and nickel based reference blocks of known electrical conductivity values. This was done to compensate for any change in temperature within the laboratory environment. Although the standard procedure of the instrument requires re-calibration for any 5°C of temperature change, in this investigation to ensure best possible accuracy, re- calibration was in fact performed every time a 1°C temperature change was detected.

b) To avoid the influence of temperature increases on the probe caused by handling, an insulated handling probe was used and manual contact with the cable probe was avoided.

c) The surfaces for electrical conductivity measurements were machined flat to eliminate the effect of curvatures on the measurements.

d) The instrument was operated at 60 kHz, which means the eddy current penetration will not be deeper than 1.6 mm for the alloy under investigation (Mil-STD-1537B 1988). In order to avoid errors in the measurements, the thickness of the test pieces was chosen to be 3 mm or thicker.

There are other possible errors. However, they are negligible as described below:

a) The lift-off effect error during this investigation was negligible. Full contact

between the test piece flat surface and the probe was always maintained. For aluminium alloys with a conductivity range up to 51% IACS, the instrument used has a lift-off effect less than 0.19% IACS, on spacing between zero to 0.51 mm.

b) Since AA 7010 has a ferromagnetic impurity of 0.05% Fe, a theoretical electrical conductivity measurement error will be present. However, the error due to this effect will be constant throughout the investigation.

c) The edge and geometry effect can be ignored in this investigation. The instrument's probe (8 mm in diameter) was electro-magnetically screened with respect to the edges. The areas to be tested on test pieces were designed to be have a width of 12.5 mm.

3.2.5 Hardness testing

All the test pieces were polished for electrical conductivity and hardness measurements prior to the heat treatments. The measurements were performed after completion of each individual precipitation age hardening treatment. On flat dog-bone tensile test pieces, the hardness measurements were performed immediately before tensile tests. The locations of measurements were on the centre of the parallel length, one side only.

Hardness measurements were carried out using a Vickers HTM 8313 hardness tester, with a 5 kg load. The measurements were performed in compliance with Airbus UK process specification (Airbus UK 2004a, BS ES ISO 6507-1-2006). The hardness tester was constantly calibrated to British Standard EN ISO 6507-2 (2006) and checked on a weekly basis with reference standard blocks of known values, which

were also calibrated in accordance with British Standard EN ISO 6507-3 (2006). The standard blocks and the tester were certified with traceability to the National Physical Laboratory. A stage binocular microscope was used to measure the hardness indentation; the indentation results were converted into Vickers's hardness values using standard tables (BS ES ISO 6507-4-2006).

In order to minimise any possible errors during Vickers hardness testing, the following precautions were taken (BS EN ISO 6507-1- 2005):

(1) Prior to the start of the hardness measurements, the accuracy of the machine was verified using standard reference blocks.

(2) The test pieces were laid firmly on the support, so that no movement took place when the testing load was applied.

(3) The distance between the centre of the indentations produced and the edge of the test piece was considerably larger than the minimum specified (3 times the mean diagonal of the indentation for light alloys).

(4) The distance between the centre points of two adjacent indentations was larger than the recommended 6 times the mean diagonal of the indentation produced.

(5) The hardness tests were always carried out on a 1 μm surface finish.

(6) The difference between the horizontal and vertical readings of the diamond indentations was always guaranteed to be < 5%.

3.2.6 Tensile testing

Mechanical testing of standard flat dog bone tensile test pieces was performed using a Denison Mayes Group testing machine, model 6157. It works with a 100 KN servo-hydraulic load frame, and was fitted with an IBM stem/2 and a 50 mm–gauge-

length extensometer 7609 DC1/7902 DC2. The load cell and extensometers were calibrated annually to the requirements of British Standard EN ISO 7500-1, 2004. The tensile tests were carried out at a strain rate of 4 x 10^{-3} s^{-1} in compliance with test pieces and test methods for metallic materials (British Standard 4A- 4 1966). In order to minimise any possible errors during the tensile tests, the following precautions were taken:

(1) On the parallel portion of the tensile test pieces, 71 mm long, several gauge length marks of 50 mm were inscribed on each respective parallel portion, to ensure that the test piece fracture occurs between two gauge marks, so that accurate elongation values were guaranteed.

(2) The thickness and width of the test pieces were measured using a calibrated and certified electronic digital calliper to an accuracy of 0.01 mm.

(3) The fracture face of every test piece tested was examined with the aid of a magnifying glass, to detect any possible defects likely to influence premature failure.

3.3 Results

3.3.1 Response of electrical and mechanical properties to age hardening

The numerical data of electrical conductivity (EC), hardness, PS, UTS and percentage elongation, obtained for the various stages of age hardening (natural ageing, artificial ageing and over ageing) (Fig. 3.4) have been compiled in Tables 3.2, 3.3 and 3.4.

Fig. 3.5 shows the changes of the hardness and electrical conductivity during natural ageing from a supersaturated solid solution for AA 7010. The electrical conductivity

changed in a reciprocal manner to hardness with ageing time. In the initial stage of natural ageing (first 24 hrs from quenching) the electrical conductivity decreased dramatically (31. 56 to 28.78% IACS), while the hardness increased with similar response (78.8 to 124 Hv). In the remaining time (up to 386 hrs) of natural ageing, the electrical conductivity continued to decrease while the hardness increased. However, the change of properties was less pronounced than in the earlier stage of natural ageing, with electrical conductivity decreasing from 28.78 to 27.26% IACS and hardness increasing from 124 to 146 Hv. The variations of hardness and electrical conductivity with ageing time, during natural ageing, appear to obey a logarithmic relations and power law, with correlation coefficients of $R^2 = 0.9459$ for hardness and $R^2 = 0.8192$ for electrical conductivity.

Fig. 3.6 shows the changes of the hardness and electrical conductivity during artificial and over ageing for AA 7010, from the natural aged condition. In the artificial age hardening stage, the electrical conductivity increased progressively with temperature and ageing time. The increase of electrical conductivity during the under ageing stage (up to 10 hrs) was moderate (27.26 to 30.17% IACS). However, at the higher temperature of 172°C, the increase of the electrical conductivity with ageing time became more pronounced for the first 8 hrs (30.17 to 38.13% IACS). The electrical conductivity increased furthermore in the next 100 hrs at 172°C from 38.13 to 44.65% IACS. The hardness, on the other hand, when aged at 120°C, experienced a notable drop from 146 to approximately 120 Hv. Following this, it increased significantly up to the onset of over ageing, when a maximum hardness of 192 Hv was attained. During the latter stage of over ageing at 172°C, the hardness dropped to 120.6 Hv.

3.3.2 Electrical conductivity and hardness

Fig. 3.7 shows the overall response of hardness and electrical conductivity to the age hardening process of AA 7010, from a supersaturated solid solution. In this graph, the hardness and electrical conductivity vary progressively with natural ageing, artificial ageing and over ageing.

In the region of natural ageing and over ageing conditions (Fig. 3.7) electrical conductivity and hardness showed a reciprocal effect, i.e. an increase in one resulted in a decrease in the other and vice versa. Although the natural and over ageing treatments resulted in a nearly linear correlation, the overall relationship between hardness and electrical conductivity is not linear. It is therefore impossible for either of these variables to be predicted from one another without the consideration of further information.

During natural age hardening at room temperature, the hardness increased from 78.8 to 146 Hv. Simultaneously, the electrical conductivity showed a decreasing trend from 31.5 to 27.26% IACS. During the artificial age hardening, overall, the hardness further increased from 146 to 192 Hv. However, with the onset of over ageing it decreased from 192 to 120 Hv. During artificial and over ageing, the electrical conductivity experienced a reversal reaction to that observed in natural ageing. In these ageing regions, conductivity increased from 27.26 to 44.65% IACS.

The reciprocal effect of electrical conductivity and hardness observed in the natural and over ageing conditions was not evident in the artificial age hardening region. Instead an overall increasing trend for both hardness and electrical conductivity was

registered.

In the initial stage of artificial ageing at 120°C (Figs. 3.6 and 3.7) there is a decrease in hardness from 146 to 120 Hv and an increase in electrical conductivity. This effect, which has been termed reversion, has been observed in many other aluminium alloys (Riontino and Abis 1991, Ferragut *et al.* 1996).

3.3.3 Electrical conductivity and strength

Figs. 3.8 shows correlations of electrical conductivity with UTS and PS. Strong similarities exist between the correlations of electrical conductivity with hardness (Fig. 3.7) and with strength (Fig. 3.8).

Fig. 3.8 presents a non-linear correlation of strength with electrical conductivity up to a value of approximately 35.9 % IACS, where the onset of over ageing condition appears to commence with the start of a near linear correlation. For electrical conductivity above this value, the PS shows a regression value of $R^2 = 0.9392$.

Figs. 3.9 shows a non-linear correlation of electrical conductivity with the strength ratio of PS / UTS. This correlation is non-linear up to an approximate value of 35.9% IACS, where the onset of over ageing condition commences with the start of a near linear correlation. Strong similarities exist between the correlations of electrical conductivity with hardness (Fig. 3.7) with strength (Fig. 3.8) and with strength ratio (Fig. 3.9).

3.3.4 Hardness and strength

Fig. 3.10 shows the correlation of hardness with strength for all three temper-conditions, i.e. natural ageing, artificial ageing and over ageing. The graph shows a linear relationship of hardness with UTS, with a correlation coefficient R^2 of 0.9765, suggesting a good correlation. On the other hand, the correlation of PS with hardness gives a lower R^2 of 0.8983, indicating a more pronounced scattering of proof strength values. Fig. 3.10 also shows different gradients of PS and UTS, i.e. 3.7162 and 2.4664 respectively, indicating a difference response of these properties to the age hardening process.

Fig. 3.11 shows the variation of hardness with strength ratio (PS/UTS). For a given value of hardness, the strength ratio can be different for different ageing conditions of natural ageing, artificial ageing and over ageing. For the same hardness, the over ageing conditions gave a higher strength ratio than the natural and artificial ageing conditions. The different strength ratios for the same hardness, appears to be inherent of the strain hardening response of the test pieces in tensile tests.

3.3.5 Hardness and elongation

Fig. 3.12 shows the relationship between hardness and elongation. In the natural ageing and artificial ageing conditions, the elongation decreased with increasing hardness. At the onset of the over ageing condition, the hardness started and continued to decrease and the elongation began to show some recovery during the over ageing stage. However, the elongation remained at a lower level indicating a loss of ductility.

3.4 Discussions

3.4.1 Response of electrical conductivity and hardness to age hardening

It is well documented that hardness and electrical conductivity are sensitive to the ageing process. The response of these properties to the variation of temperature and time can be interpreted as their dependence on the structural changes of the matrix with the age hardening process. The precipitates and their strain fields influence the electrical conductivity and hardness by scattering the conducting electrons and offering obstacles to the motion of dislocations. Therefore, the variation of hardness and electrical conductivity could be directly attributed to precipitation of different precipitates, their volume fraction and the purification effect of the matrix.

The decrease in electrical conductivity during natural ageing from the supersaturated solid solutions, as indicated in Fig 3.5, is common to other aluminium alloy systems (Kelly and Nicholson 1963) and has been associated with the formation of very small solute clusters and the GP zones (Rossister 1976, Hillel and Rossister 1981).
The relatively fast response of hardness and electrical conductivity to the ageing process at low temperature during natural ageing (Fig 3.5) is a direct consequence from fast diffusion rates of solute atoms, aided by a high concentrations of solute atoms and quenching vacancies. In this work, it appears that the diffusion rate has been enhanced by the fast speed of quenching (less than 95°C / seconds) from solution heat treatment temperature (Fig. 3.4), which generated a higher concentration of solute atoms and an increase in the number of vacancies available for natural ageing. This view is supported by the fact that a rapid quenching of heat treatable aluminium alloys from the solution heat treatment temperatures leads to high vacancy concentrations in the as quenched materials (Kelly and Nicholson

1963, Federighi and Cotterill 1965). The excess of vacancy concentration was reported to play an important role in the enhanced diffusion coefficients, which lead to significant clustering to occur, at room temperature, in aluminium alloys (Kelly and Nicholson 1963). There is also strong evidence suggesting the importance of binding between solute atoms and vacancies during the formation of clusters and GP zones (Federighi and Thomas 1962, Löffler 1995). Furthermore it has been reported that, GP zone formation in aluminium alloys at low temperature occurs at rates of seven to eight orders of magnitude greater than expected from extrapolation of high temperature diffusion data, because of the presence of these quenched-in vacancies (Bergner 1995, Staley *et al.*1984).

It has been well documented that the factors affecting diffusion in metals are solute concentration, activation energy, temperature, vacancies and time with the diffusion coefficient, D, expressed as in equation 2.4, chapter 2:

$$D = D_0 e^{-Q/RT}$$

where D_0 is the pre-exponential factor, Q is the activation energy, R is the gas constant and T is the temperature (Reed-Hill 1973). The diffusion of the solute atoms and the formation of precipitates are mainly influenced by the ageing temperature. The concentration of solute atoms and vacancies also play an important role on the diffusion rate, especially at room temperature. Fig. 3.5 and Fig. 3.6 show a significant change in hardness and electrical conductivity in the early stages of ageing at room temperature and when the temperature was increased from room temperature to 120 °C respectively, this is believed to be due to a fast diffusion rate

aided by high concentrations of solute atoms and vacancies. However, when the temperature was increased from 120 °C to 172 °C, at the early stages of ageing, a moderate change in hard and electrical conductivity was observed, Fig. 3.6. This suggests that, the concentration of solute atoms and vacancies, at this ageing stage, has considerably decreased with ageing time and temperature, reducing the diffusion rate.

The increase of electrical conductivity with increasing temperature (room temperature → 120°C→ 172°C), Fig.3.6, is believed to be associated with the purification effect of the matrix and the decrease in the number density of the new precipitates formed. This view is supported by the well established Matthiessen's law and by reports on AA 6111 which showed that: (a) the number density of precipitates is inversely related to the precipitate spacing (Esmaeili 2007), (b) during the late stages of aging at high temperatures, there was an inverse correlation between the precipitate spacing and its contribution to resistivity (Raeisinia 2006).

3.4.2 Natural age hardening

3.4.2.1 Electrical conductivity

The electrical conductivity, which is a measure of the ability of a material to conduct electrical current (Sigli *et al.* 2007), is reduced by the addition of alloying elements. The presence of these elements in solid solution depresses the electrical conductivity to a greater extent than when out of solution (Morris *et al.*1984). The electrical conductivity is therefore largely determined by the content of alloying elements in the solid solution and the amount and nature of the precipitates formed during the manufacturing and thermal processes.

Since the electrical conductivity of a material is the reciprocal of its electrical resistance, the steady decrease of electrical conductivity during room temperature age hardening (Figs. 3.5 and3.7) can be explained in terms of a progressive increase of electrical resistance of the aluminium alloy. This resistance increase, in solution heat-treated aluminium alloys from a supersaturated solid solution, has been attributed by many investigators to gradual increase in the number and size of very fine and coherent precipitates and GP zones. It is well documented that the GP zones are very effective in scattering electrons, leading to the decrease in the electrical conductivity of the matrix (Matthew *et al.* 1994). The electron scattering effect is induced by the coherent strains associated with the G.P. zone precipitates (Martin 1998).

During room temperature age hardening of AA 7010, the diffusion of solute atoms from the solid solution, to form the GP zone precipitates, will cause a purification effect of the matrix, leading to an increase of electrical conductivity. However, the net decrease in electrical conductivity (31.5 to 27.26 % IACS) observed on the natural ageing region (Figs. 3.5 and 3.7) is attributed to the electron scattering effect of the GP zones being more predominant than the purification effect.

3.4.2.2 Hardness

It is well documented that, the hardening mechanism which operates in a given aluminium alloy will depend on the type of particles precipitated (e.g. whether G.P. zone, intermediate meta-stable precipitate or a stable phase), the magnitude of the strain around the particles and the temperature of testing.

In the natural ageing region (Figs. 3.5 and 3.7) the existence of a decreasing trend of electrical conductivity suggests that the precipitates formed are of the GP zone type, which are coherent with the matrix by creating coherent strain field. This implies that during natural ageing, the alloy under investigation has become harder by both the internal strain hardening and the chemical hardening mechanisms. This hypothesis is supported by the fact that, in the early stage of ageing, there is evidence that the coherent zones are cut by dislocations moving through the matrix (Polmear 1995).

The internal strain-hardening mechanism is based on the fact that precipitation of the coherent particles having a slight misfit in the matrix gives rise to internal stress fields, which hinder the movement of gliding dislocations (Smallman 1970, Rollason 1973, Polmear 1995). On the other hand, the chemical hardening mechanism contributes to the increase of hardness or strength by providing a short-range interaction between dislocation and precipitates (Polmear 1995, Smallman 1970).

However, it has been reported that, in alloys such as Al – Zn, the zones possess no strain field and the flow stress would be entirely governed by the chemical hardening effect (Smallman 1970). Although Zn (6.3% nominal) is the main alloying element of AA 7010, the alloy also possesses a nominal copper content of 1.75%. The electrical conductivity decrease at room temperature indicates that, the precipitates formed at room temperature contained G.P. zones with strain fields. The increasing trend of hardness at room temperature from 78 to 146 Hv (Figs. 3.5 and 3.7) can be summarised as the product of a progressive increase of internal stresses due to strain fields around the GP zones and the precipitates themselves, which hinder the movement of gliding dislocations (Polmear 1995, Rollason 1973).

The contribution of coherence strain hardening and chemical hardening to the overall hardness and strength depends on the number and spacing of the zones or precipitates, and also on the degree of strain produced by them (Marshall *et al.* 2007). As the GP zones nucleate and grow an increase in hardness and strength is expected. The maximum coherency strain hardening and therefore the maximum hindrance to the dislocation motion is to be expected when the spacing between the particles is equal to the limiting radius of curvature of moving dislocation lines, i.e. about 50 atomic spacing or 10 nm. At this stage, the dominant precipitate in most alloys is the coherent GP zone (Polmear 1995).

3.4.3 Artificial age hardening

3.4.3.1 Reversion effect

The temporary decrease in hardness from 146 to 120 Hv and the increase in electrical conductivity detected at the beginning of the artificial ageing stage at 120°C (Figs 3.6 and 3.7) are believed to be inherent from a reversion effect or retrogression. The reversion effect has been a commonly observed phenomenon in age hardened aluminium alloys. A number of early investigations to the reversion in aluminium (Smallman 1970, Rollason 1973) have shown that reversion occurs when the GP zones, which have precipitated at room temperature, partially re-dissolve back into the matrix at higher ageing temperature, making the alloy softer. On prolonged heating at the artificial ageing temperature, the alloy becomes harder again. For AA 7010 under investigation reversion is expected to occur on those nuclei or zones, which are very small and unstable when the ageing temperature is raised to 120°C. From a free energy point of view, the particles with radii smaller than the critical radius tend to re-dissolve back into the solid solution. A consequence of this is that

the strains associated with the coherency of the precipitate are reduced or lost. With further heating new phases, that are less coherent or non-coherent, form. This point of view is consistent with the fact that multiple precipitate structures are observed in AA 7010 (Godard 2002).

In this investigation, when the GP zones re-dissolve back into the matrix, the expected decrease in electrical conductivity, due to the increase in solute content of the matrix, appears to have been offset by the removal of the particle coherency strain.

Recent studies also reported the reversion effect in AA 7075 and Al-Cu alloys. Studied using hardness, positron lifetime and transmission electron microscopy on AA 7075 showed that GP zones dissolve during the initial stage of artificial age hardening (Ferragut *et al.*1996). A drop in hardness and a decrease in the positron lifetime were associated with the dissolution of GP zones. With further age hardening, the hardness and positron lifetime increased with the appearance and grow of new precipitates. The dissolution of the coherent structure in the Al-Cu alloys was also studied using differential scanning calorimetric (DSC) and scanning electrical resistivity techniques (Riontino and Abis 1991). The dissolution of the coherent structure was detected by DSC technique. The net result of resistivity change was explained by considering the contribution of the matrix and the decrease of the scattering on the conducting electrons, due to the removal of strain fields associated with dissolved precipitates.

3.4.3.2 Hardness and electrical conductivity

For the alloy under investigation, the overall increase of hardness and electrical conductivity in the artificial ageing region (Figs. 3.6 and 3.7) can be attributed to the formation of the coherent and semi-coherent precipitates and their intermediate meta-stable precipitates.

The hardness is mainly dependent on the amount of coherent and semi-coherent precipitates formed in the alloy; the higher the volume fraction of the new precipitates formed the higher hardness attained. The increasing trend of hardness from 146 to 192 Hv (Figs. 3.6 and 3.7) can therefore be summarised as the product of a progressive increase of internal stresses due to strain fields around the coherent precipitates and the precipitates themselves, which hinder the movement of gliding dislocations. The hardening mechanism most likely to be active in this alloy, for artificial aged samples, is expected to be a combination of the coherency strain and the chemical hardening mechanisms. The continuous increase of electrical conductivity with ageing suggests that, during the progress of artificial ageing, the chemical hardening mechanism is likely to become more predominant than the coherency strain hardening mechanism.

The maximum hardness or strength attained, consistent with the fully aged condition, can be found within a wide range of electrical conductivity values, that is between 32 to 36.5% IACS (Figs. 3.7 and 3.8). This clearly suggests that, if this alloy was to be heat treated to peak hardness at ageing temperature of 120°C for 10 hours followed by 172°C, the ageing time for the second ageing temperature could exist within a wide tolerance range.

The increase of electrical conductivity registered during the artificial ageing stage is considered to be the contribution of two effects: the purification effect of solute elements from the solid solution and the effect of formation of a new precipitate which gradually becomes less effective in scattering the conducting electrons. The purification effect arises when the alloying elements such as Zn, Mg and Cu diffuse out from the solid solution to form the precipitate. The result is an increase in the electrical conductivity due to a more pure matrix. The precipitates formed at artificial ageing temperatures have been reported to be coarser (transition phase η') than the room temperature precipitate (Ferragut *et al.* 1998) and less effective in scattering the electrons than the GP zones (Raesignia 2006). The hardness plateau attained before the onset of over ageing (Fig. 3.7) can be understood in terms of the net result of two age hardening mechanisms with opposing effects on hardness. The continuous nucleation and growth of new particles ensure the presence of either the coherence strain mechanism or chemical hardening mechanism or both, which increase the hardness. On the other hand, the over ageing of large precipitated particles has been related to the dispersion hardening mechanism, by which continuous growth of precipitates lowers the hardness. Since the continuous growth of both large and small particles has different effects on hardness, the effect of these opposing ageing mechanisms must be balanced on the plateau region. With prolonged artificial ageing, the over ageing mechanism becomes predominant and the hardness starts to drop. This is due to the fact that the loss of coherence between the large particles and the matrix is more predominant than the coherency produced by the new precipitated particles.

3.4.4 Over ageing

The progressive decrease in hardness (192 to 120 Hv) and the continuous increase in electrical conductivity (36.5 to 44.65% IACS) observed in the over ageing region (Fig. 3.7) are due to the formation of incoherent precipitates. The beginning of the hardness drop trend is in agreement with the generally accepted concept that the over-ageing of aluminium alloys starts when the intermediate or fully formed precipitate begins to become incoherent with the matrix and the internal lattice strains are lost. It has been well documented (Matthew *et al.* 1994) that on prolonged heating at ageing temperatures, precipitation hardening leads to over-ageing, when the precipitates increase in size, become less numerous and lose coherency with the matrix.

Within the over ageing region (Fig.3.7) the inversely proportional correlation between hardness and electrical conductivity is in agreement with the works reported by Raesignia (2006) and Orowan (1948), which showed direct correlation of the precipitate particle spacing and electrical resistivity (Raesignia 2006) and a direct correlation between the precipitate particle spacing and the flow stress (Orowan 1948). Orowan (1948) demonstrates that, when moving dislocations by-pass the precipitates by the bowing mechanism, the yield stress, which is the stress necessary to expand a loop of dislocation between the precipitates, is inversely proportional to the particle separation. This clearly infers that the flow stress decreases as the distance between the precipitates increases. Therefore, the dispersion hardening mechanism accounts for the over-aged condition on this alloy. This view is further supported by the fact that, when the precipitates become incoherent with the matrix and dislocations are no longer able to cut trough them, the dispersion hardening

mechanism becomes predominant over the chemical hardening mechanism (Marshall *et al.* 2007). In this case, the dislocations by-pass the precipitate by either bowing, climbing or cross slip.

Furthermore, recently reported studies for AA 6111 (Raesignia 2006) showed that the precipitates formed during high ageing temperatures (350 – 560°C) have insignificant contribution to the resistivity. However, at lower temperatures, the effect of precipitates must be taken into account. Raesignia (2006) proposed a modified Matthiessen's law, which included the resistivity contribution due to the scattering by the precipitates:

$$\rho = \rho_{pure}(T) + \Sigma \rho_i C_i + \rho_{ppt} \qquad (3.1)$$

where ρ is overall resistivity, $\rho_{pure}(T)$ is the temperature dependent resistivity, ρ_i is the resistivity specific of the ith solute, C_i is the concentration of the solute and ρ_{ppt} is the resistivity contribution due to the scattering of the precipitate. Raesignia (2006) showed that the contribution of resistivity from the precipitates does decrease as the precipitate spacing increases.

Therefore, the inversely proportional correlation between hardness and electrical conductivity in the over ageing region (Fig. 3.7) can be interpreted as a direct correlation between the precipitate particle spacing with hardness and electrical resistivity.

When the precipitation has reached an equilibrium, the over ageing treatment is

completed. Further precipitation of alloying elements from the solid solution is not possible and the final equilibrium precipitate structure η ($MgZn_2$) is attained. With prolonged heating the larger precipitated particles continue to grow at the expense of the smaller ones (Reed – Hill 1991). However, the hardness and electrical conductivity values attained for the most extreme case of over ageing 120 Hv and 44.65% IACS (Fig. 3.7) suggest that the equilibrium state has not been fully attained.

3.4.5 Strength correlations

The overall lack of a linear correlation of strength with electrical conductivity (Figs. 3.8 and 3.9) is mainly due to the different nature of precipitates (GP zones, coherent and semi-coherent precipitates) formed during the age hardening process. Due to the presence of these precipitates, the electrical conductivity and strength responded with different and some times contradicting trends. In two out of three age hardening stages, each property showed opposing effects during age hardening. During natural ageing the strength increased and the electrical conductivity decreased; during artificial ageing both properties increased; and during over ageing the strength decreased and conductivity increased.

The observed increasing trend of strength and the decreasing trend of electrical conductivity in the room temperature age hardening stage (Fig. 3.8) can be explained by the gradual increase of the volume fraction of the GP zones. As the volume fraction of the coherent precipitate increases, the degree of the strained matrix also gradually increases, resulting in a progressive increase of resistances to the motion of dislocation and to the electron flow.

In the artificial age region (Fig. 3.8), the precipitates formed are expected to be larger and less coherent with the matrix than those formed at room temperature. The continued increase of strength in this region is most likely due to the new precipitates being larger and still coherent with the matrix, which have a more effective chemical hardening mechanism and maintain a further contribution from the strain hardening mechanism. The moderate increase of electrical conductivity, between the ends of room temperature ageing to peak strength, appears to be due to a nearly balanced opposing effects of the electron scattering of the strained matrix and the purification of the matrix on electrical conductivity. The purification effect of the matrix appears to be slightly predominant over the scattering effect of the strained matrix.

The constant high strength maintained with a continued increasing trend of the electrical conductivity (the plateau effect observed in Figs. 3.8 and 3.9) in the artificial ageing region is due to a balanced effect of the strength hardening mechanism in operation. In this region, it appears that the dispersion hardening mechanism, which infers a loss of strength due to some over ageing, negates the beneficial effects on strength of the chemical hardening mechanism. In the over ageing stage (Fig. 3.8 and 3.9), the strength decreased and the electrical conductivity continued increasing. The decrease in strength can be explained by the onset of over ageing. In this ageing stage, the dispersion hardening or the Orowan strengthening is the predominant hardening mechanism. This view is supported by the fact that, when the dispersion hardening mechanism is in operation, the flow stress is inversely proportional to the spacing between the precipitates (Orowan 1948).

The continued electrical conductivity increase is inherent from the loss of coherency of the precipitate with the matrix and a continued purification effect of the matrix. Non-coherent precipitates do not significantly affect the electrical conductivity (Raesignia 2006).

The overall non-linear correlations of electrical conductivity with hardness and with strength (Figs. 3.7, 3.8 and 3.9) are the result of the different responses of electrical conductivity and hardness to the precipitation age hardening process. However, the over ageing region showed an inversely proportional correlation between hardness and electrical conductivity (Fig. 3.7) and between strength and electrical conductivity (Figs. 3.8 and 3.9). The correlations appear to be the consequence of the inverse relationship between the precipitate particle spacing with electrical resistivity (Raesignia 2006) and the precipitate particle spacing with strength (Orowan 1948) respectively.

3.4.6 Strength prediction

The difference in gradients of the strength-hardness correlations (Fig. 3.10) indicates that the PS is more responsive to the age hardening process than the UTS. Therefore, as the alloy age hardens with time and temperature, the gap between 0.2 % PS and UTS decreases and the strength ratio (PS / UTS) increases with increasing hardness (Fig. 3.11). The pronounced gradient of PS, in comparison with that of UTS, appears to be influenced by the strain hardening characteristics of the alloy. This view is supported by the simultaneously loss of ductility observed (Fig. 3.12) where the percentage elongation of the alloy simultaneously decreases with the age hardening process. The abilities of the alloy to strain harden is reduced during the age

hardening process, since the strain hardening is related to the ductility and strain hardening exponent (Riggs *et al.* 1984).

The good liner relationship between UTS and hardness (Fig. 3.10) as indicated by the high regression R^2 value of 0.9765, suggests that the prediction of UTS from a given hardness value can be made with a reasonable degree of accuracy. On the other hand, the prediction of PS is less accurate due to a lower R^2 value (0.8983). Other investigators have reported similar correlation of yield strength with hardness, for example, for AA 7075 (Koch and Colijn 1979), AA 2090 and binary Al 2.2% Li alloy (Brasche *et al.* 1989), for AA 2219 (Natan and Chihoski 1983). For Al-7 wt% Si alloys with different levels of Mg, the strength-hardness relationship, on both yield and tensile strengths, changes linearly with Mayer hardness (Tiryakioglu *et al.* 2000).

The lack of accuracy in predicting 0.2 % PS from hardness values, in comparison to the prediction of UTS, appears to be a result of different ductility or strain hardening characteristics between test pieces with the same hardness. This assumption is based on observations made from Figs. 3.11 and 3.12. From Fig. 3.11 it can be seen that for the same hardness the strength ratio can be different. The over ageing conditions gave higher values of strength ratio than the under-aged conditions. Fig. 3.12 shows that for a similar hardness a different ductility can be obtained depending on the ageing condition of the test pieces.

However, the accuracy in predicting the PS can be improved by assessing the hardness and electrical conductivity simultaneously. Specifically, the age condition

can be determined by examining both the hardness and electrical conductivity values from Fig. 3.7. With the established ageing condition, the UTS and the strength ratio for the corresponding age condition the PS can be determined with better degree of accuracy for any given hardness value. Furthermore, the PS can also be determined from the electrical conductivity-strength ratio correlation (Figs. 3.9) or from the PS – EC correlation (Fig. 3.8b) for any ageing condition with electrical conductivity value greater than 35.9% IACS. For example, in the over ageing region (Fig. 3.8b) the regression value R^2 is 0.9392.

During this investigation, before the re-heat treatments commenced, a lack of property uniformity was noticed on test pieces from different plate thicknesses. A notable difference in electrical conductivity and hardness was observed between test pieces in the as received heat treatment condition. The inhomogeneity across plate thickness will be studied in Chapter 4.

The findings from the correlation of hardness with strength for AA 7010 should not be extrapolated to other aluminium alloys. Each alloy should be assessed on its own merit, as non-consistency between different alloys is possible.

3.5 Summary

In the present work, electrical conductivity and hardness measurements were combined to evaluate the age hardening phenomena in AA 7010.

The properties are sensitive to processing parameters such as temperature and ageing time. When ageing conditions are changed, differences in hardness and electrical conductivity are detected.

The response of hardness and electrical conductivity to the age hardening process for AA 7010 can be interpreted as their dependence on the structural changes of the matrix. The precipitates formed and their strain fields influence the electrical conductivity and hardness by scattering the conducting electrons and offering obstacles to the motion of dislocation. The variation of hardness and electrical conductivity could be directly attributed to the formation of different precipitates, their volume fractions and the purification effect of the matrix.

The formation of the precipitate is mainly dependent upon the diffusion and precipitation rate, which in turn depends mainly on temperature. The fast speed of quenching before natural ageing enhances the diffusion rate because of the inherent high concentration of both solute atoms and vacancies retained in the matrix. This was evidenced by the dramatic speed of response of hardness and electrical conductivity to the age hardening process during the initial stage of natural ageing. For the full range of ageing conditions, there is an overall non-linear correlation of electrical conductivity with hardness (Fig. 3.7) and with strength (Figs. 3.8 and 3.9). It is possible to have two different hardness and strength values for the same electrical conductivity value, or vice versa. Therefore, the prediction of strength or hardness from electrical conductivity value alone is not possible. However, the over ageing region of Figs. 3.7, 3.8 and 3.9 showed an inversely proportional correlation between electrical conductivity with hardness or strength. Therefore, the hardness or strength can be determined with reasonable accuracy on AA 7010 for any electrical conductivity value beyond 35.9% IACS.

For the full range of age hardening, a linear correlation was established between the strength and hardness of AA 7010, where the strength can be predicted with a reasonable accuracy. The linear relationship of hardness with UTS gave a correlation coefficient R^2 of 0.9765, suggesting a good correlation. On the other hand, the correlation of PS with hardness gives a lower R^2 of 0.8983, indicating a more pronounced scattering. However, when the hardness and conductivity properties are assessed in combination, they can provide the initial step to non-destructively predict the PS with an improved accuracy for any age condition for AA 7010.

Table 3.1 Chemical composition of AA 7010

Chemical elements	Zn	Mg	Cu	Zr	Fe	Si	Ti	Ni	Mn	Cr
Nominal Wt %	6.30	2.34	1.75	0.12	0.05	0.04	0.03	0.01	0.00	0.00
Minimum Wt %	5.7	2.1	1.5	0.10	-	-	-	-	-	-
Maximum Wt %	6.7	2.6	2.0	0.16	0.15	0.12	0.06	0.05	0.10	0.05

Table 3.2 Properties of specimens after solution heat treatment at 473°C for 50 minutes, quenched in water (>95°C/s) and naturally aged at different times

Test Piece ID	Ageing Time (hrs)	EC (%IACS)	Hardness (HV)	0.2% PS (MPa)	UTS (MPa)	Elongation (%)
1A	0.25	31.56	78.8	104	303	
1B	0.5	31.24	86.7		307	31.2
2A	1.25	30.86	88.9	107	327	31
2B	1.5	30.74	91.1		334	32
3A	2	30.5	92.3	95.5	323	30
3B	3.25	29.4	104	133	361	30.5
4A	4.5	29.28	101	169	357	28
4B	5.25	28.76	104	222	374	31
5A	6	28.79	102	221	368	
5B	7	28.74	113	224	373	30
6A	8	28.54	111	230	376	28
6B	9	28.33	111	244	399	28
7A	11	28.19	115	258	408	26
7B	13	28.03	118	254	409	27
8A	16	29.86	107	240	389	25
8B	18	27.88	118	252	403	27
9A	20	29.74	106	248	402	24
9B	24	27.88	124	276	431	30
10A	33	27.68	131	270	418	29.5
10B	46	27.52	130	291	446	28
11A	63	27.38	133	299	450	29
11B	91	27.45	133	266	457	25.5
12A	116	27.26	138	302	446	26
13A	163	27.31	141	312	475	25
13B	199	27.26	139	288	484	24.5
14A	247	27.2	140	325	486	24.5
15B	386	27.26	146	308	496	25.5

Table 3.3 Properties of specimens after solution heat treatment at 473°C for 50 minutes, quenched in water (>95°C/s), naturally aged for 16 days and artificially aged at 120°C and 172°C for different times

Test Piece ID	Ageing temp.	Time (hrs)	EC (%IACS)	Hardness (Hv)	0.2% PS (MPa)	UTS (MPa)	Elongation (%)
21A	120°C	0	27.47	135.7	317.9	468	23.5
21B		0	29.74	119.7	322.4	452.7	22.5
22A		0.02	30.29	124	300	443	22.5
22B		0.03	28.9	147.3	308	470	21.5
23A		0.07	29.26	157.3	324.4	508	20
23B		0.1	29.62	162	311.9	505	19
24A		0.13	29.51	165.7	434	530	19
24B		0.26	29.65	163.7	415	515	18
25A		0.36	29.66	169	320.8	539	20
25B		0.5	29.5	170.3	404	539	18
26A		0.45	29.63	170.5	345	523	19
26B		1	31.4	160.7	400	524	17
27A		1.5	29.78	176	407	552	19
27B		2	29.77	176.3	366	538	20
28A		3	29.36	181.2	465	562	18
28B		4	30.01	180.6	402.3	574	18.5
29A		5	31.7	170	540	553	17.5
29B		6	31.88	170.3	479	554	14.5
30A		7	30.21	182.6	469	554	17
30A		8	30.05	182.3	492	574	17.5
31A		9	30.14	183.3	481	553	18
31B		10	30.17	187	417.1	577	18
32A	172°C	0.16	31.4	184	492	565	15.5
32B		0.25	31.72	191	459	567	16
33A		0.33	33.4	178.7	498	555	15
33B		0.41	32.1	186.7	532	576	14
34A		0.75	32.5	192	531	568	13.5
34B		0.58	32.26	190.3	508	565	13.5
35A		1	34.64	182	525	570	12
35B		1.25	35.15	177.3	527	567	11.5
36A		1.5	36.22	178.8	540	575	11.5
36B		2	35.2	191.8	563	589	12.5
37A		2.5	35.9	187.3	549	587	12.5
37B		3	36.22	187	542	584	12.5
38A		3.5	36.41	191	521	585	12.5
38B		4	36.53	190.3	535	572	11
39A		4.5	36.81	186.7	530	572	11
39B		5	37	186.7	538	582	13
40A		5.5	37.17	187.3	514.7	568	13
40B		6	37.14	187.7	526	569	12.5
41A		6.5	38.33	180.7	515	558	11.5
41BC		7	37.41	180.7	508.3	556	13
42A		7.5	37.29	185.3	516	566	12.5
42B		8	38.13	176.7	508	558	12.5

Table 3.4 Properties of specimens after solution heat treatment at 473°C for 50 minutes, quenched in water (>95°C/s), naturally aged for 16 days, artificially aged at 120°C and 172°C and over aged at 172°C for different times

Test Piece ID	Ageing Time (hrs)	EC (%IACS)	Hardness (HV)	0.2% PS (MPa)	UTS (MPa)	Elongation (%)
43A	Std. H/T	37.44	188	530	581	10.5
43B	1	37.88	185	512	563	10.5
44A	2	38.14	181.3	501	556	13
44B	4	38.89	179	490	549	12
45A	6	40.05	164	467	527	11.5
45B	8	40.91	158.7	448	513	11
46A	9	40.95	154	440	507	11
46B	10.5	40.63	164.3	429	507	11
47A	12	40.9	161.3	426	509	14
47B	13.5	41.77	150.3	406	482	13
48A	15.25	41.17	155	407	494	13
48B	17	41.4	156.3	407	489	13
49A	19	41.55	157	407.7	489	12
49B	21	41.83	148	339	489	13
50A	23	42.02	151.2	403	492	13.5
50B	25	41.97	146	385	483	14
51A	27	42.06	146.3	380	476	14
51B	29	42.22	152.3	380	474	13
52A	31	42.21	147.6	384	478	13
52A	34	42.25	147.3	380	472	13.5
53A	37	42.61	147.7	374	475	13.5
53B	40	42.41	141	369	465	12
54A	44	42.71	143	368	464	12
54B	48	42.71	140.8	359	456	12
55A	56	43.16	144.6	354	455	13.5
55B	64	42.91	141	358	447	11.5
56A	77	44.21	124.7	325	421	11.5
56B	100	44.65	120.6	312	409	12

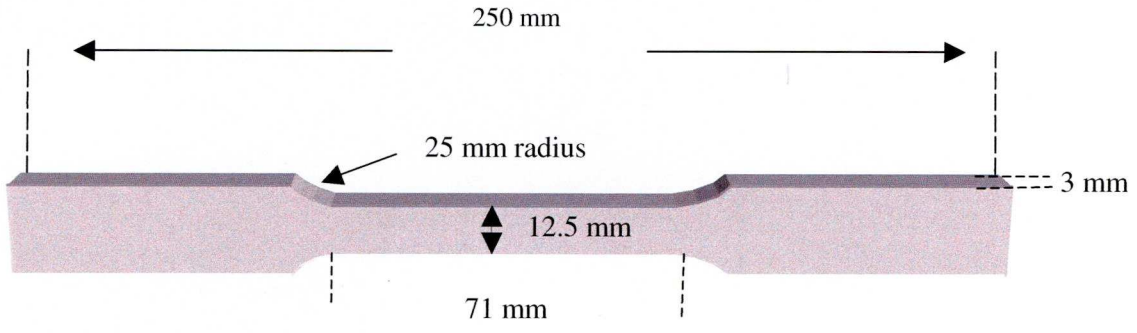

Fig. 3.1 Geometry of flat dog-bone tensile test pieces

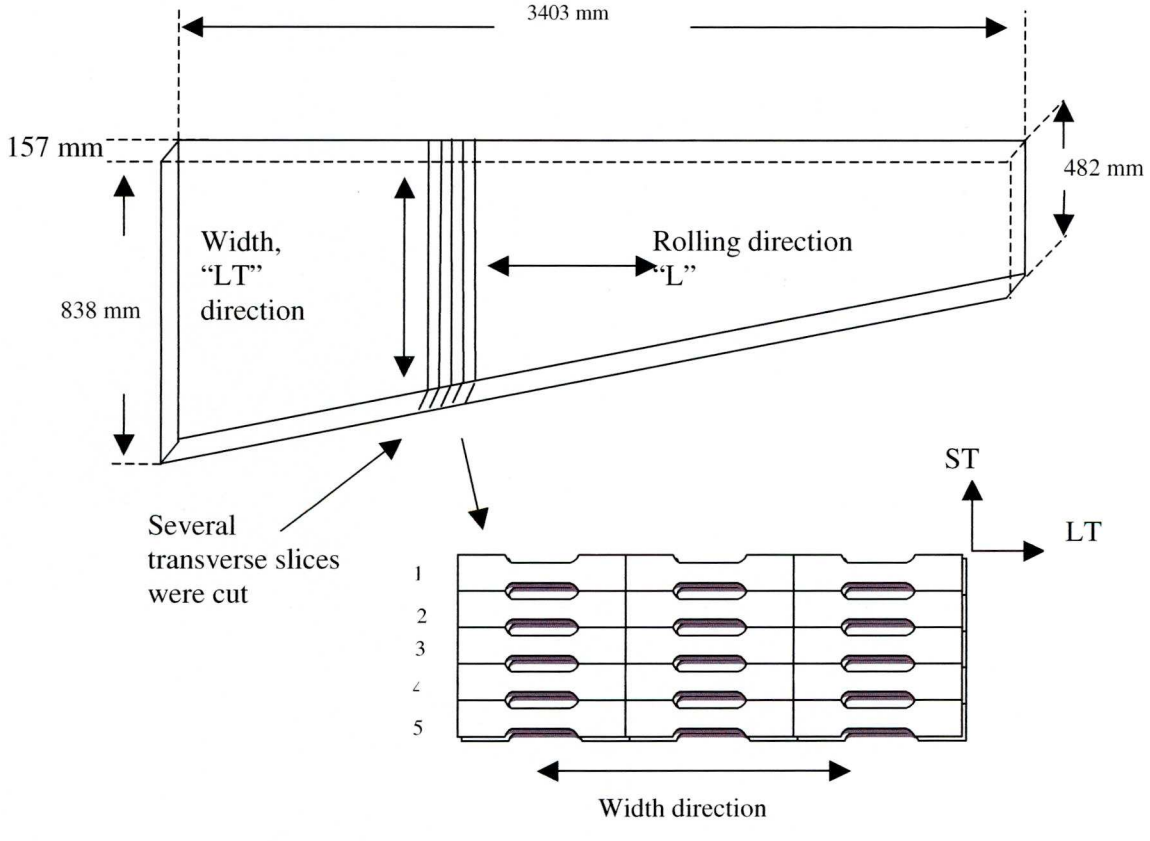

Fig. 3.2 Schematic of rolled plate indicating location and orientation of flat dog-bone tensile test pieces. L, Lt and ST indicate the rolling direction, long transverse and short transverse directions, respectively.

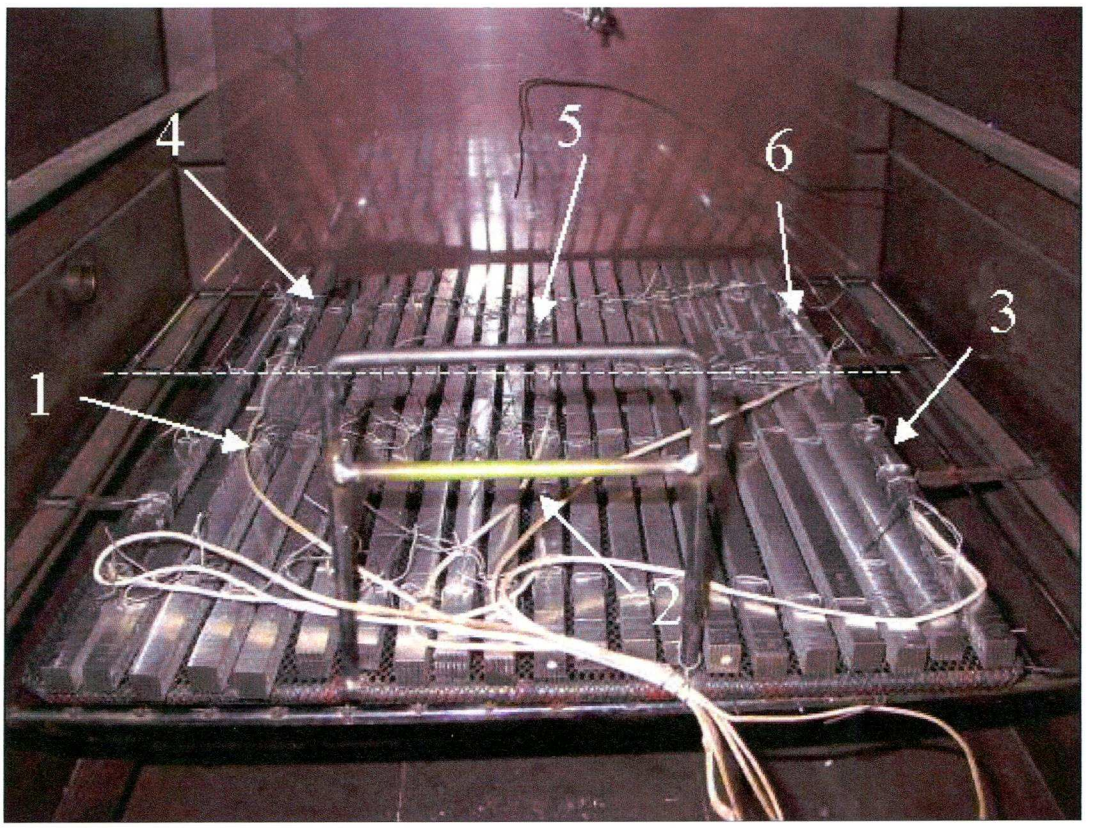

Fig. 3.3 Arrangement of test blanks on the solution heat treatment rack. Arrows indicate positions of thermocouples, which were numbered 1 to 6 and were equally spaced on the charge

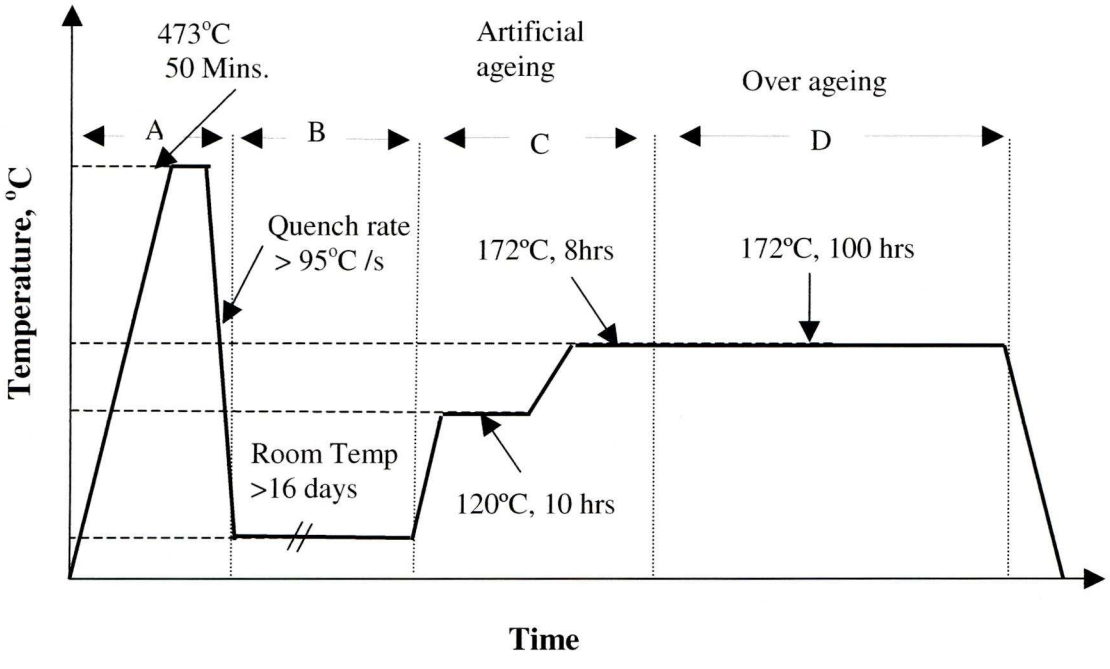

Fig. 3.4 Schematic representation of the thermal cycle for flat dog-bone samples

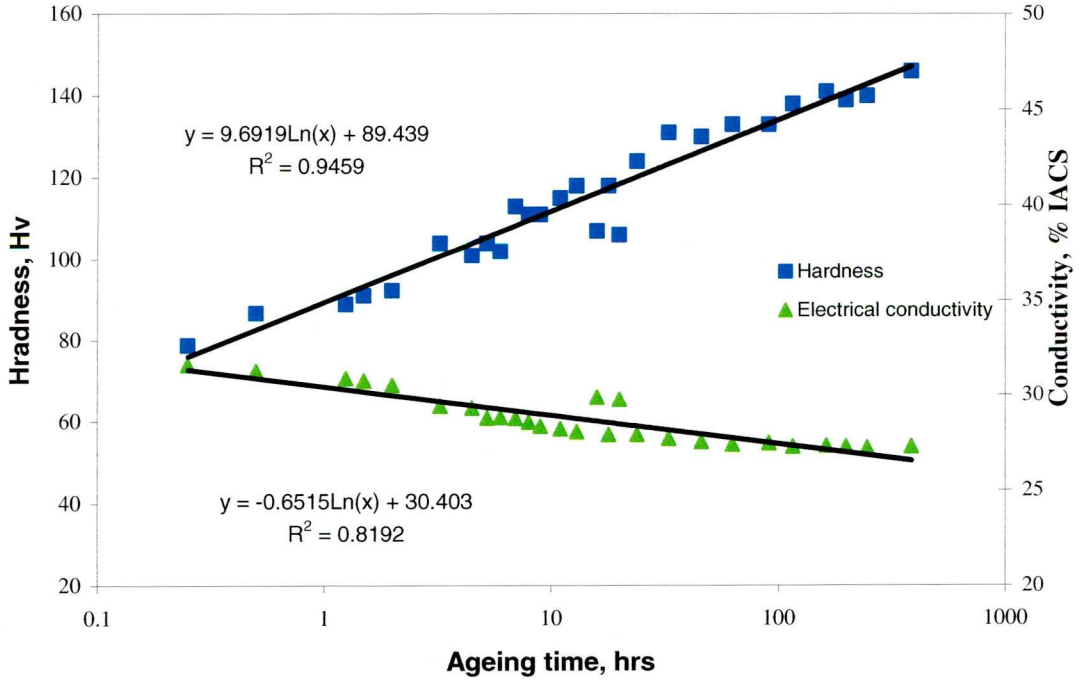

Fig. 3.5 Evolution of hardness and electrical conductivity of AA 7010 from a supersaturated solid solution during natural age hardening

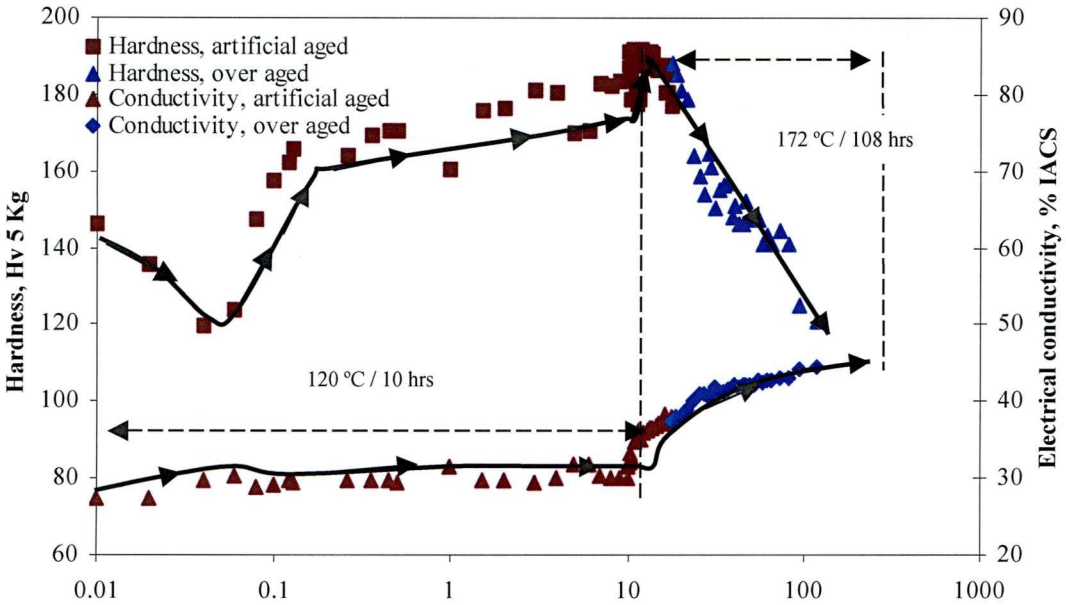

Fig. 3.6 Evolution of hardness and electrical conductivity of AA 7010, from natural ageing condition, during artificial ageing at 120°C and over ageing at 172 °C.

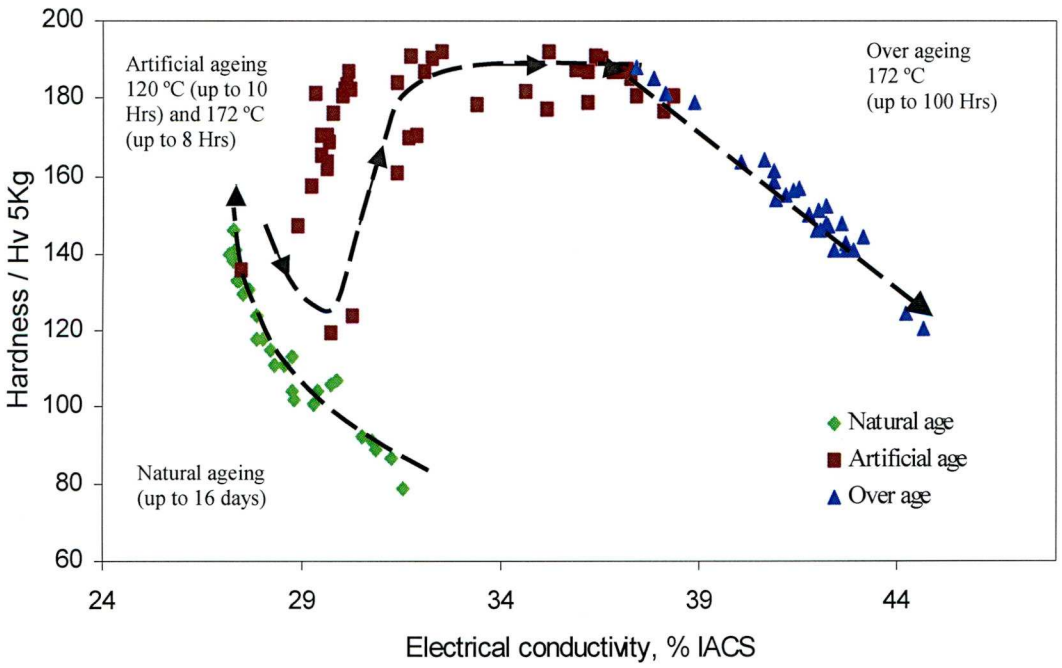

Fig. 3.7 Electrical conductivity and hardness response of AA7010 age hardened from saturated solid solution. Arrows indicate the progress of the different age hardening stages with temperature and time.

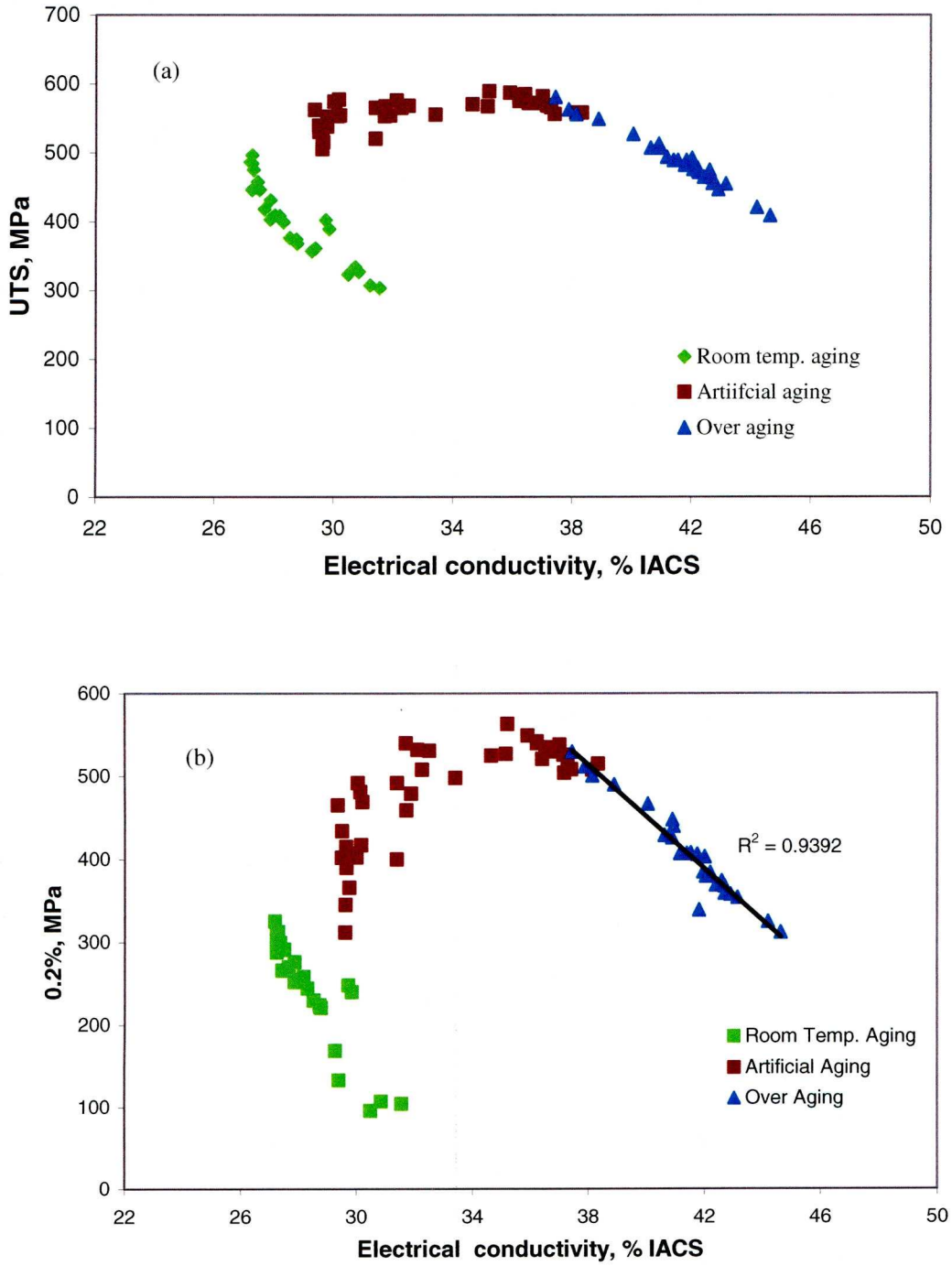

Fig. 3.8 Correlation of strength and electrical conductivity:
(a) UTS and (b) 0.2% PS

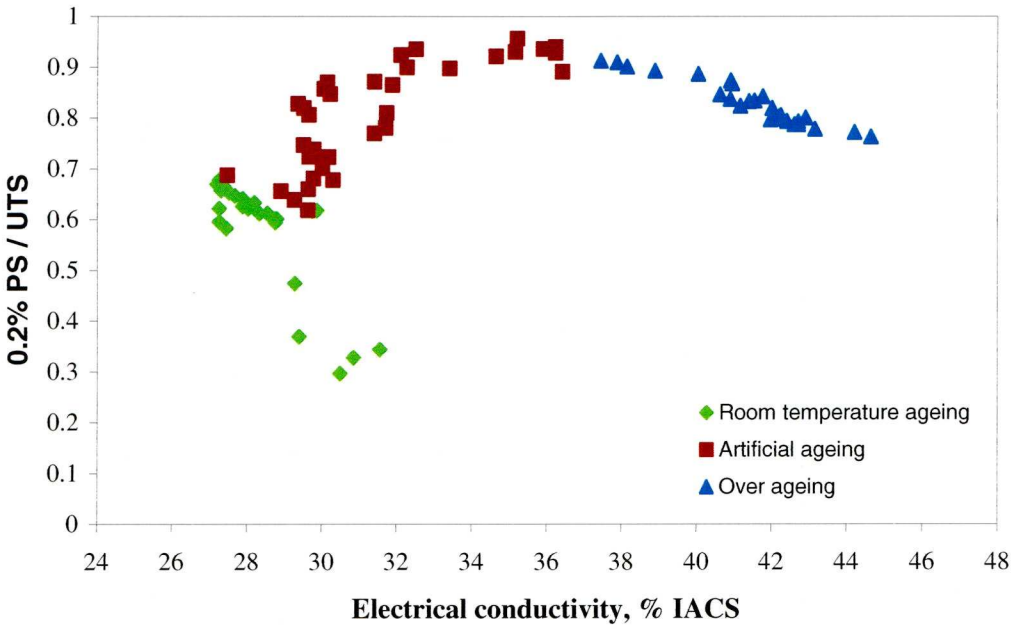

Fig. 3.9 Correlation of strength ratio (PS/UTS) with electrical conductivity in different age hardening conditions

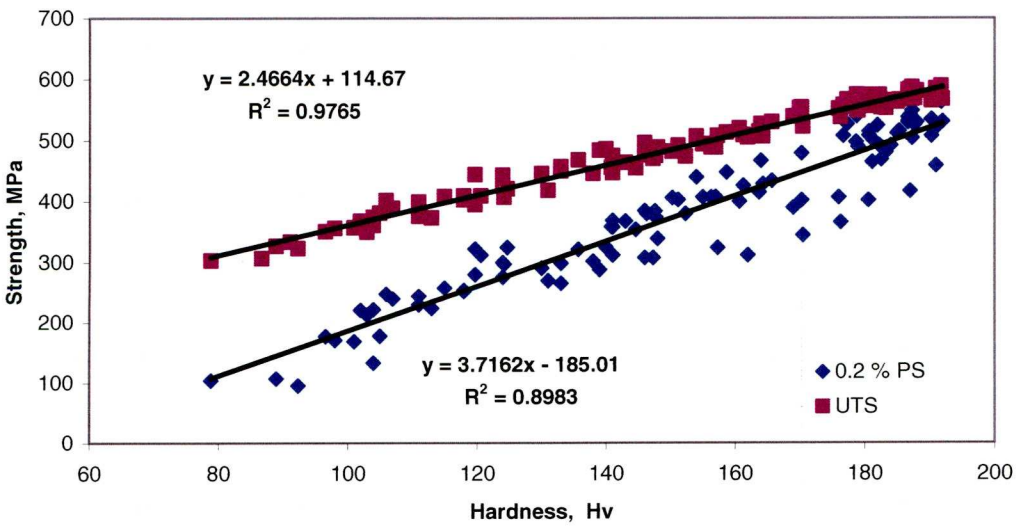

Fig. 3.10 Relationships of UTS and 0.2% PS with hardness

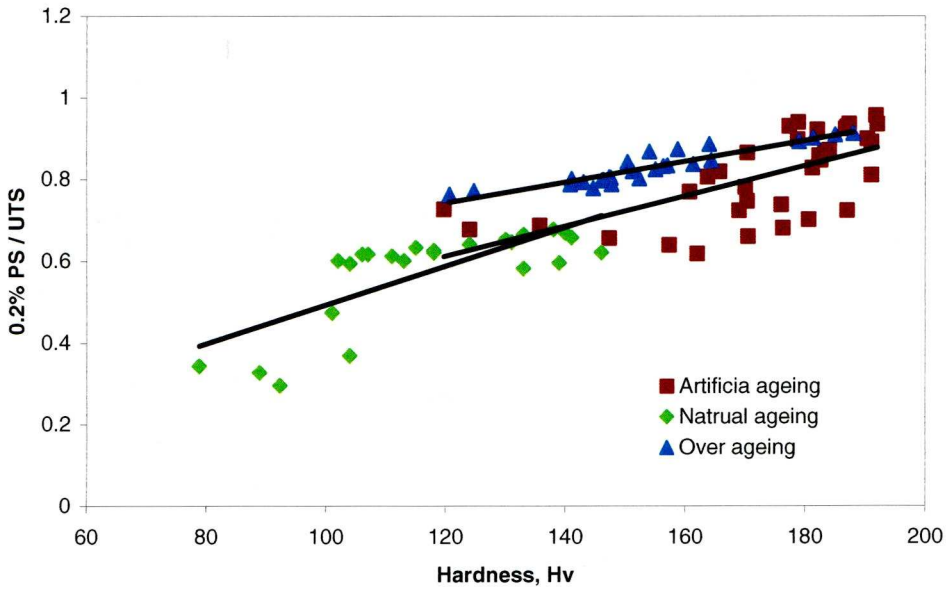

Fig. 3.11 Correlation of strength ratio (0.2% PS / UTS) with hardness

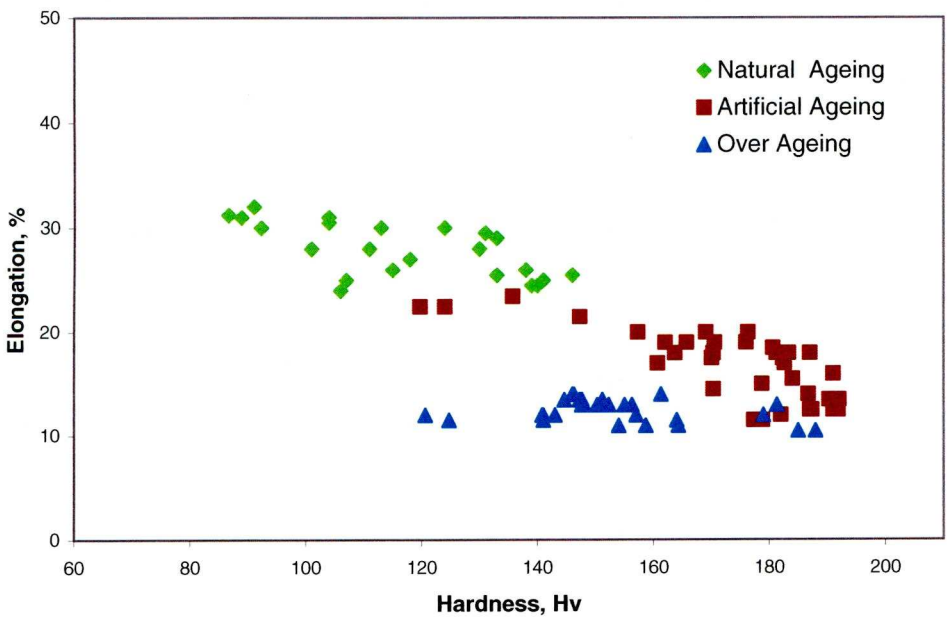

Fig. 3.12 Correlation of elongation with hardness in different ageing conditions

Chapter 4

Property assessment across plate thickness of AA 7010

4.1 Introduction

The mechanical properties of high strength aluminium alloys are influenced by their chemical composition and the heat treatments. When selecting these alloys for structural parts, careful consideration is also given to the product form. The minimum values of tensile properties are governed not only by the section thickness but also by the direction of the wrought product, from which the components are made from (Nielson et al 1984).

AA 7010 in the T7651 temper condition is one of the aircraft industry standards for thick plates, due to a combination of good strength, good fracture toughness and high resistance to stress corrosion cracking (Reynolds 1976, Military Handbook 5G 1994). It is well documented that the anisotropy of properties becomes very important as the plate thickness increases. Normally, tensile properties are higher in the longitudinal than in the transverse direction. The properties are dependent upon the test direction in relation to the rolling direction of the plate or the orientation of grain structure and second phase constituents.

The suppliers of thick plates of AA7010 commonly use NDT of electrical conductivity and hardness to monitor the quality consistency during manufacturing. Due to their accuracy and fast response, hardness and electrical conductivity measurements have also been used extensively to study the age hardening process

and the associated precipitation mechanism in many heat treatable aluminium alloys.

In the aircraft industry these non-destructive inspection techniques are also used to assess the indications of overheating due to machining operations, when previously detected by chromic acid anodising. AA 7010 under investigation, it has been observed that, even when no indication of overheating is detected by chromic acid anodising, the electrical conductivity and hardness change notably from the outside surface towards the centre of the plate. This suggests a lack of property homogeneity through the plate thickness. For AA 7050, through-thickness anisotropy of tensile yield strength was reported (Chakrabarti 1996). For AA 7075 the quenching-rate gradient from solution heat treatment temperatures was reported to be a major factor leading to the property differences in thick sections (Staley et al 1984). The property inhomogeneity through the thickness can also be a result of other factors, such as the segregation of alloying elements during solidification and the subsequent thermo-mechanical processing, especially when subjected to prolonged high temperature during rolling. This view is supported by the fact that the orientation dependence of mechanical properties in aluminium alloys can arise for several reasons, e.g. mechanical fibrin, internal stresses and crystallographic texture. Mechanical fibrin results from changes in grain shape or alignment of second phase particles in a heavy worked material (Polmear 1995).

However, very little information is available to explain the lack of homogeneity of properties for thick products of AA7010. This chapter aims to identify the main contributors to the property inhomogeneity through the plate thickness of AA 7010

and to gain an understanding of the metallurgical phenomena involved, with the objective to improve the manufacturing efficiency of the structural aircraft parts.

4.2 Experimental

4.2.1 Material

The material assessed in this investigation was a plate of AA 7010 with the T7651 temper condition. Details of the thermo-mechanical manufacturing route, the dimensions and the chemical composition of the plate have been specified in section 3.2.1.

4.2.2 Test pieces

A total number of 11 test pieces were taken at different locations from the AA7010 plate for electrical conductivity, hardness, chemical analysis, metallography and tensile tests. Fig. 4.1 shows the locations and orientations of the test pieces. Test piece 1 was selected at a random location as shown in Fig 4.1 and was used for assessing the homogeneity of electrical conductivity, hardness, chemical composition and microstructure through the plate thickness. Test pieces 2-5 were taken at different locations along the long transverse (LT) direction in a slice cut from the end of the plate. Test pieces 6 and 7 were taken at two different locations along the LT direction, at a distance of 200 mm from each other, in two slices parallel to the rolling (L) direction. Test pieces 8 and 9 were taken at two different locations along the rolling direction, at a distance of 340 mm from each other, in two slices perpendicular to the rolling direction. Test pieces 10 and 11 were taken at two different locations along the LT direction, at a distance of 200 mm from each other, in two slices parallel to the rolling (L) direction.

Test pieces 1-7 were used to study the property homogeneity of electrical conductivity and hardness perpendicular (1-5) and parallel (6-7) to the rolling direction. Test pieces 8 - 9 and 10 - 11 were used to study the property homogeneity of tensile strength, electrical conductivity and hardness perpendicular and parallel to the rolling direction. Test pieces 8-11 were also used for making samples for tensile tests.

Test piece 1 is rectangular with dimensions of 157×100×3 mm, as shown in Fig. 4.2. The longest dimension represents the original thickness of the plate. The test piece was marked near the centre into 31 different areas of 25 mm^2 for electrical conductivity and hardness measurements. Chemical analysis was performed by taking milling samples at different depths of the plate, starting from the outside surface towards the centre of the plate, as illustrated in Fig 4.2. Metallographic examinations were performed on six different areas across the plate thickness, as indicated in Fig. 4.2.

Tensile test samples were cut from test pieces 8-11 as shown in Fig. 4.1. Fig. 4.3 shows the geometry of the tensile test samples and the locations from which these samples were taken. A plate of 250 mm in length and 157 mm in width was cut from each test piece (11 mm thick) and was further cut along the length into 13 rectangular bars (11×11×250 mm), representing 13 different depths across the plate thickness with Bars No. 1 and No. 13 representing the outside areas of the plate and Bar No 7 the centre of the plate. From each rectangular bar, a tensile test specimen was machined. The specimen has a diameter of 7.98 mm, a minimum parallel length of 65 mm, a gauge length of 40 mm, a minimum transition radius of 8 mm,

and was consistent with the requirements of British Standard BS 4A – 4 (1966). The square ends of the specimen used for gripping were also used for electrical conductivity and hardness tests.

The specimens are taken parallel to the rolling direction for test pieces 10 and 11 and perpendicular to the rolling direction for test pieces 8 and 9.

4.2.3 Thermal treatment

Re-heat treatment was performed on test pieces 1-5, meanwhile test pieces 6-11 were tested in the as received condition (heat treated by the supplier), the locations of which in the plate are shown in Fig. 4.1. Fig. 4.4 is a schematic diagram of the re-heat treatment process. The re-heat treatment included solution heat treatment at 473°C for 50 minutes and quench in water (Stage A), natural age hardening at room temperature for 30 days (Stage B), and artificial age hardening at 120°C for 10 hours and then at 172°C for 8 hours (Stage C).

4.2.4 Electrical conductivity

The electrical conductivity measurements were carried out using a Forster SIGMATEST Ec 2.068 electrical conductivity meter. These measurements, which are based on the eddy current method, were performed in compliance with the Airbus UK process specifications (Airbus UK 2005). The precautions taken to minimise any possible error during the electrical conductivity measurements have already been discussed in section 3.2.4.

Electrical conductivity was measured on all test pieces 1 to 11, the locations of which in the plate are shown in Fig. 4.1. However for test pieces 1, 4, 6, 7, 8, 9,10 and 11 the measurements were conducted in the as received condition. Test pieces 1, 2, 3, 4 and 5 were tested after every stage of the re-heat treatment. All the test samples were polished before the electrical conductivity assessments.

4.2.5 Hardness

Hardness measurements were carried out using a Vickers HTM 8313 hardness tester, with a 10kg load. The measurements were performed in compliance with Airbus UK process specification (Airbus UK 2004a) and British Standard BS ES ISO 6507-1 (2005). Details of calibration and the precautions taken to minimise any possible errors during hardness testing were discussed in section 3.2.5.

Hardness was measured on all test pieces 1 to 11, the locations of which in the plate are shown in Fig. 4.1. However on test pieces 1, 4, 6, 7, 8, 9, 10 and 11 the measurements were conducted in the as received condition. Test pieces 1, 2, 3, 4 and 5 were also tested after every stage of the re-heat treatment. Hardness measurements were conducted after electrical conductivity measurements.

4.2.6 Chemical analysis

Samples of 0.2 grams of millings were extracted from test piece 1 in the 10 different areas from one surface to the centre of the plate, as identified in Fig 4.2. These areas were adjacent to the locations where the electrical conductivity and hardness measurements were made. Bulk chemical analysis was performed on each sample using the ion couple plasma technique.

4.2.7 Tensile Testing

Tensile tests, on the cylindrical tensile test specimens as illustrated in Fig. 4.3a, were performed using a Denison Mayes Group testing machine, model 6157. The test machine worked with a 100 KN servo-hydraulic load frame and was fitted with an IBM stem/2 computer and a 50 mm gauge length extensometer 7609 DC1/7902 DC2. The tensile tests were carried out at a strain rate of 4×10^{-3} s^{-1} in compliance with British Standard BS 4A – 4 (1966). Details of calibration and the precautions taken to minimise any possible errors during tensile tests were discussed in section 3.2.6.

4.2.3 Results

4.3.1 Numerical data

The numerical values of electrical conductivity, hardness, chemical composition and tensile strength of the test pieces across the plate thickness are compiled in Tables 4.1 (1), 4.2 (1), 4.3 (2,3, and 5), 4.4 (4), 4.5 (6 and 7), 4.6 (8), 4.7 (9), 4.8 (10) and 4.9 (11). The numbers in the brackets indicate the identification numbers of the test pieces.

4.3.2 Variation of hardness and conductivity with plate thickness

Fig. 4.5 shows how the hardness and electrical conductivity change across the plate thickness of test piece 1 in three different temper conditions. The hardness and electrical conductivity vary in a reciprocal manner, i.e., an increase in one results in a decrease of the other and vice versa. Figs. 4.5(a) shows that the hardness in the as received condition generally decreases with increasing distance from the edge towards the centre across the plate thickness. The respective reciprocal change of

electrical conductivity is also observed. Fig. 4.5(b) shows that the hardness and electrical conductivity of the plate in the re-solution heat treated and naturally aged condition do not change significantly in the first 40 mm from either side of the plate; however, notable changes are evident at the plate centre, where a drop in hardness is accompanied by an increase in electrical conductivity. Fig. 4.5(c) shows a gradual increase in hardness up to 6.5 Hv and a respective conductivity drop of -0.3% IACS from the surface to approximately one-quarter of plate depth in the artificially aged condition. The differences in hardness and electrical conductivity from approximately one-quarter of the plate depth from the edges to the plate centre are approximately -9.5 Hv and +0.7% IACS, respectively.

Three repeated heat treatment cycles of re-solution heat treatment and artificial age hardening of test piece 1 gave the same profiles for hardness and electrical conductivity as in the single heat treatment cycle (Fig. 4.5c). However, three heat treatment cycles with prolonged soaking time and full age hardening resulted in higher hardness values and lower electrical conductivity values than those in the single heat treatment condition.

Fig. 4.6 shows the variation of hardness and electrical conductivity across the plate thickness in test pieces 4, 6 and 7, all in the as-received condition. Comparing Figs. 4.5(a) and 4.6 shows that there exist no significant differences in the hardness and electrical conductivity trends between the four plate locations. The profiles of hardness and electrical conductivity across the plate thickness between the test pieces perpendicular (Figs. 4.5(a) and 4.6(a)) and parallel (Figs. 4.6(b) and (c)) to the rolling direction are also very similar.

Fig. 4.7 shows the variation of hardness and electrical conductivity across the plate thickness in test pieces 2-5, all in the re-solution heat-treated and artificially aged condition. Comparing Figs. 4.5(c) and 4.7 shows that all five test pieces from different locations on the plate (Fig. 4.1) have similar, but not identical, variation profiles in the re-solutionised and artificially aged condition. The hardness generally increases progressively from either edge of the plate towards approximately one-quarter of plate thickness and then deceases towards the plate centre. The respective reciprocal change of electrical conductivity is also observed through the thickness. Fig. 4.5c is equal to Fig.4.7c, on the other hand Fig. 4.7a is equal to Fig. 4.7d.

The hardness values for the re-solution heat treat and artificial ageing condition, Figs. 4.5(c) and 4.7, are higher than those for the as received condition, Figs. 4.5(a) and 4.6. On the other hand, the electrical conductivity values for the re-treated condition were lower than those for the as received condition. Although test pieces in the as received and in the re-treated conditions show different hardness profiles through the plate thickness, they have very similar electrical conductivity profile patterns.

The variations of hardness across the plate thickness in all the test pieces in the age hardening conditions showed consistent "M" shaped profiles, with that in the re-solution heat treated and artificially aged condition being more pronounced. The variations of electrical conductivity across the plate thickness in all the test pieces with different ageing conditions, including natural aged condition (Fig. 4.5b) showed essentially the same flattened "W" shaped profile.

Variations of hardness and electrical conductivity for test pieces 8-11 are shown in Figs. 4.8-11. The electrical conductivity values of the test pieces tested in the as received condition are within the material specification requirements. However, the hardness values at the centre of the plate were marginally below the minimum (160 Hv) on six test pieces out of eight. The test pieces with hardness below the specification were: 4, 6, 7, 8, 9 and 11.

4.3.3 Variation of strength with plate thickness

Figs. 4.8-11 show variations of hardness, electrical conductivity, UTS and PS with plate thickness in test pieces 8-11. There is little correlation between the hardness profile and PS or UTS profile across the plate thickness. Generally, in all the four test pieces, the hardness, UTS and PS decreased from the outside faces towards the centre of the plate. The strength variation through the plate thickness shows a flattened "M" shaped profile, specifically between the plate locations of approximately 40 to 115 mm from one edge.

It most be bore in mind that, on each test piece (Figs. 4.8 to 4.11) a single measurement of the tensile properties (proof strength and ultimate tensile strength) was performed at different depths from the plate surface. The fluctuation in tensile properties across the plate thickness may be due to statistical / experimental errors, as well as other factors discussed in section 4.4.5

Figs. 4.8-11 show that all test pieces have similar hardness and electrical conductivity profiles. However, the profiles of UTS and PS show noticeable differences between the long transverse direction (Fig. 4.8b and 4.9b) and the

rolling direction (4.10b and 4.11b). The strength in the rolling direction shows a sharper "M" shaped profile than that in the LT direction. This is particularly noticeable towards the centre of the plate, where the strength is higher than that at the one-quarter depth of the plate.

4.3.4 Variation of chemical composition with plate thickness

Fig. 4.12 shows the variation of chemical composition of test sample 1 from the outside surface to the centre of the plate. Fig. 4.12a shows the variations in concentrations of the major alloying elements Zn, Cu and Mg. They increase slightly from the surface to approximately a depth of 32 mm of the plate thickness and then decrease slightly towards the centre. Fig. 4.12b shows the variations in concentrations of the minor alloying elements Zr, Fe, Si and Ti. There are some changes of Fe and Si concentration through the plate thickness, but the variation of Si in particular may be due to possible experimental scattering in measurements. The maximum changes of Zn, Cu, Mg, Fe and Si between the surface and this depth were 0.3%, 0.15%, 0.13%, -0.01 and -0.01%, respectively. The remaining elements Ti, Zr and Mn did not change much through the thickness, except for higher Ti and Zr concentrations at the centre of the plate.

4.3.5 Microstructure

Fig. 4.13 shows typical microstructures of the AA7010 plate. The samples for the metallographic examinations were taken from test piece 1, the location of which is shown in Fig. 4.1. The micrographs of the microstructure perpendicular to the rolling direction (Fig. 4.13a - 4.13d) of the plate show that the mean grain size varies across the plate thickness, with the grains at the centre being coarser than

near the edge. This grain structure also shows indication of grain spread in the long transverse direction. The average grain sizes, measured by quantitative metallography, are approximately 90 μm at the outside edge and 120 μm at the centre, respectively. The micrographs of the microstructure perpendicular to the long transverse direction (Fig. 4.13e – 4.13h) of the plate show that the grains are elongated on the rolling (longitudinal) direction and the grains gradually coarsen from the edge of the plate to the centre. The change in shape and orientation of the grains through the plate thickness indicate slight fibrin effect due to the rolling operation.

The micrographs showed that primary coarse inter-metallic particles or constituents are predominantly irregular in shape and are mainly confined to the grain and sub-grain boundaries. There is an apparent gradual change in the number and size of these constituents through the plate thickness. They appear to be larger and slightly less numerous at the centre than towards the edge of the plate.

4.4 Discussion

4.4.1 Relationships between composition, microstructure and properties

The hardness and electrical conductivity of an aluminium alloy are dependent upon the composition and microstructure of the aluminium alloy. The alloying elements can exist in the matrix as solute or form coarse primary intermetallic particles or dispersoids and fine precipitates. The intermetallic constituents, which are relatively large particles and formed during solidification, cannot be dissolved completely during homogenisation, high temperature rolling and solution heat treatment, or in the age hardening treatment (Morris *et al.* 1984, Hamerton 2000).

They are present in the natural and artificially aged conditions. In the 7000 series aluminium alloys, Fe, Si and Mn containing dispersoids and other micro constituents have a constant or little contribution to the hardness and electrical conductivity (Morris *et al.* 1984).

It is well established that the hardness and strength are largely determined by the amount of fine precipitates in the alloy formed during age hardening; the higher the volume fraction of the fine precipitates, the higher the hardness and strength would be. All known metallic additions to aluminium reduce its electrical conductivity; metals in solid solution depress the conductivity to a greater extent than out of solution (Morris *et al.* 1984). The electrical conductivity is therefore largely determined by the amount of alloying elements in the solid solution and the amount of fine precipitates. The effect of grain size on electrical conductivity for commercial materials is negligible (Frank *et al.* 1984). However, grain size influences the strength of aluminium alloys (Orowan 1948).

4.4.2 Variations in hardness and conductivity

The variations in hardness and electrical conductivity across the plate thickness are normally in a reciprocal relationship, i.e. higher hardness corresponds to lower electrical conductivity and vice versa. This is because higher hardness is associated with GP zones or fine strengthening precipitates generating more distortion or more strain in the crystal lattice, which also leads to more scattering to electron movement and thus lower electrical conductivity.

The general differences in hardness and electrical conductivity between the as-received, the re-solution heat treated / naturally age hardened and the re-solution heat treated / artificially age hardened conditions, as shown in Fig. 4.5, can be explained by the amount of alloying elements in the solid solution and the amount of strengthening precipitates. In the naturally age hardened condition, only a small fraction of the alloying elements are precipitated as fine and coherent particles (GP zones). Because of this, the aluminium alloy in the naturally age hardened condition has much lower hardness than in the as received and the re-solution heat-treated / artificial age hardened conditions. Because a large fraction of the alloying elements are still dissolved in the solid solution, the aluminium alloy in the naturally age hardened condition has much lower electrical conductivity than in the as received and the re-solution heat-treated / artificial age hardened conditions.

The high hardness and low electrical conductivity values across the plate thickness in the re-solution heat treated / artificially age hardened condition (Figs. 4.5c and 4.7), in comparison with the as-received condition (Figs. 4.5a and 4.6), are mainly due to the difference in quenching rate after solution heat treatment. With a thickness of only 3 mm, the laboratory re- solution heat-treated and artificially aged test samples have a higher quenching rate than that of the as received plate (157 mm thick). The test samples will therefore have reduced quench-induced precipitates, increased solute content and quenched-in vacancies in the solution. This in turn leads to a more efficient artificial age hardening and an increase in the amount of strengthening precipitates. This re-solution heat-treated and artificially age hardened condition will lead to higher hardness. In comparison, the as-received condition is expected to have a greater level of quenching induced precipitates than

the laboratory-retreated test samples, due to the low quenching rate and prolonged manufacturing operations at high temperature (Martin 1998). A low quenching rate from solution heat treatment temperatures leads to heterogeneous precipitation on primary dispersoids and at grain boundaries (Godard *et al.* 2002). As a consequence, the amount of alloying elements available for age hardening is reduced.

The differences in electrical conductivity and hardness values and profiles though the plate thickness between the as received and the re-treated conditions are also affected by the absence of controlled stretching on the re-treated samples. It was reported that the stretching could introduce uniformly distributed dislocations into the alloy prior to age hardening, which leads to a more uniform distribution of coherent and semi - coherent precipitates and therefore more homogeneous properties (Martin *et al.* 1989).

In the present investigation, the stretching effect was removed during re-solution heat treatments. For this reason, the re-treated and artificial age hardening samples showed more pronounced changes in hardness and electrical conductivity than the as received condition. However, the net result of higher hardness and lower electrical conductivity values, for the re-solution heat-treated and artificially aged condition, is a direct consequence of the faster quenching rate.

It was reported that the quenching-rate gradient in the solution heat treatment was the major factor leading to the property differences in thick sections of AA 7075 (Staley 1984). In the present investigation, the quenching rate for the re-solution

heat-treated test pieces 1 to 5 (3 mm thick) were much higher than that of the as received condition. However, the profiles of hardness and electrical conductivity through the plate thickness remained essentially the same as those of the received condition. Furthermore, repeated re-solution heat treatments, with longer soaking time, and full ageing of test piece 1 showed the same trend of properties. Therefore, the quench rate gradient from the surface to the centre of plate is not a major contributing factor for the low hardness at the plate centre in the present investigation.

The variations in electrical conductivity and hardness through the plate thickness of test pieces 1 to 7, for AA 7010, showed "W" and "M" shaped profiles, respectively (Figs. 4.5-7). The variations are considered to be inherent from the parameters governing the ingot casting, which lead to some degree of segregation of the alloying elements, and partly due to the rolling process parameters and the thermal gradients in the heat treatments. The variation in electrical conductivity is mainly due to changes in chemical composition, the nature of the precipitates formed, or both (Morris *et al.* 1984). The variation in hardness, on the other hand, is most likely due to a combination of chemical composition change and the effects of the thermo-mechanical processes.

Since the chemical composition of the plate is very similar between the outside face and the centre (Fig. 4.12), the drop in hardness and the corresponding increase in electrical conductivity at the plate centre, in the three different age harden conditions, are mainly due to the depletion of alloying elements from the solid solution at mid-plate. This occurs because the formation of equilibrium precipitates

(η) on the primer dispersoids during the high temperature manufacture of the plate and during the artificial age hardening. A similar effect was reported on Al-Li-Cu-X alloys, where decreases in the UTS and yield strength in the T6 and T86 temper conditions were attributed to the formation of coarse heterogeneous precipitates, which consumed Cu and thereby reduced the number density of the fine strengthening precipitates (Csontos *et al.* 2000).

4.4.3 Microstructural inhomogeneity

Optical microscopy examination through the thickness of the AA7010 plate showed that the grains at the plate centre are much coarser than at the surface (Fig. 4.13). A notable difference in the size and number of primary constituents between the surface and centre of the plate was also observed. It is indicated that the centre part of the plate was subject to low cooling rate during solidification and prolonged high temperature during the homogenisation and thermo-mechanical manufacturing operations. During the solidification of a large ingot, the dendrites containing peritectic and eutectic intermetallic compounds can be broken away and transported towards the ingot centre by the liquid metal flow, resulting in the formation of primary dispersoids containing elements such as Zr, Fe, Mg and Si (Morris *et al.* 1984, Hamerton 2000). High temperature precipitates can also form heterogeneously on the dispersoids during the thermo-mechanical operations.

The difference in the content of dispersoids also supports the view that the hardness drop and electrical conductivity increase at the plate centre are inherent of the solidification and thermo-mechanical processes of the product. The majority of the dispersoids are most likely Al_3Zr, which forms very rapidly in solidification due to

its similar crystallographic structure and low misfit with the aluminium matrix (Nes 1972). The formation and growth of the dispersoids at the centre could decrease the amount of solute elements within the solid solution, which otherwise would be available for artificial age hardening. The lack of strengthening alloying elements (Zn, Cu and Mg) within the solid solution may have resulted in the lower hardness and higher electrical conductivity observed at the centre of the plate. This view is supported by the findings of Deschamps (1998) and Godard (2002). They reported for Al-Zn-Mg-Cu alloy that, during slow quench, extensive nucleation of precipitates occurs. The quench induced precipitates occur mainly on Zr containing dispersoids. This induced a decrease of the solute available for the fine-scale precipitation.

The fibrin effect (change in shape and size of grains) observed through the thickness of the plate is due to the nature of mechanical deformation during hot rolling. The mechanical deformation also influenced the differences in size and number of the constituents present through the microstructure. The constituents have been broken down into smaller sizes near the surface of the plate than at the centre.

4.4.4 Effect of chemical composition changes

The difference in hardness and electrical conductivity values through the plate thickness (Fig. 4.5c) is considered to be influenced by the slight variations in the major alloying elements through the plate thickness (Fig. 12a) and by the nature of the precipitates formed by the strengthening alloying elements (Zn, Cu and Mg). At the plate centre, the level of non-strengthening precipitates would be higher than at

the surface.

Variations of chemical composition of alloying elements can occur within a single plate, typically due to macro segregation carried forward from the original ingot (Rummel and Arbegast 1981). The variations in chemical composition can result in variations in electrical conductivity values within the plate. According to Morris (1984), a 1 wt% increase in Zn, Cu, Mg, Zr, Fe, Ti, Mn or Si in solid solution in aluminium alloys would result in an increase in resistivity of 0.094, 0.344, 0.54, 1.74, 2.56, 2.88, 2.94 and 1.02 μΩ cm, respectively. The measured concentrations of Zn, Cu, Mg, Zr, Fe, Ti, Mn and Si at the surface and at 32 mm from the surface of the AA7010 plate were (6.1%, 1.69%, 2.26%, 0.1%, 0.06%, 0.03%, 0.01% and 0.05%) and (6.64%, 1.84 %, 2.39%, 0.1%, 0.05%, 0.03%, 0.01% and 0.04%), respectively. Using the above principle, these alloying elements would result in increases in resistivity of pure aluminium (2.65 μΩ.cm at 20°C) by approximately 2.87 μΩ.cm for the outside face and 3.01 μΩ.cm at 32 mm from the surface. The corresponding values of electrical conductivity for these locations would be estimated to be 31.24% IACS and 30.48% IACS, respectively. Although the estimated values are different from the measured values, because of ignoring the precipitation effects, they clearly demonstrate the possible cause of the difference in electrical conductivity between the two locations.

The change of chemical composition registered at the location 32 mm from the surface is most likely inherent from the cast ingot from which the plate was rolled. During the solidification of a large ingot, the microstructure changes from equiaxed to columnar and to equiaxed again from the surface to the centre (Higgins 1983).

As a consequence, the alloying elements are pushed inwards until a new solidification mode becomes dominant. The subsequent homogenisation and hot rolling operations cannot remove the compositional inhomogeneity completely. The registered increases in the major alloying elements at 32 mm from the surface might coincide with the transition zone between the equiaxed and columnar regions (Higgins 1983). The high levels of Ti and Zr concentrations at the plate centre, as shown in Fig. 4.12b, are also a result of the solidification-induced inhomogeneity.

4.4.5 Variations in strength

The UTS and PS values showed noticeable differences in the longitudinal and long transverse directions (Figs. 4.8-11). The anisotropy appears to be due to the fibrin and texture in the AA7010 plate, the fibrin is evidenced in Fig. 4.13. It has been reported that anisotropy can also be influenced by preferred precipitation during age hardening on specific crystallographic planes. Bate *et al.* (1981) showed that the habit plane of the precipitates are important in relation to the orientation dependence of their strength effects. Precipitates can impart a directionality in properties, which either enhances or diminishes the effect attributed to texture alone.

The main reasons for the variations in UTS and PS across the plate thickness are similar to those discussed, for the variation in hardness, in section 4.4.2. However, the fluctuation in tensile properties across the plate thickness may also be influenced by statistical / experimental errors.

The contributing factors to the through thickness anisotropy of strength are most likely the gradients of crystallographic texture and thermal history from the surface to the centre. This view is supported by a report on AA 7050, which showed that the texture gradient from the surface to the centre contributes strongly to the differing yield strength pattern through the thickness in the longitudinal, long transverse and short transverse directions (Chakrabarti 1996). Other investigators have drawn similar conclusions. Solas *et al.* (1996) showed that the variation of macro yield strength was mainly a crystallographic texture effect for AA7010. Chen *et al.* (2008) observed a pronounced texture variation through the plate thickness for AA 7055, with β fibre texture at the centre and shear type texture at the surface.

4.5 Summary

The investigation on the variations of hardness, electrical conductivity and strength across the thickness of an AA 7010 plate under the temper condition of T7651 showed considerable inhomogeneity in these properties. Whereas the hardness and strength varied simultaneously through the thickness, the electrical conductivity responded in a reciprocal manner to hardness and strength. A test piece from the plate subjected to re-solution heat treatment / natural age hardening and re-solution heat treatment / artificial hardening showed similar tendencies in property changes as in the as-received raw material. This suggested that the lack of property homogeneity across the plate thickness was inherent of the manufacturing route. The differences in properties through the plate thickness were due mainly to the changes in the concentrations of the strengthening alloying elements in the solid solution and the associated changes in microstructure. These changes were due to

the different thermal histories experienced at different locations across the plate thickness during solidification, homogenisation and rolling operations.

Table 4.1

Hardness and electrical conductivity of test piece 1, in the as received, re-solution heat-treated naturally aged and artificially aged conditions. The thermal re-treatments were performed as indicated in Fig. 4.4.

		As received		Naturally aged		Artificially aged	
Location on thickness	Distance from edge	Electrical conductivity	Hardness	Electrical conductivity	Hardness	Electrical conductivity	Hardness
	mm	% IACS	Hv 10 kg	% IACS	Hv 10 kg	% IACS	Hv 10 kg
1	5	39.84	172.5	27.38	147	38.69	179
2	10	39.74	174.5	27.34	145.5	38.63	180.5
3	15	39.62	171.5	27.4	146	38.59	181
4	20	39.6	174	27.4	146	38.52	183
5	25	39.62	174	27.4	147.5	38.52	184
6	30	39.67	171.5	27.4	145.5	38.5	185
7	35	39.76	170	27.42	146	38.47	186
8	40	39.78	171.5	27.36	147.5	38.52	185.5
9	45	39.85	169	27.42	145.5	38.53	185
10	50	39.97	171	27.57	145.5	38.57	184
11	55	40.09	167	27.72	143.5	38.64	182
12	60	40.21	166	27.81	144.5	38.84	180
13	65	40.31	165	27.98	145	38.93	177
14	70	40.57	164.5	28.12	140.3	39.05	178
15	75	40.79	164	28.51	139.3	39.19	177
16	80	40.69	163	28.65	137	39.22	176
17	85	40.81	163.5	28.6	139	39.29	175.5
18	90	40.76	164.5	28.35	140	39.14	177
19	95	40.52	166	27.91	139.5	38.88	178
20	100	40.22	168.5	27.72	144	38.8	178.5
21	105	40.1	168.5	27.67	144.5	38.72	180.5
22	110	40.02	171	27.64	143.7	38.74	180.5
23	115	39.88	171	27.45	145.5	38.62	181
24	120	39.8	171.5	27.34	144.5	38.62	181.5
25	125	39.66	172	27.36	145.3	38.59	184
26	130	39.57	173	27.32	146	38.6	185
27	135	39.53	172.5	27.34	146	38.67	184.5
28	140	39.52	171.5	27.35	146.7	38.67	183
29	145	39.64	170.5	27.34	146	38.71	181
30	150	39.76	171.5	27.36	146	38.76	179.5
31	155	39.76	171.5	27.41	147	38.81	178.5

Table 4.2

Chemical composition through half the plate thickness in test piece 1. The locations of chemical analysis are indicated in Fig. 4.1.

Depth of plate	**Zn**	**Mg**	**Cu**	**Zr**	**Fe**	**Si**	**Ti**	**Mn**
mm	Wt %	Wt %	Wt %	Wt %	Wt %	Wt %	Wt %	Wt %
0.1	6.1	2.26	1.69	0.1	0.06	0.05	0.03	0.01
15.7	6.3	2.34	1.79	0.1	0.06	0.04	0.03	0.01
23.6	6.3	2.35	1.81	0.1	0.06	0.04	0.03	0.01
31.4	6.4	2.39	1.84	0.1	0.05	0.04	0.03	0.01
39.3	6.3	2.33	1.81	0.1	0.05	0.05	0.03	0.01
47.1	6.2	2.32	1.78	0.1	0.06	0.04	0.03	0.01
55.0	6.2	2.3	1.72	0.1	0.05	0.04	0.03	0.01
62.8	6.1	2.29	1.72	0.1	0.05	0.04	0.03	0.01
70.7	6.1	2.24	1.68	0.1	0.04	0.04	0.03	0.01
78.5	6.1	2.21	1.64	0.11	0.04	0.04	0.04	0.01
Uncertainty Wt %	0.02	0.07	0.04	*	0.04	*	0.03	0.01

* Values were not supplied by chemical test house

Table 4.3

Hardness and electrical conductivity of test pieces 2, 3 and 5, in the re-solution heat-treated and artificial aged condition, as indicated in Fig. 4.4.

		Test piece 2		Test piece 3		Test piece 5	
Location on thickness	Distance from edge	Electrical conductivity	Hardness	Electrical conductivity	Hardness	Electrical conductivity	Hardness
	mm	% IACS	Hv 10 kg	% IACS	Hv 10 kg	% IACS	Hv 10 kg
1	5	38.36	185.5	38.31	182	38.81	177
2	10	38.41	183.5	38.22	184	38.79	178
3	15	38.36	182.5	38.19	181	38.78	178.5
4	20	38.34	183	38.22	182.5	38.72	180
5	25	38.16	186.5	38.24	181.5	38.67	179
6	30	38.09	186.5	38.16	180.5	38.67	180
7	35	38.21	185.5	38.1	180.5	38.66	179
8	40	38.22	183	38.03	183.5	38.67	179
9	45	38.28	185.5	38.02	184	38.71	178.5
10	50	38.26	185	38.1	185	38.71	178.5
11	55	38.28	184	38.19	183	38.78	177.5
12	60	38.4	182.5	38.19	182.5	38.84	175
13	65	38.47	179.5	38.43	181.5	38.95	174
14	70	38.66	177	38.62	177.5	39.02	173
15	75	38.62	175.5	38.95	176.5	39.05	172.5
16	80	38.67	176	38.9	176	39.07	173.5
17	85	38.55	178	38.88	177	39.12	173
18	90	38.59	176.5	38.71	177.5	39.1	173.5
19	95	38.5	179	38.43	178	39	174
20	100	38.43	178.5	38.36	180.5	38.86	177
21	105	38.47	180	38.29	181.5	38.83	178.5
22	110	38.38	182	38.21	184.5	38.66	181
23	115	38.34	184	38.14	182	38.6	181.5
24	120	38.29	183.1	38.19	184	38.62	182
25	125	38.29	185.5	38.14	184	38.69	180
26	130	38.33	184	38.12	186	38.72	178.5
27	135	38.31	184.5	38.14	184.5	38.67	180
28	140	38.31	185	38.21	181.5	38.69	179
29	145	38.29	182.5	38.28	183.5	38.76	178.5
30	150	38.34	182	38.33	182	38.78	178
31	155	38.38	183.5	38.4	181.5	38.81	177.5

Table 4.4

Hardness and electrical conductivity of test piece 4 in the as received condition, and re-solution heat-treated and artificially aged condition as indicated in Fig. 4.4.

		As received		Artificially aged	
Location on thickness	Distance from edge	Electrical conductivity	Hardness	Electrical conductivity	Hardness
	mm	% IACS	Hv 10 kg	% IACS	Hv 10 kg
1	5	39.63	172.5	38.48	179
2	10	39.52	174.5	38.41	180.5
3	15	39.34	173	38.31	182.5
4	20	39.39	174	38.28	183
5	25	39.27	172.5	38.17	182.5
6	30	39.29	171.5	38.12	184
7	35	39.43	169.5	38.14	185.5
8	40	39.35	171	38.09	185
9	45	39.35	169	38.03	185
10	50	39.52	169.5	38.12	182.5
11	55	39.69	168.5	38.24	184.5
12	60	39.71	166	38.34	180
13	65	39.97	165.5	38.59	178.5
14	70	40.33	164	38.81	178
15	75	40.53	161	38.93	176
16	80	40.42	159	38.95	172
17	85	40.68	160.5	39.16	172.5
18	90	40.53	159	38.91	172.5
19	95	40.33	163	38.69	175.5
20	100	39.83	164	38.41	179
21	105	39.69	167.5	38.31	182.5
22	110	39.57	169	38.29	184.5
23	115	39.42	172	38.16	187
24	120	39.3	171	38.12	187
25	125	39.26	173.5	38.19	185.5
26	130	39.13	172	38.16	184
27	135	38.9	174	38.05	184
28	140	39.14	175	38.29	183.5
29	145	39.31	173	38.38	182.5
30	150	39.33	174	38.33	182.5
31	155	39.29	172.5	38.34	180.5

Table 4.5

Hardness and electrical conductivity of test pieces 6 and 7 in the as received condition, thermally treated by the manufacturer. The test pieces are parallel to the rolling direction and 200 mm apart.

		Test piece 6		Test piece 7	
Location on thickness	Distance from edge	Electrical conductivity	Hardness	Electrical conductivity	Hardness
	mm	% IACS	Hv 10 Kg	% IACS	Hv 10 Kg
1	5	40.95	164.5	40.10	167.5
2	10	40.79	166	39.83	169
3	15	40.66	166	39.72	168.5
4	20	40.64	167	39.69	168.5
5	25	40.66	166.5	39.76	169
6	30	40.64	164.5	39.81	167
7	35	40.79	164.5	39.86	166
8	40	40.86	162	39.91	166.5
9	45	40.93	163.5	40.03	165
10	50	40.98	162	40.10	168
11	55	41.12	161.5	40.26	166
12	60	41.34	160.5	40.41	164.5
13	65	41.45	159	40.59	163
14	70	41.67	159.5	40.84	159.5
15	75	41.74	158.5	40.97	155
16	80	41.81	156.5	40.81	156
17	85	41.79	159	40.97	155.5
18	90	41.78	159	40.91	157.5
19	95	41.55	160	40.53	159
20	100	41.36	162	40.36	161.5
21	105	41.14	162	40.26	162
22	110	40.98	164	40.05	166.5
23	115	40.98	166.5	39.97	163
24	120	40.84	167.5	39.91	165
25	125	40.60	168	39.81	165.5
26	130	40.66	167	39.79	166.5
27	135	40.60	167.5	39.72	168
28	140	40.55	169.5	39.71	169
29	145	40.66	167.5	39.78	168.5
30	150	40.74	167	39.93	168
31	155	40.98	166	40.17	165.5

Table 4.6

Mechanical properties of tensile test piece 8

Test piece location	Plate depth mm	UTS MPa	O.2% PS MPa	Elongation %	Hardness Hv 10	Conduct. % IACS
1	6	538.108	482.3376	12.2037	170	39.72
2	18	530.5977	480.5827	12.8341	174	39.45
3	30	518.2068	467.6686	10.3743	172	39.59
4	42	518.3943	465.0464	11.4329	171.25	39.69
5	54	524.6134	465.8518	3.1907	166.25	40.03
6	66	528.1587	471.2668	6.3974	164	40.62
7	78	523.2226	464.1392	8.3459	160	40.76
8	90	527.1202	469.2275	8.5765	163.25	40.74
9	102	522.3163	462.9197	10.8229	168.25	40.29
10	114	519.8116	465.8433	10.0478	171.75	39.74
11	126	518.9666	467.6108	11.4394	172	39.69
12	138	528.7204	478.8449	10.1989	173.25	39.52
13	150	533.7147	477.4883	12.1884	172.5	39.79

Table 4.7

Mechanical properties of tensile test piece 9

Test piece locations	Plate depth mm	UTS MPa	O.2% PS MPa	Elongation %	Hardness Hv 10	Conduct. % IACS
1	6	538.5239	477.5091	12.5632	172	40.42
2	18	531.3614	479.2471	10.9658	174.5	40.18
3	30	522.5788	471.0835	11.9114	172.5	40.29
4	42	521.5664	467.1235	10.5767	169	40.78
5	54	528.6685	469.8949	8.9789	164	41.14
6	66	534.8448	477.3001	7.6943	165.5	41.24
7	78	528.4593	469.5948	9.1254	159.5	41.34
8	90	538.3787	479.3783	13.9183	165.5	41.19
9	102	529.1253	470.8485	8.5369	168.5	40.78
10	114	527.2493	473.0614	11.6574	170	40.5
11	126	528.368	477.594	11.1364	172	40.25
12	138	532.9723	480.4958	13.3468	174.5	40.18
13	150	529.2444	470.967	10.1614	172.75	40.76

Table 4.8

Mechanical properties of tensile test piece 10

Test piece locations	Plate depth	UTS MPa	O.2% PS MPa	Elongation %	Hardness Hv 10	Conduct. % IACS
1	6	545.63	473.94	13.5	169.5	39.99
2	18	559.03	474.4	12.11	169.5	39.83
3	30	534.3	466.42	10.69	166.25	39.9
4	42	525.64	457.9	9.72	165.25	40.1
5	54	521.19	455.13	8.32	164	40.37
6	66	529.63	461.18	8.17	160	40.66
7	78	524.56	455.58	9.79	158.5	40.8
8	90	529.51	447.93	8.62	159.25	40.71
9	102	530.68	447.47	8.79	161.25	40.28
10	114	529.34	460.85	10.64	164.75	40.07
11	126	537.66	470.92	11.67	168	39.88
12	138	552.35	474.67	12.16	170	39.8
13	150	545.84	472.84	11.76	170.5	40.05

Table 4.9

Mechanical properties of tensile test piece 11

Test piece locations	Plate depth	UTS MPa	O.2% PS MPa	Elongation %	Hardness Hv 10	Conduct. % IACS
1	6	555.5	484.1	9.04	172	40.22
2	18	545.8	479.4	10.12	169.8	40.1
3	30	528	461.9	9.72	166.3	40.22
4	42	523.7	456	9.91	166.3	40.35
5	54	527.7	460	13.97	166.8	40.64
6	66	530.6	462.5	12.32	163.8	40.99
7	78	525.6	458.6	13.34	159.5	41.09
8	90	529	460.8	13.45	159.5	41
9	102	535.8	467	14.13	162	40.63
10	114	535	466.6	12.91	165.5	40.36
11	126	544.3	473.3	12.76	166.5	40.16
12	138	555.5	487.5	13.1	168.8	40.09
13	150	546.9	474.7	14.72	166	40.39

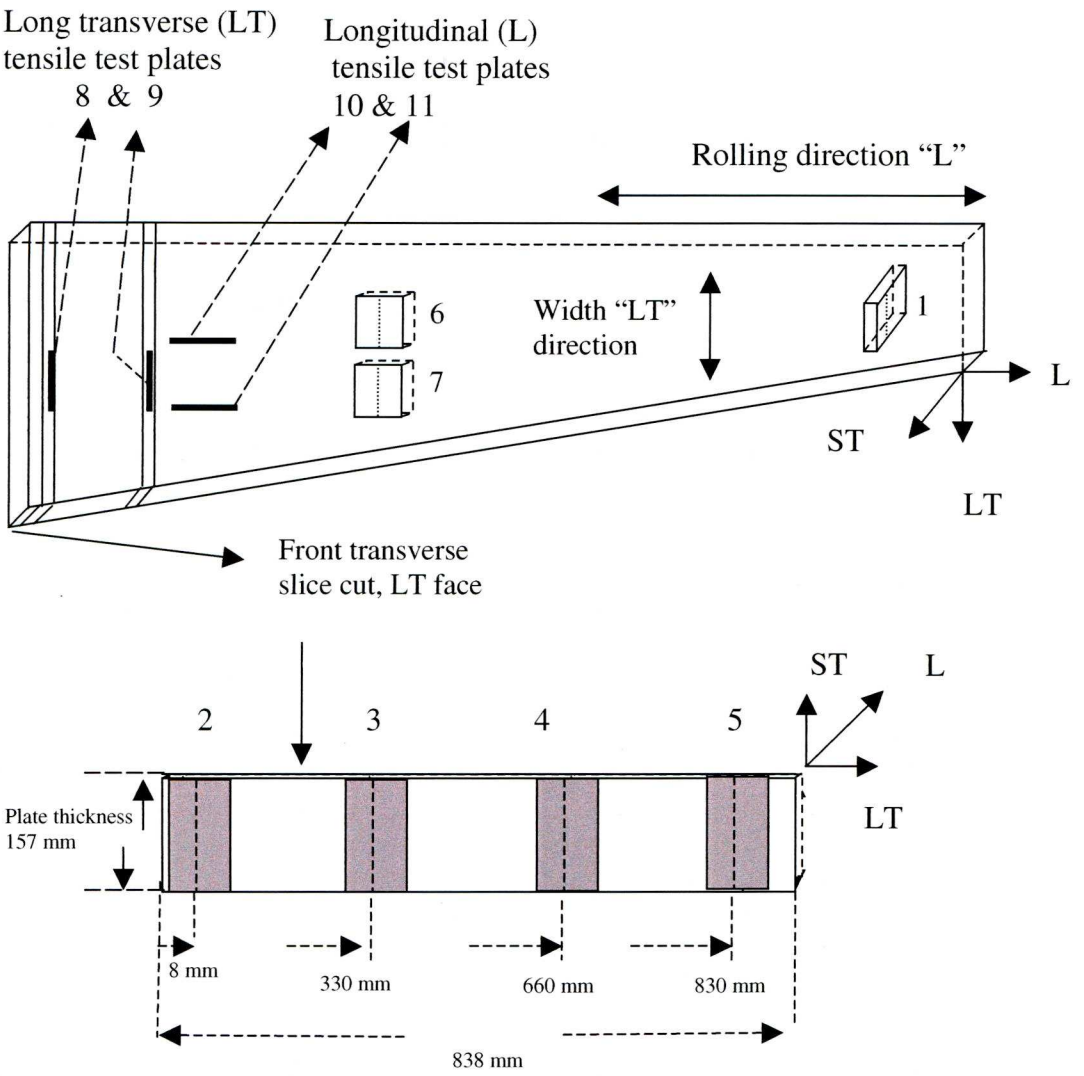

Fig. 4.1 Schematic diagrams indicating the locations and orientations of the test pieces 1-11. The letters L, LT and ST indicate the rolling, long transverse and short transverse directions, respectively.

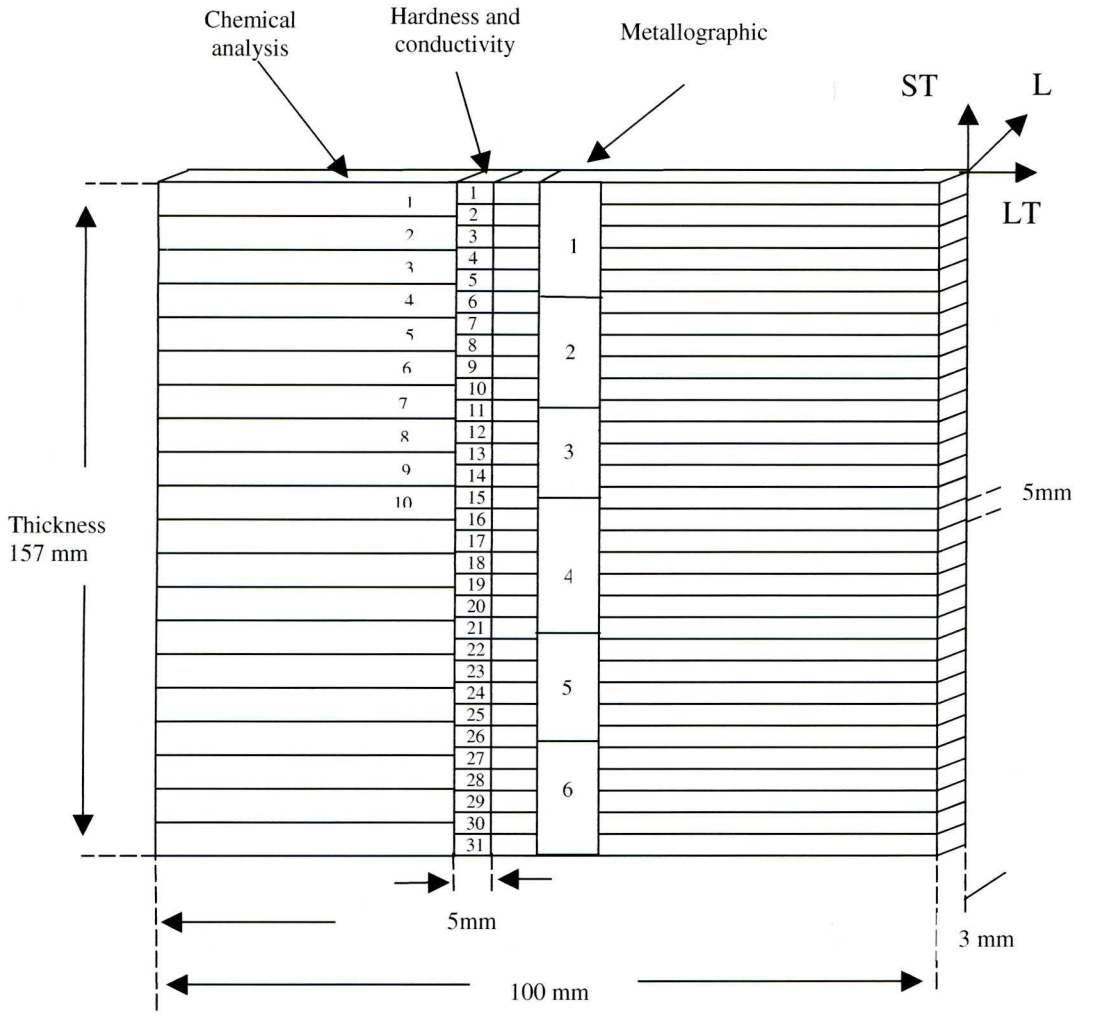

Fig. 4.2 Schematic diagram of test piece 1 showing the locations of the test samples for electrical conductivity, hardness, chemical analysis and metallographic tests. The letters L, LT and ST indicate the rolling, long transverse and short transverse directions, respectively.

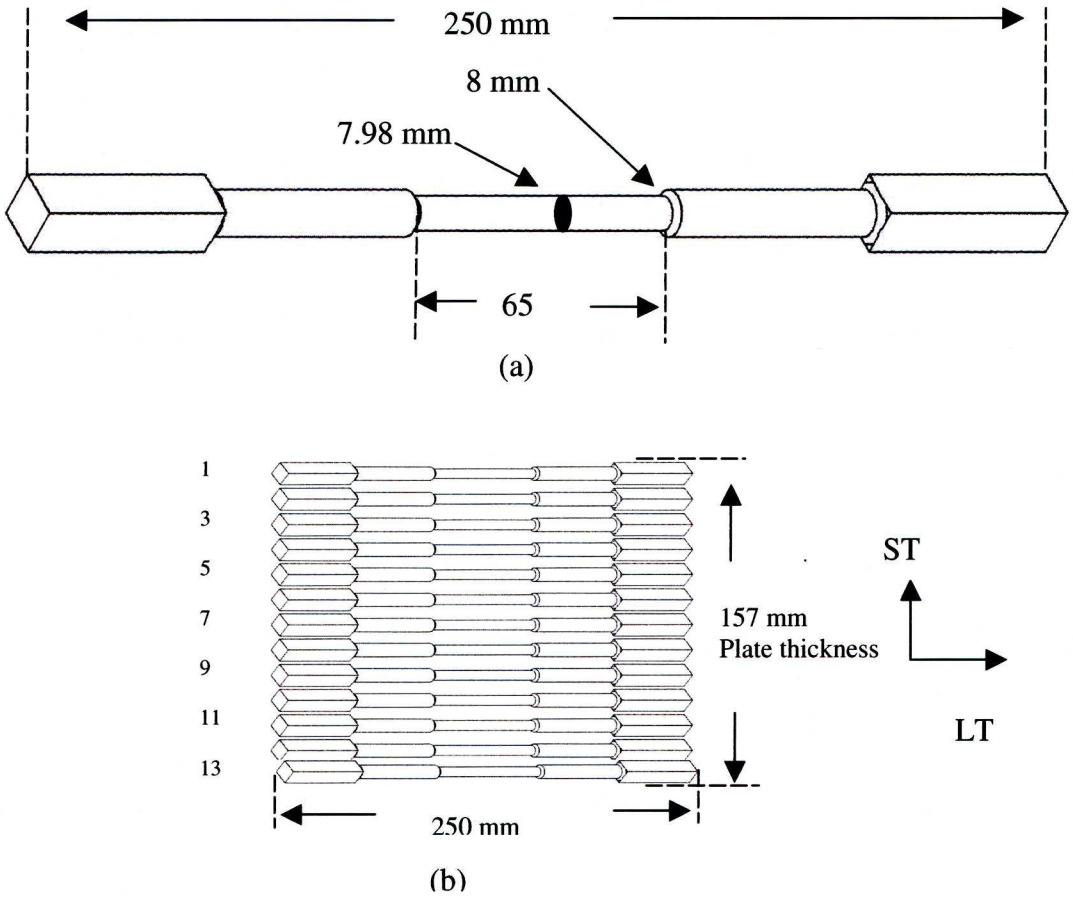

Fig. 4.3 Schematic diagrams showing (a) geometry of a typical cylindrical tensile test sample and (b) the locations of the samples across the plate thickness

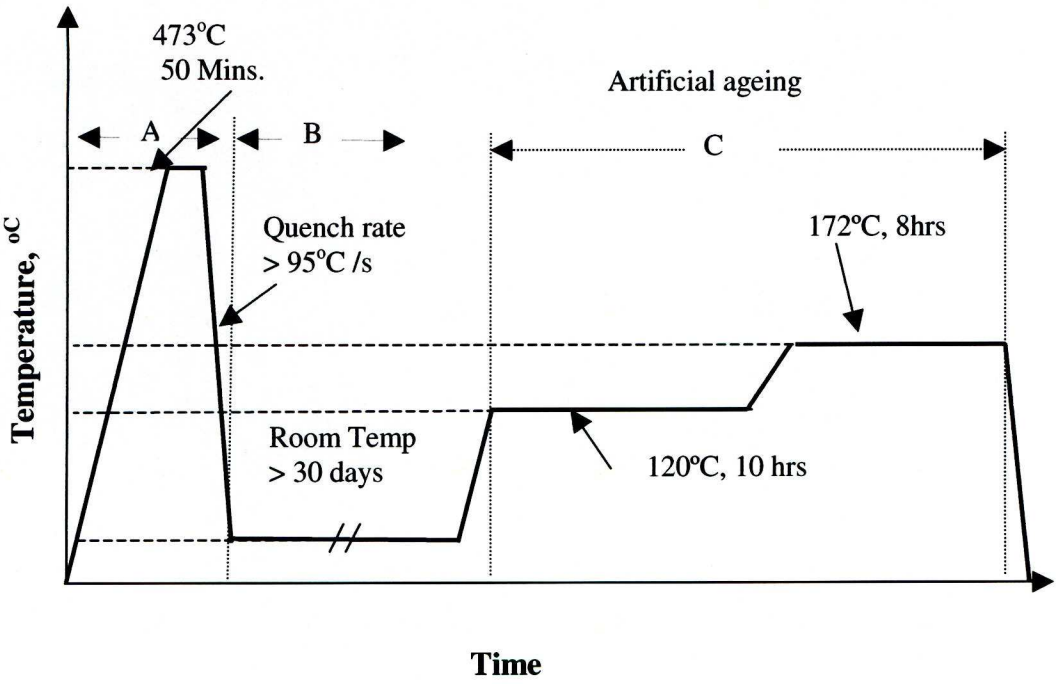

Fig. 4.4 Schematic representation of the re-heat treatment

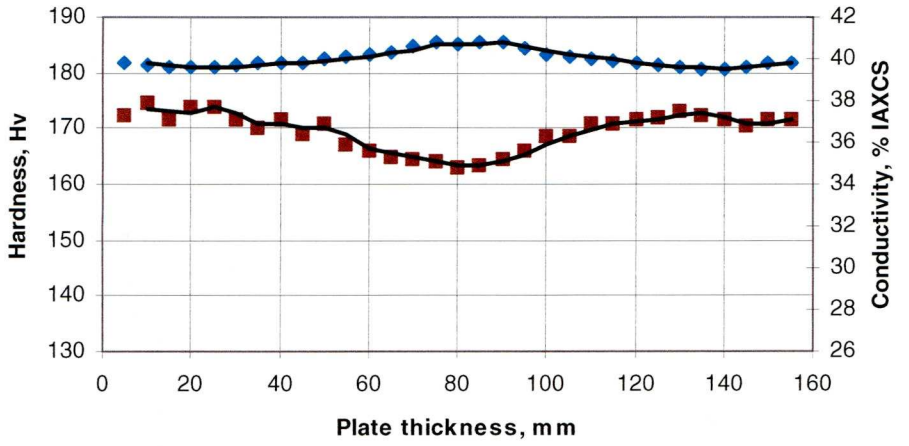

(a)

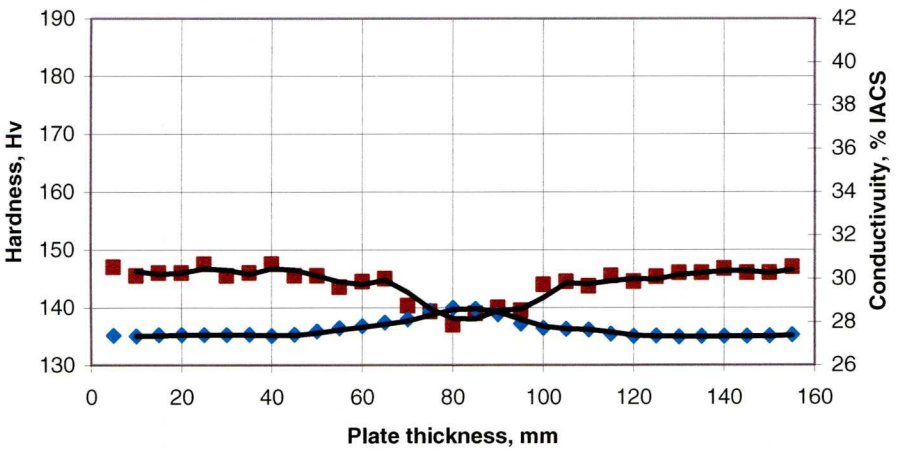

(b)

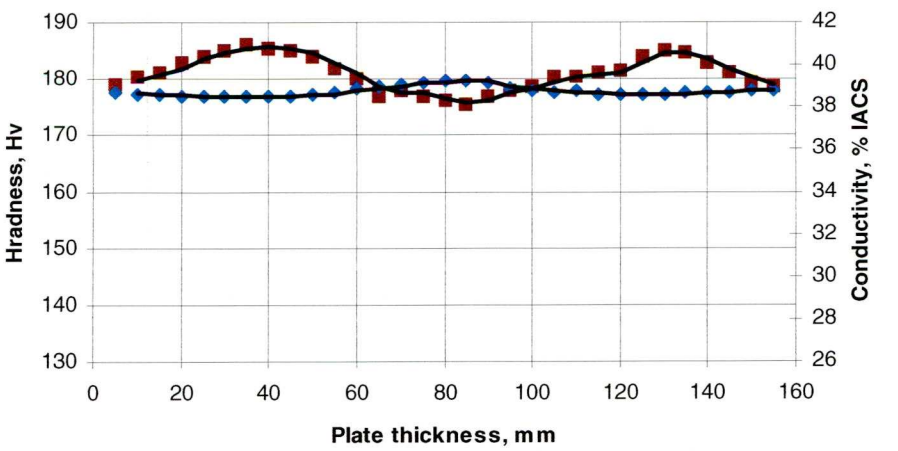

(c)

Fig. 4.5 Variations of hardness (■) and electrical conductivity (♦) across the plate thickness of test piece 1 in three conditions: (a) as received, (b) naturally aged and (c) artificially aged.

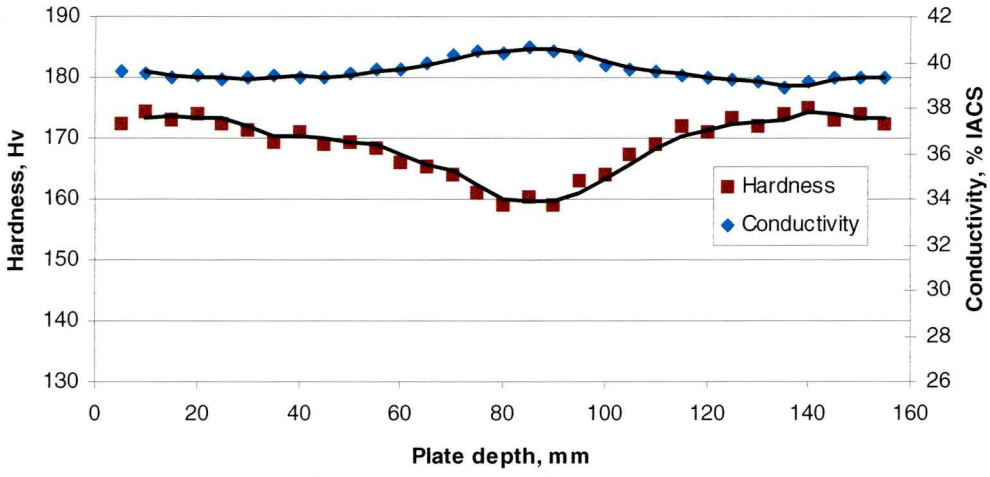

(a)

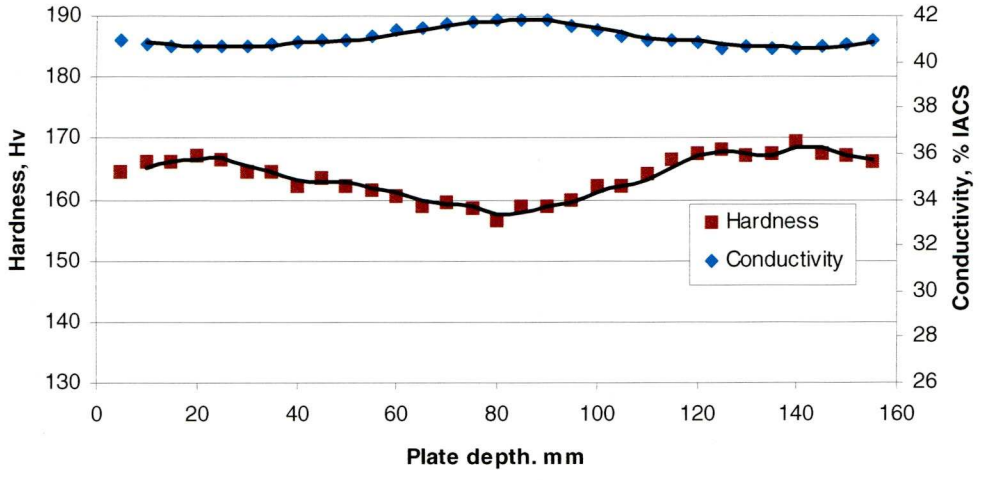

(b)

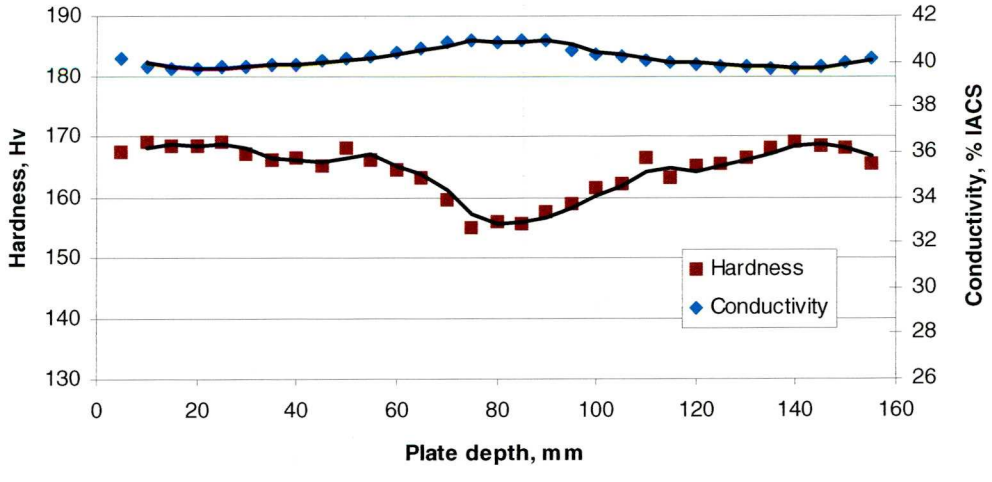

(c)

Fig.4.6 Variations of hardness (■) and electrical conductivity (◆) across the plate thickness in the as received condition in (a) test piece 4, (b) test piece 6 and (c) test piece 7.

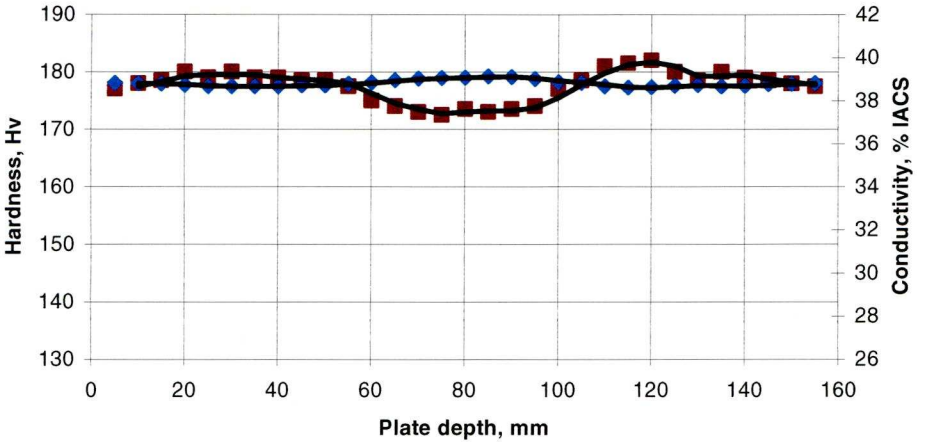

(a)

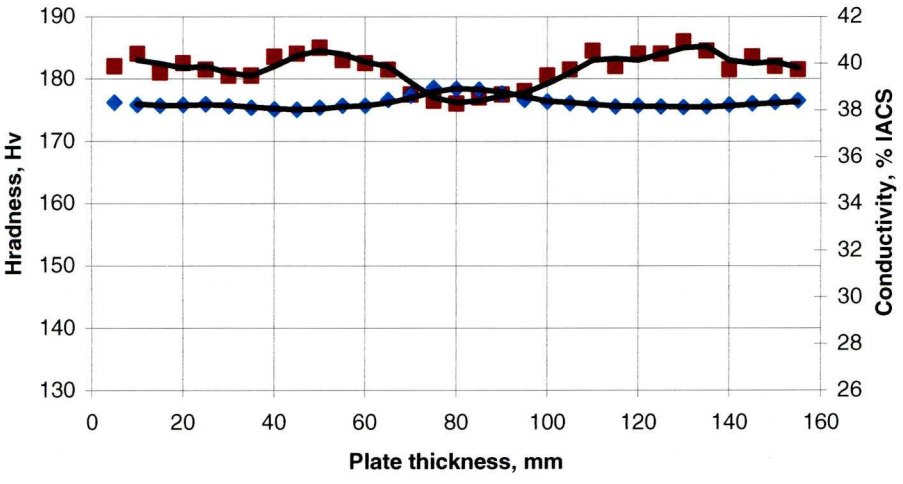

(b)

to be continues

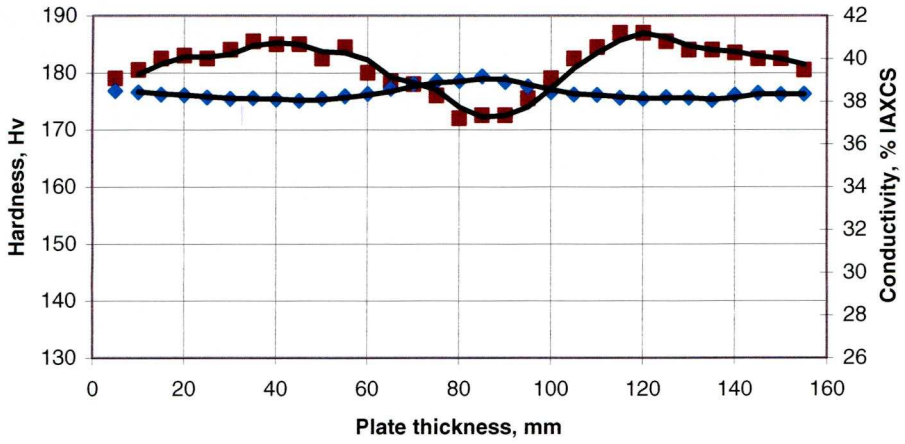

(c)

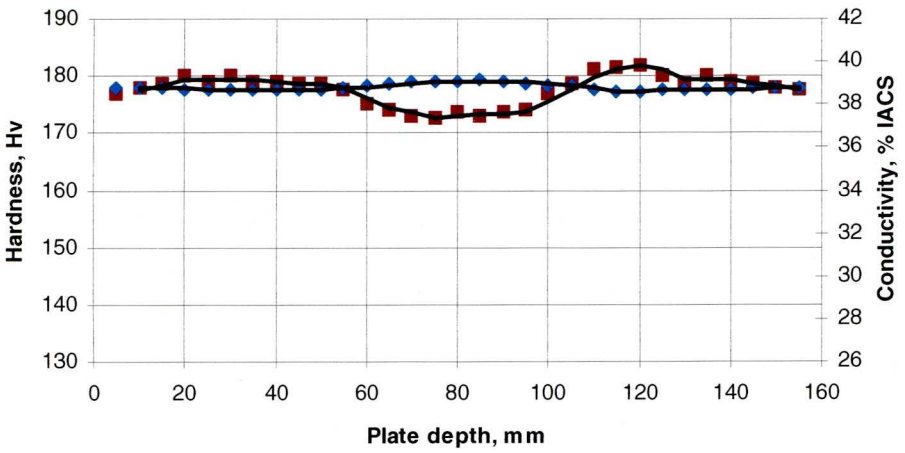

(d)

Fig.4.7 Variations of hardness (■) and electrical conductivity (♦) across the plate thickness in the re-solution heat treated and artificially aged condition in (a) test piece 2, (b) test piece 3, (c) test piece 4 and (d) test piece 5

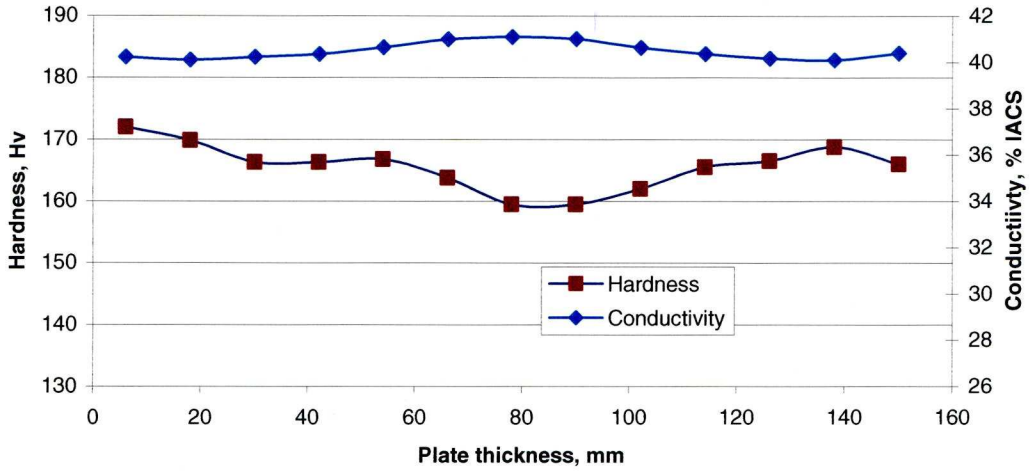

(a)

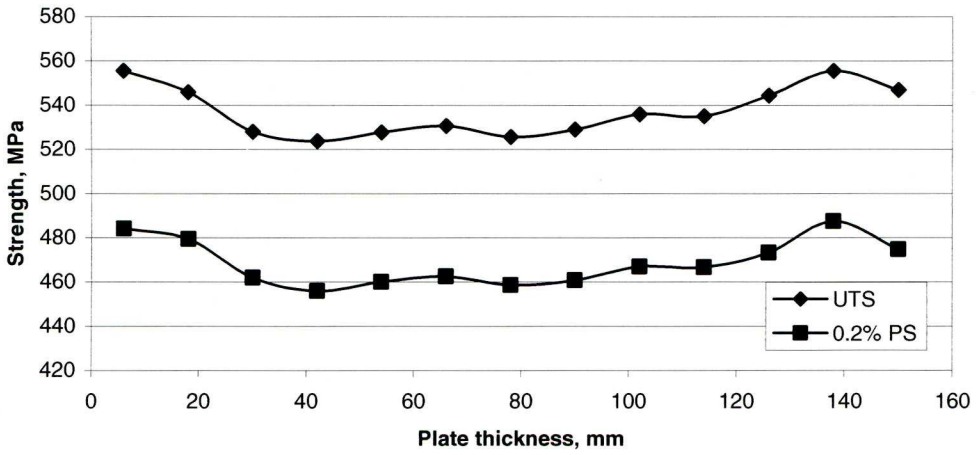

(b)

Fig.4.8 Variations of (a) hardness and electrical conductivity and (b) UTS and 0.2% PS properties with plate thickness in test piece 8

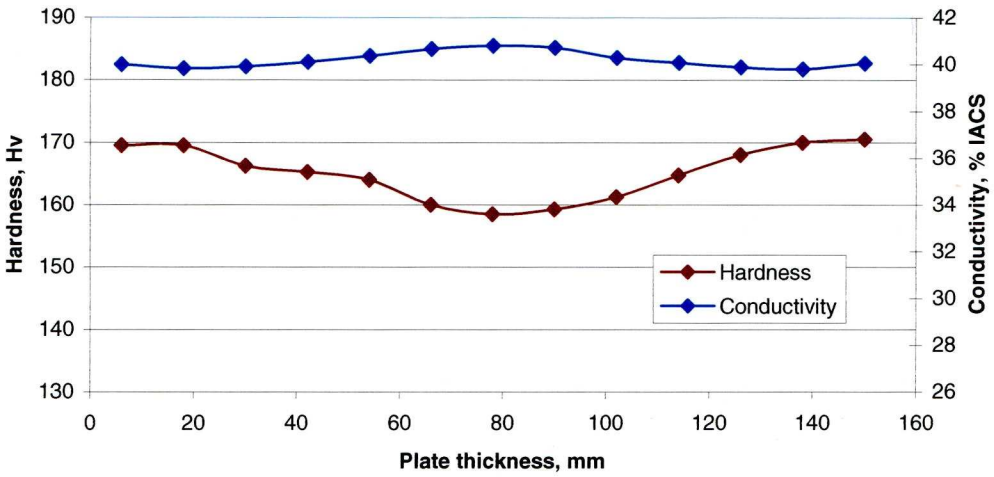

(a)

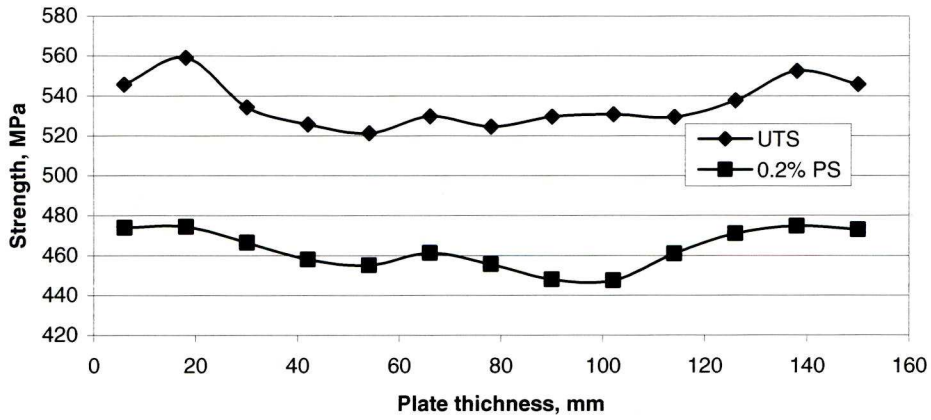

(b)

Fig.4.9 Variations of (a) hardness and electrical conductivity and (b) UTS and 0.2% PS with plate thickness in test piece 9

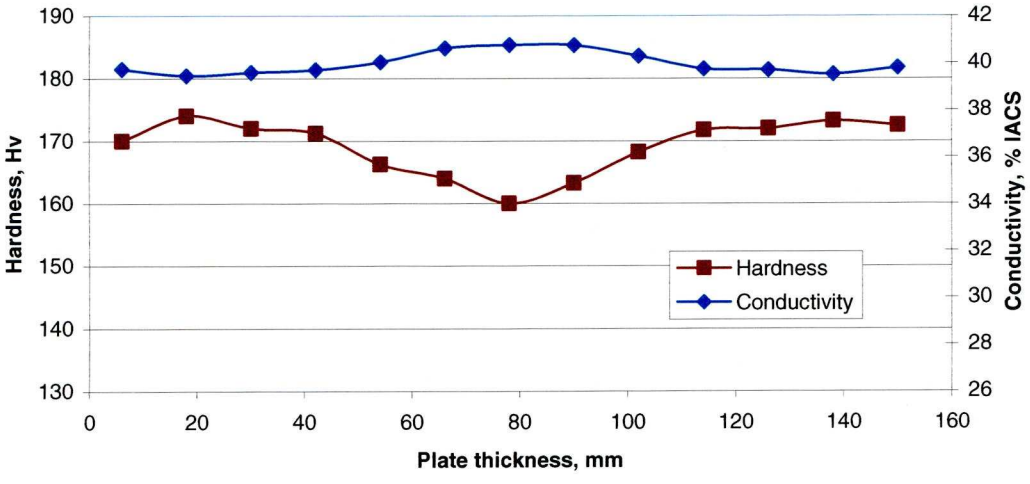

(a)

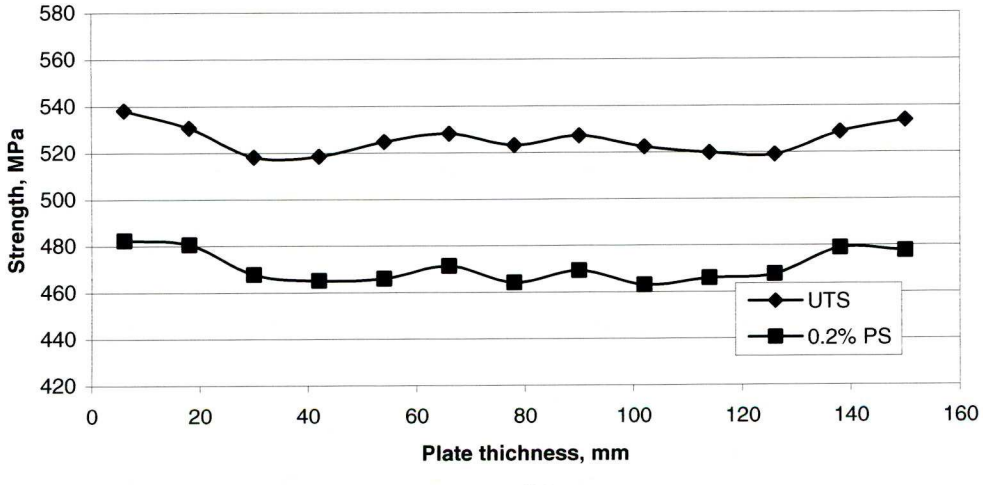

(b)

Fig.4.10 Variations of (a) hardness and electrical conductivity and (b) UTS and 0.2% PS with plate thickness in test piece 10

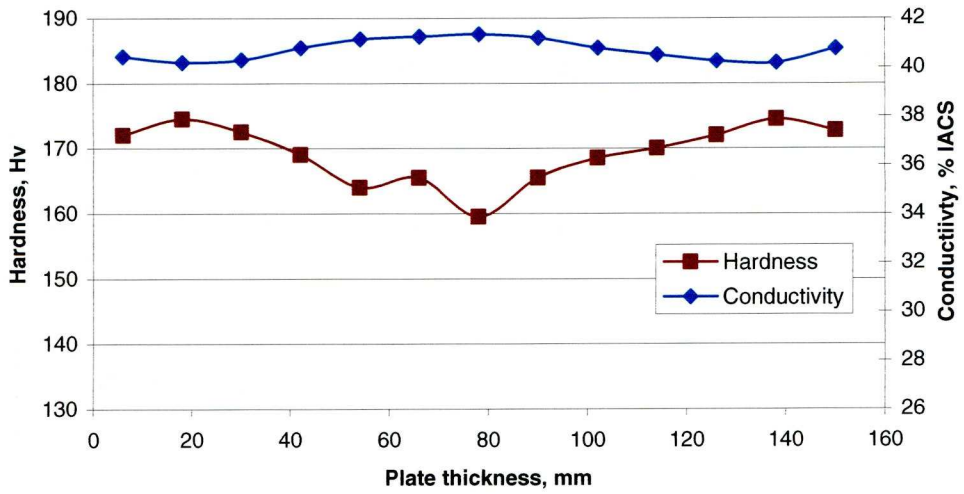

(a)

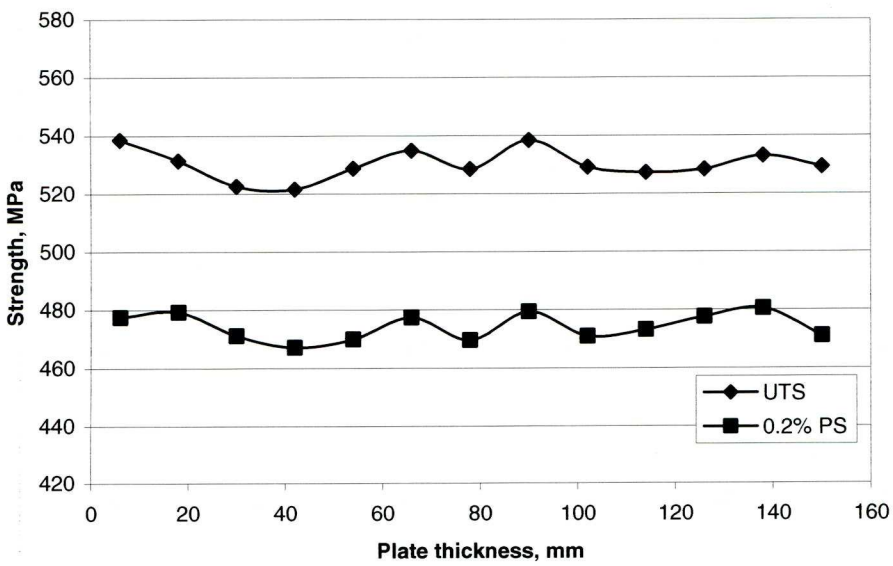

(b)

Fig.4.11 Variations of (a) hardness and electrical conductivity and (b) UTS and 0.2% PS with plate thickness in test piece 11

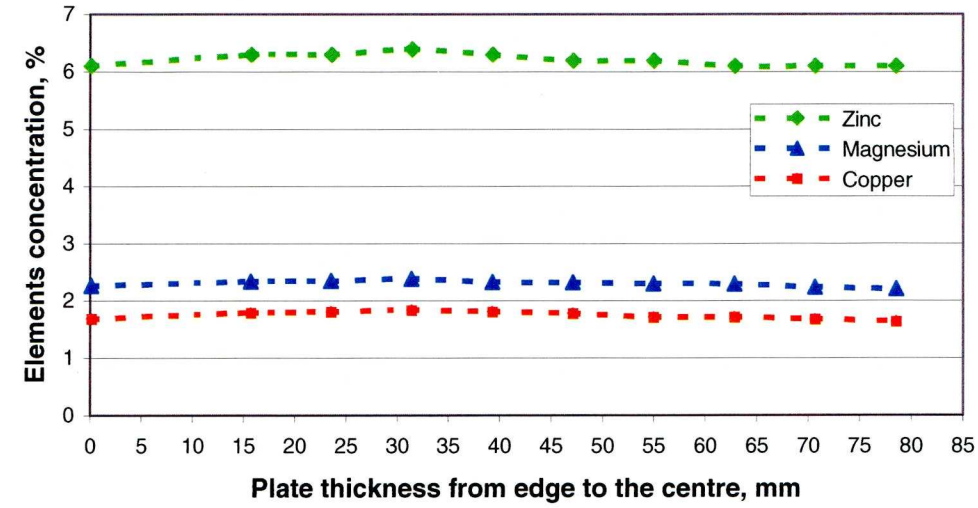

(a)

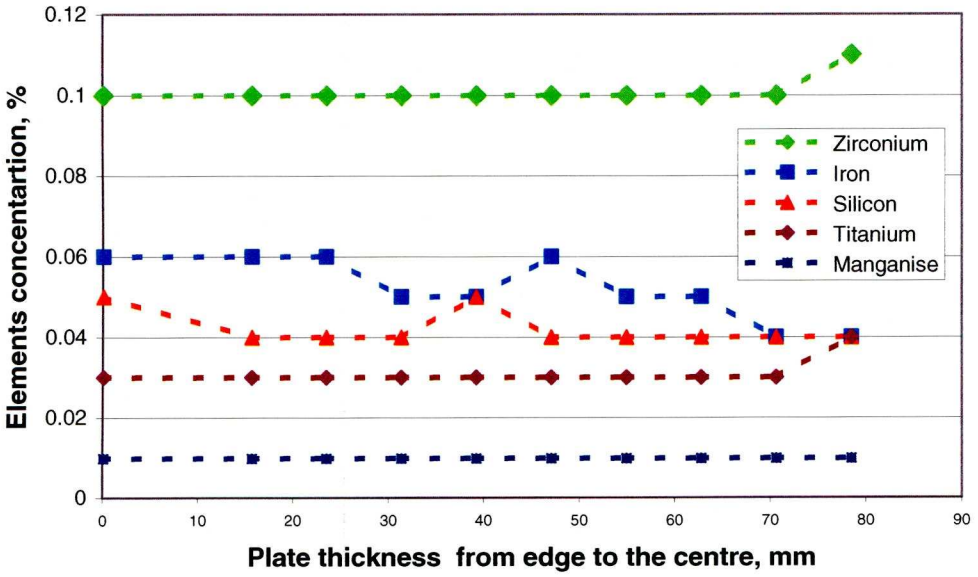

(b)

Fig. 4.12 Variation of chemical composition across half plate thickness: (a) Zn, Mg and Cu; and (b) Zr, Fe, Si, Ti and Mn

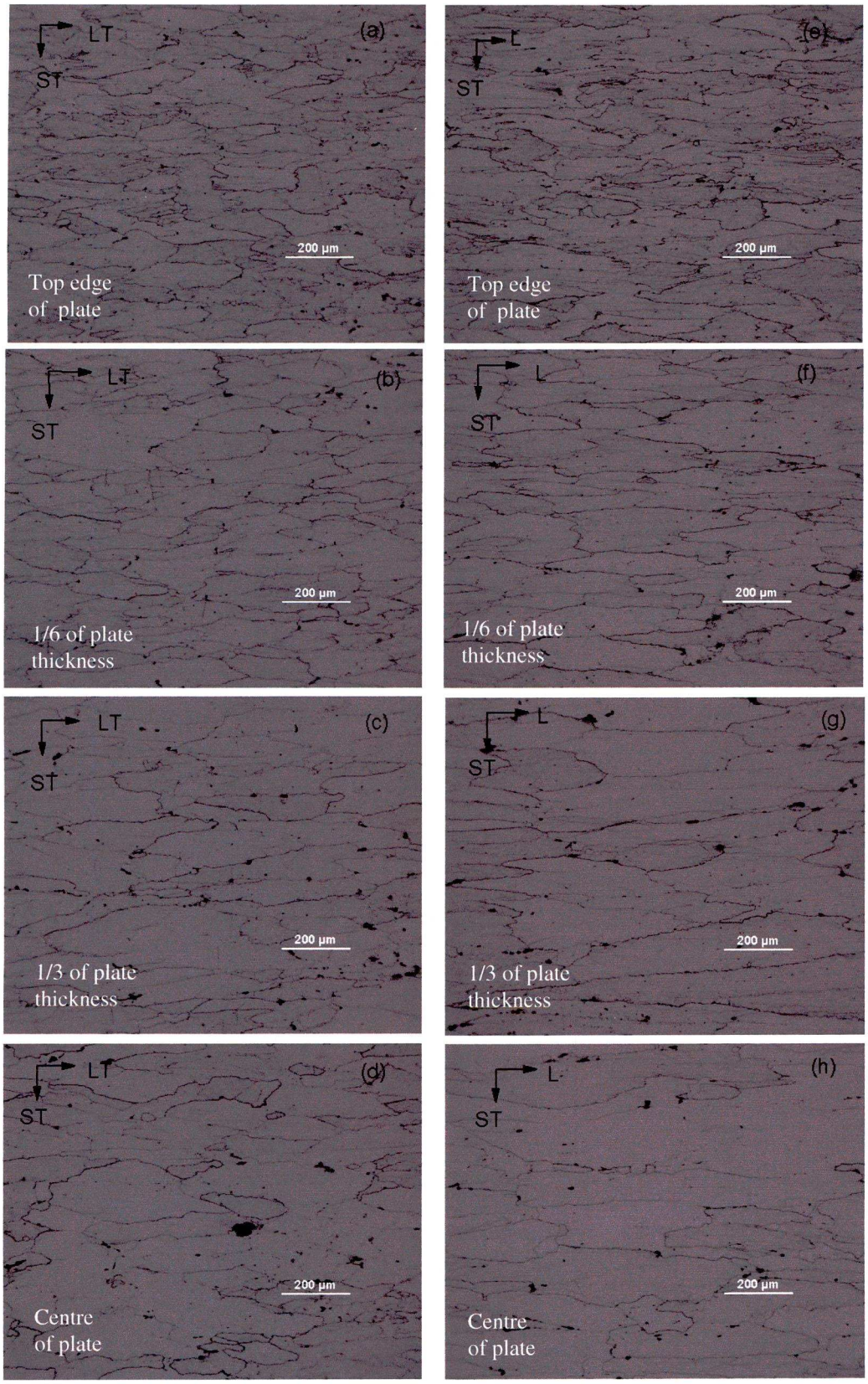

Fig. 4.13 Microstructure of plate at different depth locations: (a - d) perpendicular to the rolling direction, (e-h) parallel to the rolling direction. L, LT and ST represent longitudinal, long transverse and short transverse directions, respectively.

Chapter 5

Effect of quench rate on properties

5.1 Introduction

In solution heat treatment of heat treatable aluminium alloys, all soluble alloying elements are expected to dissolve into the solid solution (Staley *et al.* 1984). The quenching operation will retain these elements in the supersaturated solid solution, provided that the quenching operation is rapid enough to prevent diffusion and precipitation at high temperature. On slow cooling from the solution heat treatment temperature, however, the alloying elements will start to precipitate heterogeneously at a temperature just below the solvus at locations of easy nucleation, for example, grain boundaries (Reed – Hill 1991). The alloying elements precipitate out of solution and form stable or equilibrium precipitates, which are coarse particles and non-coherent with the matrix. In this case, nearly all of the solute finds its way to the second phase at the grain boundaries (Reed – Hill 1991). The solute concentration in the matrix is continually reduced. Therefore, the alloying elements will be unavailable for strengthening (Aluminium Association Inc. 1982).

In AA 7010, zirconium is added to control the grain size and to lower the quench sensitivity. The low quench sensitivity makes this high strength aluminium alloy particularly suitable for thick plates and large forgings (Reynolds 1976, Martin 1998). At low artificial ageing temperatures, the precipitation in AA 7010 is predominantly homogeneous. However, heterogeneous formation of quench-induced precipitates can also occur when there is a slow or sluggish cooling during quenching

(Godard 2002). The heterogeneous equilibrium precipitate phase (η) nucleates on dispersoids and at grain boundaries (Staley *et al.* 1984). The temperature range for rapid formation of η precipitates was determined to be from 350 to 250°C (Goddard 2002). For most aluminium alloys the temperature range where quench rate is critical is approximately 400 – 290°C (Staley *et al.* 1971).

Natan and Chihoski (1983) reported that when a sub-standard quench delay operation was employed for AA 2219, quench-induced precipitates were formed and coarsened, leading to low hardness and high electrical conductivity. The effect was found to be associated with increasing amounts and sizes of primary θ' and θ, developed during quenching. These high temperature precipitates were minimised by faster quenching.

After the quenching operation, the maximum strength attained upon artificial ageing largely depends on the amount of alloying elements retained within the solid solution, or on the initial amount of quench-induced precipitates developed during the quenching operation. The quenching operation following the solutionising treatment is therefore considered to be one of the most critical steps in the manufacture of high strength aluminium alloys.

This chapter reports the study on the effect of quenching rate on the properties of AA 7010, including electrical conductivity, hardness, UTS and PS.

5.2 Experimental

5.2.1 Test Pieces

The material assessed in this investigation was an AA 7010 plate with the T7651 temper condition. The details of the thermo-mechanical manufacturing route, the dimensions and the chemical composition of the plate were specified in section 3.2.1.

The test pieces for electrical conductivity, hardness and tensile tests were manufactured from a location near the wide end of the plate, as shown in Fig. 5.1. From this location, a number of slices (11 mm thick), which were perpendicular to the rolling direction, were saw-cut. Each slice was further cut along the long transverse direction into thirteen rectangular bars, representing different depths across the plate thickness, with bars No 1 and 13 representing the outside areas of the plate and bar No 7 representing the centre of the plate. From each bar, a number of test blanks were cut to length, to approximate dimensions of 11×11×228 mm.

The test blanks were then machined to tensile test pieces with a cylindrical gauge length and square ends, as illustrated in Fig. 5.2. The tensile test specimens were machined to be consistent with requirements of British Standard BS 4A – 4 (1966), with a diameter of 7.98 mm, a minimum parallel length of 65 mm, a gauge length of 40 mm and a minimum transition radius of 8 mm. The electrical conductivity and hardness of the test pieces were first measured before tensile testing.

5.2.2 Thermal Treatments

Seven groups of tensile test pieces, 31 in each, were thermally treated. Fig. 5.3 shows the applied thermal treatments, which consisted of solution heat treatment,

cooling in air at different cooling times followed by quenching, natural age hardening at room temperature and artificial age hardening at various temperatures and ageing times. Each group of test pieces was solution heat treated in an individual run. In each run, six thermocouples (type K) were attached to the middle of the six test pieces, as illustrated in Fig.3.3, so that the cooling history was monitored and recorded.

Fig. 5.4 shows the cooling curves for the seven groups of test pieces. Each group of test pieces was first solution heat treated at 475°C for 75 minutes. Afterwards they were removed from the furnace and allowed to cool in air for a different delay time and then fast quenched in water at room temperature. The cooling delay times of the first six groups were 3, 71, 113, 198, 474 and 813 seconds, corresponding to pre-quenching temperatures of ~475, 394, 363, 324, 240 and 200°C, respectively. The cooling condition of the group with a delay time of 813 seconds was slightly different from the others. Instead of cooling in air at room temperature, the cooling was performed with the test pieces placed on the heat treatment rack and covered with a metal hood, so that a lower cooling rate before quenching was maintained. The last group of test pieces were cooled in air to room temperature without quenching.

The seven groups of test pieces were then all allowed to naturally age hardened at room temperature for more than 30 days, as illustrated in Fig. 5.3. These test pieces were split into 31 sets, each of which contained one test piece from each of the seven groups. The test pieces in each set represented different cooling delays as illustrated in Fig. 5.4, i.e. 3, 71, 113, 198, 474 and 813 seconds plus complete air-cooling. All

the 31 sets of test pieces were then artificially aged, with each set representing a different condition. The full cycle of the artificial age hardening treatment, as indicated in Fig. 5.3, was 120°C for 10 hours, 172°C for 24 hrs, 190 C for 4 hrs and 200°C for 12 hrs. During each artificial ageing temperature stage, several sets of test pieces were removed from the ageing furnace, each at a different time interval. Eight sets of test pieces were removed from the furnace at 120°C, nineteen sets at 172°C, one set at 190°C and three sets at 200°C. By removing a set of test pieces at a different time at each ageing temperature, a wide range of ageing conditions could be studied. Table 5.1 summarises the age hardening treatments for the 31 sets of test pieces, including the ageing temperatures and the ageing times at these temperatures. A set of test pieces without any artificial ageing is also included and designated as Set 0.

Hardness and electrical conductivity tests were performed on the test pieces immediately after the artificial age hardening treatment in order to avoid any possible secondary ageing. The test pieces were then left at room temperature for around nine months. Hardness and electrical conductivity tests were performed again, followed by tensile testing.

5.2.3 Electrical Conductivity

The electrical conductivity measurements were carried out using a Forster SIGMATEST Ec 2.068 electrical conductivity meter. These measurements, which are based on the eddy current method, were performed in compliance with the Airbus UK process specifications (Airbus UK 2005). The precautions taken to minimise any possible error during the electrical conductivity measurements have already been

discussed in section 3.2.4.

5.2.4 Hardness

The hardness measurements were carried out using a Vickers HTM 8313 hardness tester with a 10kg load. The measurements were performed in compliance with Airbus UK process specification (Airbus UK 2004a) and BS ES ISO 6507-1 (2006). Calibration of the hardness tester, standard reference blocks and the stage binocular microscope was performed to the respective British standard and with traceability to the National Physical Laboratory. Details of this and the precautions taken to minimise any possible error during hardness testing have already been discussed in section 3.2.5.

5.2.5 Tensile Testing

Mechanical testing was performed using a Denison Mayes Group testing machine, model 6157. The tensile test machine worked with a 100 KN servo-hydraulic load frame and was fitted with an IBM stem/2 and a 50 mm gauge length extensometer 7609 DC1/7902 DC2. The tensile tests were carried out at a strain rate of 4×10^{-3} s^{-1} in compliance with British standard BS 4A – 4 (1966). The details of calibration of the load cell and extensometers and the precautions to minimise any possible errors during tensile testing have already been discussed in section 3.2.6.

5.3 Results

5.3.1 Numerical data

The numerical values of electrical conductivity and hardness for the test pieces with different quench delays, measured immediately after the artificial ageing treatment,

are compiled in Tables 5.2. The numerical values of electrical conductivity and hardness together with mechanical properties for the test pieces with different quench delays, measured nine months after the artificial ageing treatment, are compiled in Tables 5.3 to 5.9.

Comparing the electrical conductivity and hardness values measured immediately and nine months after the artificial ageing treatment shows that they do not change very much. This indicates that secondary ageing is insignificant.

5.3.2 Variation of hardness and electrical conductivity

Fig. 5.5 shows the variations of hardness and electrical conductivity, measured immediately after the artificial ageing treatment (Table 5.2), with artificial age hardening for the seven groups of test pieces with different quench delays. The hardness and electrical conductivity are sensitive to changes of cooling rate and artificial age hardening condition. Both hardness and electrical conductivity gave similar trends of response for different quench delays. However, the values of the properties were very different between the different quench delays. The salient points evident from Fig. 5.5 are described as follows.

After having been solution heat-treated and naturally aged but before the artificial age hardening, the test pieces with different quench delays showed distinct differences in the electrical conductivity and hardness values. The group of test pieces with the shortest quenching delay exhibited the lowest electrical conductivity and the highest hardness values. On the other hand, group of test pieces with the longest quench delay showed the highest electrical conductivity and the lowest

hardness values. In general, decreasing quench delay, i.e. increasing cooling rate, reduces the electrical conductivity values and increases the hardness values.
The groups of test pieces with short quench delays (3 to 198 seconds) showed a typical response of age hardening of aluminium alloys. Generally, the hardness increased rapidly with increasing ageing time and temperature. The increasing trend in hardness was maintained until the ageing temperature changed from 120 to 172°C, at which a sudden drop was experienced in all the ageing curves. The drop in hardness is believed to be inherent from a retrogression effect of GP zones or fine precipitates formed during the first stage of artificial ageing at 120°C . This drop was immediately followed by a second rapid increase in hardness trend up to the peak hardness. There was a short plateau around the maximum hardness on each curve. Following this plateau region was the onset of over ageing and the hardness experienced the downward trend.

The groups of test pieces with long quench delays (474 to 813 seconds) showed different behaviour. Although the hardness also increased with ageing time and temperature, their curves exhibited three drops in hardness. In addition to the hardness drops at the ageing temperature change from 120 to 172°C and the onset of over ageing, there was a hardness drop at the beginning of the artificial age hardening at 120°C. This additional drop (first drop) was also due to the retrogression effect of GP zones and fine precipitates formed during cooling and during the first stage of artificial ageing at 120°C.

Upon artificial ageing, the electrical conductivity increased with increasing age hardening time and temperature for all quench delays. As ageing progressed, the

difference in electrical conductivity between the curves became smaller, especially so towards the end of the over ageing region, when the equilibrium steady state condition was approached.

When the test pieces were artificially age hardened up to the material specification requirements (120°C for 10 hrs followed by 172°C 8 hrs) (Airbus UK 2003), satisfactory values of hardness and electrical conductivity were obtained for all the curves with quench delays between 3 and 198 seconds. The results indicate that a wide range of quench delays or cooling rates are allowed for AA7010 test pieces with a limiting ruling section less than 11×11 mm^2.

For the same artificial age hardening treatment, different quench delays resulted in different responses of hardness and electrical conductivity values to the ageing condition. The hardness-conductivity curves in a wide range of ageing conditions thus formed a network. From a combination of hardness and electrical conductivity values, it is possible to identify a unique approximate temper condition from this network of curves. In other words, the combination of hardness and electrical conductivity can be used as a non-destructive inspection tool for thermal treatment quality.

5.3.3 Variation of strength

Fig. 5.6 shows the correlation of hardness with strength for all the test pieces with seven different quench delays. There was a good linear correlation of hardness with both UTS and PS, with the correlation coefficients of $R^2 = 0.96$ and $R^2 = 0.94$ respectively. The fitted lines for UTS and PS had different gradients of 2.43 and 3.10

respectively, indicating different responses of these properties to the age hardening process. It was also clear from Fig. 5.6 that both UTS and PS increased with decreasing quench delay time.

5.4 Discussions

5.4.1 Precipitation during quench delay

The metallurgical mechanisms involved in solution heat treatment, quenching and subsequent age hardening for aluminium alloys are summarised in Sections 2.3 and 2.5. It is a well-known fact that heterogeneous precipitation can develop in aluminium alloys during quenching. The impact of this precipitation on mechanical properties after ageing has been widely studied (Evancho and Staley 1974). For example, 7000 series alloys generally require a rapid quench to prevent heterogeneous precipitation from occurring at elevated temperatures, which can lead to a reduction of strength after age hardening (Hughes *et al.* 1984).

For the Al-Zn-Mg-Cu alloy, extensive nucleation of precipitates occurs during slow quench (Deschamps 1998, Godard 2002). The quench-induced precipitates form mainly on zirconium containing dispersoids. This results in a decrease of the solute available for the fine-scale precipitation during ageing and therefore a reduction in hardness and an increase in electrical conductivity. For AA 7010, it is also expected that the increase in the amounts and sizes of high temperature precipitates during quenching will lead to a decrease in hardness and an increase in electrical conductivity. Similarly, the opposite effect is expected when the amount and size of these incoherent precipitates are diminished by faster quenching.

Indeed, Fig. 5.5 shows that the hardness and electrical conductivity values are sensitive to the changes of quench delays. The differences in hardness and electrical conductivity between the test pieces with different quench delays can be attributed to the differences in the heterogeneous quench-induced precipitates formed during cooling and the homogeneous precipitates formed during artificial age hardening. The contribution from excess vacancies can be important with fast quench or short delay conditions (Kelly and Nicholson 1963).

During cooling from solution heat treatment temperature, various amounts of alloying elements can diffuse away from the solid solution to form precipitates. The concentration of alloying elements remaining within the solution in turn depends on the extent of diffusion that takes place during cooling, which is a function of temperature and time (Reed Hill 1973, Askeland 1992). The extent of retained quench-in vacancies during the cooling is also related to the cooling path. It is well established that rapid quenching of heat treatable aluminium alloys from the solution treatment temperatures leads to a concentration of excess vacancies in the as quenched materials (Kelly and Nicholson 1963, Bergner 1995). Therefore, the thermal history of cooling from the solution treatment temperature to room temperature has a strong effect on the formation of both quench-induced precipitates and vacancies. The effect of quench delay on the properties of the test pieces can be explained based on this effect.

5.4.2 Electrical conductivity

The electrical conductivity of aluminium alloys is mainly determined by the distribution of the alloying elements in the alloys. Alloying elements affect the

electrical conductivity more when they are in solid solution than when they are precipitated (Morris *et al.* 1984). The lower the impurity within the solid solution, the higher the electrical conductivity and vice versa. For each curve in Fig. 5.5, the electrical conductivity increases with ageing temperature and ageing time, because of the reduced alloying element in solution accompanying the precipitation. Under the same ageing condition, the difference in electrical conductivity between the curves, as shown in Fig. 5.5, is a consequence of the initial different levels of alloying elements within the solid solution prior to ageing, which is inherent from the cooling path of the quenching operation. In other words, significant differences in alloying element concentration within the solid solution must have existed between the test pieces with different quench delays.

Fig. 5.5 shows that there is a significant difference in electrical conductivity between the 7 groups of test pieces before artificial ageing. Because the natural ageing process was the same for all sets of test pieces, the difference in electrical conductivity between the test pieces with different quench delays can only be inherent from two conditions: different concentrations of solute alloying elements and quench-in vacancies within solid solution before ageing; and different concentrations of primary dispersoids inherent from the manufacturing history of the plate. As the seven groups of test pieces were taken from different locations of the plate, the amounts of primary dispersoids were likely to be slightly different among the seven groups of test pieces, especially at the plate centre where high concentrations of Zr and Ti elements were determined. However, this effect is considered to be small. The main cause is believed to be the different concentrations of solute and quench-in vacancies simultaneously induced in the test pieces when

they were exposed to different cooling paths before quenching.

The progressive increase of electrical conductivity with artificial age hardening is a function mainly of the purification effect of the solid solution (Morris *et al.* 984). The relatively fast increase in electrical conductivity following the increase of ageing temperatures from 120°C to 172°C is likely to be an effect of the initially high concentration of vacancies, which are in equilibrium with the previous temperature. Diffusion of alloying element during precipitation age hardening can be enhanced by the presence of high-concentration quench-in vacancies, which quickly decrease with increasing ageing temperature and ageing time (Morris *et al.* 1984).

With increasing artificial ageing time, the differences in electrical conductivity between the seven curves became smaller. This is because, as precipitation age hardening progresses with time, less alloying elements are left in solid solution and the difference in the amount of alloying elements in solid solution between the seven groups also becomes smaller. When the equilibrium steady state condition is attained at the end of the over ageing condition, the concentration of alloying elements in the solid solution will not change and the conductivity will remain constant (Reed Hill 1991). In theory, there should be little difference between the seven groups of test pieces. Any difference in electrical conductivity between the curves in the steady state condition is most likely due to the slightly different nature of the precipitates formed during high temperature precipitation and the inherent segregation or texture from solidification.

5.4.3 Hardness

Like electrical conductivity, the variation of hardness under normal age hardening conditions is also a function of the kinetics of precipitation of the aluminium alloy. Because of the same underlining mechanisms, the variations of hardness and electrical conductivity are often related, as discussed before in Section 4.4.2. Under normal age hardening conditions, the effect of quench delay on hardness evolution is reciprocal to that on electrical conductivity, as shown in Fig. 5.5. This can be explained in a similar way as in the previous section for electrical conductivity.

The hardness of the seven groups of test pieces with different quench delays responded with a similar trend as age hardening progressed with time and temperature, as shown in Fig. 5.5. However, there are considerable differences in hardness response between the curves. Because the natural and artificial ageing conditions were identical for all the different quench delay curves, the differences in hardness values attained are inherent of the initial differences of alloying elements and quench-in vacancies within the solid solution after the quenching operation. Fast quenching leads to higher contents of alloying elements and quench-in vacancies within the solid solution, which promote the formation of a large volume of fine-scale η' precipitates during artificial ageing. As a consequence, there is a higher hardness response during ageing. For long quench delays, i.e. slow quenching, the reverse was observed.

The curves with short quench delays showed a fast response of hardness at the early stages of artificial ageing at 120°C and when the temperature changed from 120 to 172°C. The fast responses appear to be the effect of the high level of solute elements

and excess of quench-in vacancies within the solution, which promoted a fast precipitation age hardening reaction. It is well known that diffusion of alloying element during precipitation age hardening is enhanced by the presence of high contents of quench-in vacancies (Staley *et al.* 1984). Early research postulated that vacancy concentration might aid the precipitation hardening process at low temperatures by binding with solute atoms or solute-vacancy clusters and zones (Federighi and Thomas 1962). More resent work (Bergner 1995) confirmed this theory in aluminium, where diffusion is predominantly supported by the single vacancy mechanisms.

The fast response in hardness is not observed on the curves with long quench delays. This can be explained by the presence of low solute elements and low vacancy concentration within the solid solution before ageing. The low solute content is a result from heterogeneous precipitation of solute elements at point defects during slow cooling from the solution treatment temperature. Another cause for the low vacancy content is that excess vacancies anneal out by migrating to the vacancy sinks such as grain boundaries and dislocations (Hirsch *et al.* 1958).

For curves with long quench delays (474 seconds, 813 seconds and complete air cooling in Fig. 5.5), the hardness decreased instead of increased with increasing ageing time at the start of the artificial ageing at 120°C. This notable anomaly in hardness evolution is due to the effect of the retrogression phenomenon, which is the reversion or dissolution of the strengthening precipitates and the relaxation of the associated strain fields. The retrogression process leads to loss of hardness and an overall increase in electrical conductivity.

In slow cooling, an unexpected age hardening effect could have occurred when the temperature dropped to the range of approximately 240 to 200°C. During this temperature range, homogeneous or coherent precipitation took place, slightly strengthening the matrix. This view is supported by previous work of Tanner (2004), which showed that age hardening can occur during slow cooling in AA 7010 when the temperature falls to the age hardening temperature range. Coherent precipitates η' and s' have been reported to be present in AA 7010 in the 240 – 200°C temperature range (Godard 2002). The s' which is the precursor of the equilibrium S phase is orthorhombic with a chemical composition close to Al_2CuMg.

At the beginning of artificial ageing at 120°C, the strengthening precipitates formed during cooling before the final quenching are relatively small due to a short ageing time (Reed Hill 1973). These small and coherent particles can re-dissolve back to the solid solution, removing the related strain field. This is supported by the work of Bartŭska *et al.* (1979) for Al-Zn alloys that metastable transition phases precipitated and grown to various sizes at 200°C can decompose at room temperature ageing.

Retrogression largely follows the inverse process of the formation of the GP zones (Shimizu and Kimura 1969). When the temperature is increased from room to artificial ageing temperature, the stability of the GP zones or the strengthening precipitates is dependent on the particle size or the length of ageing at the previous temperature. The time for the dissolution of particles during reversion seems to depend upon the previous ageing conditions. The longer the age hardening at a given temperature, the more stable the GP zone or fine precipitates formed will be at the new ageing temperature.

The sudden drop in hardness when the ageing temperature was increased from 120°C to 172°C is also a consequence of the dissolving of the smaller strengthening GP zones and precipitates. The smaller the GP zones, the more thermally unstable they will be at the new increased temperature. The dissolution of these precipitates is accompanied by the disappearance of their associated strain fields, leading to the drop in hardness. Once the new thermally stable and coherent precipitates start to nucleate and grow at the new ageing temperature, the hardness starts to increase again.

A contradicting feature of this supposition needs some discussion. The dissolution of the strengthening precipitate should not only lead to a decrease in hardness, but also to a decrease in electrical conductivity; however, the latter is not observed. The reason for this is the existence of two possible mechanisms with opposite effects on electrical conductivity. On the one hand, the dissolution of the precipitates should decrease the electrical conductivity due to the increase of impurity in the solid solution. On the other hand, the increased temperature will remove the strain field and purify the solid solution due to the induced precipitation hardening, both of which increase the conductivity of the matrix. The latter is apparently the predominant mechanism, so the overall conductivity increased with temperature. This assumption is supported by the work of Matthew *et al.* (1994) on AA 7010. They reported that particle dissolution during retrogression is accompanied by little changes in conductivity, because the increase in the matrix solute content is offset by the removal of the particle coherency strain. In addition, when the temperature is raised during artificial ageing, retrogression occurs rapidly and is accompanied by precipitation hardening leading to an increase in the size and spacing of the

precipitate particles (Matthew *et al.* 1994). Large particles affect the electrical conductivity less than small particles (Raesignia 2006).

For all curves, the maximum hardness was attained during ageing at 172°C and a plateau profile was observed (Fig. 5.5). The hardness plateau is a manifestation of two different effects of the continuous age hardening process: the over ageing of already large precipitate particles; and a continuous nucleation and growth of new particles. In the plateau region, these two ageing mechanisms, which have opposite effects on the hardness, are balanced. With increasing ageing time further, the over ageing mechanism becomes predominant and the hardness starts to drop. This is because the loss of coherency between the large particles and the matrix is more pronounced than the coherency gain by the new particles formed.

5.4.4 Strength

The causes behind the effect of quench delay on strength are the same as those for hardness as discussed in the previous section. Regardless of the thermal history of the test pieces, there is a good liner relationship between hardness and UTS or PS as indicated by the high regression correlation coefficients, as shown in Fig. 5.6. It suggests that different quench delays and the resultant different types of precipitates do not affect the linear correlation between hardness and strength. Therefore, UTS and PS can be predicted from a given hardness value with a reasonable degree of accuracy for this aluminium alloy. However, the prediction of PS is slightly less accurate than the UTS. The lower linear correlation of hardness with yield strength has also been reported in other aluminium alloys, e.g. AA 7075 (Koch and Colijn

1979), AA 2090 and Al-2.2% Li (Brasche *et al.* 1989), and AA 2219 (Natan and Chihoski 1983).

5.4.5. Quench sensitivity

When the age hardening temperatures and ageing times were consistent with the heat treatment parameters of the required material specification ABM 3-1030 (Airbus UK 2003), all the curves with a quench delay up to 198 seconds yielded satisfactory hardness and electrical conductivity values. This suggests that the quench sensitivity for this aluminium alloy with a ruling section of 11×11 mm^2 is within 198 seconds. The wide range of quench delays, or low quench sensitivity, of AA7010 is largely due to the addition of zirconium as a dispersoid former, which is less effective in aiding the nucleation of the high temperature precipitates of the alloying elements (Reynolds 1976, Aluminium Association Inc. 1982, Martin 1998).

5.4.6 Thermal history

With the same solution treatment and artificial age hardening conditions, different quench delays resulted in different hardness and electrical conductivity values. As explained previously, the differences in hardness and electrical conductivity are a function of the different concentrations of alloying elements within the solid solution before age hardening, which are inherently related to the cooling path before quenching. The higher the initial concentration of alloying elements within the solid solution, the higher the hardness plateau and the lower electrical conductivity attained upon artificial ageing. On the other hand, the lower the initial concentration of alloying elements within the solid solution, the lower the hardness plateau and the higher the electrical conductivity values. A network of curves of the wide range of

values under different quench delays demonstrated the interdependence between hardness, electrical conductivity and quenching rate.

This network of curves, as shown in Fig. 5.5 for AA7010, can give useful information about the thermal history of the alloy when both the hardness and electrical conductivity are assessed simultaneously. With a known set of values of hardness and electrical conductivity, the unknown temper condition could be estimated for an AA 7010 product using Fig. 5.5. However, caution must be exercised with respect to attempts to establish direct correlations between hardness and electrical conductivity values. Although both properties are a function of the precipitation process, a value of one of the two variables can give multiple results of the other, and vice versa.

5.5 Summary

The effect of quench delay on electrical conductivity, hardness and mechanical properties for AA 7010 was investigated. The electrical conductivity and hardness values are sensitive to the processing parameters such as ageing temperature and ageing time. The variations of hardness and electrical conductivity are attributed to the formation of precipitates and their continuous change of size and volume fraction when ageing conditions are changed. The evolution of electrical conductivity, hardness and strength was found to be sensitive to the variation of quench delays. In general, short quench delays lead to higher hardness or strengths and low electrical conductivity; long quench delays resulted in low hardness or strength and high electrical conductivity. The dependence of these properties on quench delay appears to be dictated by the extent of high temperature diffusion of alloying elements from

the solid solution and their subsequent heterogeneous precipitation as an equilibrium phase prior to quenching.

7000 series aluminium alloys normally requires a rapid quench to prevent diffusion and heterogeneous precipitation from occurring during cooling (Staley *et al.* 1984). For AA 7010, however, a cooling path with quench delays up to 198 seconds, followed by a final fast quench into water at room temperature and subsequent artificial ageing to the thermal requirements of the material specification, produced satisfactory properties. Cooling paths with quench delays longer than 198 seconds resulted in properties below the material specification requirement.

For all quench delays, the variations of electrical conductivity and hardness with age hardening have very similar trends before over ageing. They both increase through the regions of artificial under ageing and peak age hardening up to the onset of over ageing. Afterwards, the hardness starts to decrease and the electrical conductivity continues to increase with increasing ageing time, which is characteristic of over ageing.

The network of hardness versus electrical conductivity curves under a wide range of ageing conditions is the result of different kinetics of precipitation induced by the different quench delays. Although direct correlations between hardness and electrical conductivity values are not possible, useful information can be obtained from the network of curves when both hardness and electrical conductivity are assessed simultaneously. With a known set of values of hardness and electrical conductivity, the history of temper conditions could be estimated.

There is a linear correlation between hardness and strength for AA 7010. The correlation coefficient for hardness with UTS is 0.96 and for hardness and PS is 0.94. The strength can be predicted with a reasonable accuracy independent of its temper condition.

Table 5.1 Artificial ageing conditions for the 31 sets of test pieces

Artificial Ageing sets	Ageing times at specified age hardening temperatures, hrs			
	120 °C	172 °C	190 °C	200 °C
0	-	-	-	-
1	0.25	-	-	-
2	0.5	-	-	-
3	1.5	-	-	-
4	3	-	-	-
5	4.5	-	-	-
6	6	-	-	-
7	8	-	-	-
8	10	-	-	-
9	10	0	-	-
10	10	0.17	-	-
11	10	0.33	-	-
12	10	0.5	-	-
13	10	0.75	-	-
14	10	1	-	-
15	10	2	-	-
16	10	3	-	-
17	10	4	-	-
18	10	5	-	-
19	10	6	-	-
20	10	7	-	-
21	10	8	-	-
22	10	10	-	-
23	10	12	-	-
24	10	14	-	-
25	10	16	-	-
26	10	20	-	-
27	10	24	-	-
28	10	24	4	-
29	10	24	4	4
30	10	24	4	8
31	10	24	4	12

Table 5.2 Electrical conductivity and hardness for the test pieces with different quench delays, measured immediately after the artificial ageing treatment

Set	3s before quench		71s to 394°C		113s to 363°C		198s to 324°C		474s to 240°C		813s to 198°C		Air cooling	
	EC %IACS	Hv	EC %IACS	Hv	EC %IACS	Hv	EC %IACS	Hv	EC %IACS	Hv	EC %IACS	Hv	EC %IACS	Hv
0	27.24	162.5	27.65	158.5	28.39	157	29.69	140.5	31.63	135	33.08	126	32.91	131
1	28.25	163.5	28.79	162	29.36	159.5	30.45	149	32.34	136.5	33.74	123.5	33.3	130
2	28.66	168	29.11	168	29.61	162	30.88	153	32.85	137	34.27	123.5	33.72	129.5
3	29.05	174	29.49	176	30.18	166.5	31.57	156	33.32	134	34.85	123	34.12	129
4	29.28	181.5	29.71	180	30.49	169	31.87	159	33.7	138	35.12	127	34.42	136
5	29.55	184	29.96	185	30.8	173.5	32.17	162.5	34.1	141	35.48	129	34.74	141.5
6	29.8	186	30.19	186	30.9	175	32.33	168.5	34.25	145	35.58	131	34.81	144
7	29.95	188.5	30.43	188	31	180	32.49	171	34.56	148	35.78	135.5	34.88	145.5
8	30.08	190.5	30.5	189	31.12	181	32.63	172	34.74	150	35.81	137	34.93	147.25
9	31.08	185	31.46	183	32.12	177.5	33.86	164	35.15	146	36.43	134.5	35.44	145
10	31.57	193	31.85	190	32.53	183.5	34.3	163.5	35.62	147	36.79	136.5	35.81	146
11	31.94	193.5	32.11	191	32.89	187	34.56	166	35.86	148	37.08	138	36.22	147
12	32.36	196	32.47	193	33.38	187	34.9	170	36.22	150	37.34	138	36.44	147
13	32.55	196	32.79	193	33.61	187.5	35.32	171	36.42	151	37.63	139	36.74	148
14	33.08	197	33.32	194	34.25	188	35.54	172	37.1	152	38.07	140	37.25	151
15	34.04	198.5	34.23	195.5	35.17	188	36.64	172.5	37.92	152	38.77	140.5	37.96	150
16	35.18	195	35.25	195	35.84	189	37.48	172	38.8	149	39.67	138.5	38.81	150.25
17	35.82	194.5	35.9	192	36.66	186.25	37.71	171	39.17	148	40.08	138	39.29	149.5
18	36.17	193	36.29	191	36.79	185.5	38.03	170.5	39.59	147	40.4	137	39.65	147
19	37.03	188.5	37.06	190.5	37.73	179.5	38.83	167.5	40	145.5	40.71	135	39.93	146.25
20	37.48	185.5	37.55	187	38.29	178	39.22	167.5	40.46	143.5	41.06	134.5	40.63	143.5
21	38.35	179	38.48	181.5	39.05	176.5	39.77	162	40.91	143	41.54	133	41	141.5
22	39.02	174.75	39.01	175.5	39.73	168.5	39.97	160	41.13	140	42.03	131	41.41	136
23	39.56	171	39.48	171.5	40	167.5	40.35	159	41.61	137.5	42.53	129	41.89	135
24	39.86	167	39.76	169	40.4	161	40.75	157	41.86	135.5	42.71	127	42.13	133.5
25	40.2	165.5	40.26	164.5	40.84	158.5	41.23	153.5	42.34	134	43.03	125	42.37	132
26	40.57	161.5	40.61	164	41.14	153.5	41.61	151	42.5	133	43.15	123.5	42.52	131
27	40.93	160.5	40.92	160.5	41.51	152.5	41.96	147.5	42.96	131	43.59	122.5	43.02	129
28	41.79	147	41.93	148	42.77	140	42.52	135.5	43.56	120.5	44.03	116	43.67	117
29	43.17	129	43.25	127.5	43.5	121.25	43.81	115.5	44.14	107	44.73	102.5	44.26	106.5
30	43.48	123.5	43.69	123.5	43.85	115.5	44.06	113	44.5	105	44.89	97.8	44.48	104
31	43.85	120	44.04	116	44.13	106.85	44.42	96	44.79	89.8	45.22	86.7	44.81	89.55

Table 5.3 Properties for test pieces with a quench delay of 3 seconds, measured nine months after the artificial ageing treatment

Set	EC	Hardness	UTS	0.2% PS	Elongation.
	%IACS	Hv	MPa	MPa	%
0	27.65	158.5	547.7	402.3	20.1
1	28.25	168	553.5	421.5	19.87
2	28.56	173	554.1	425.3	20.45
3	29.1	175	578.8	459.1	21.61
4	29.51	180	578.4	472.5	21
5	29.67	185	587.4	483.8	21.46
6	29.83	187	588.4	489.6	18.95
7	29.98	187	590.8	497.7	18.53
8	30.04	188	593.2	500.6	21.28
9	31.1	184	571.4	511	14.86
10	31.61	185	575.3	495.7	19.06
11	31.99	187	575.3	523.6	14.07
12	32.42	192	586.9	519.5	16.77
13	32.6	196	592.4	541.3	16.99
14	33.21	195	582.9	541.1	14.06
15	34.11	190	592	553.2	15.36
16	35.38	190	592.8	550.9	16.57
17	36.06	187	586	543.4	15.61
18	36.42	185	590.5	546.3	15.28
19	37.22	185	577.2	529.9	17.63
20	37.69	183	562.7	512.4	14.59
21	38.34	179	553.3	502.6	15.86
22	38.94	176	559.7	500	16.84
23	39.46	174	540	478.5	19.99
24	39.72	168	538.2	473.7	16.59
25	40.1	167	524.7	456.2	16.12
26	40.5	163	514.1	442.6	15.36
27	40.86	162	509.3	437.1	15.63
28	41.69	148	468.7	378.4	16.97
29	43	129	421.9	317.4	18.67
30	43.22	126	407.6	301.6	17.14
31	43.51	122	392.2	287.4	15.89

Table 5.4 Properties for test pieces with a quench delay of 71 seconds, measured nine months after the artificial ageing treatment

Set	EC	Hardness	UTS	0.2 % PS	Elongation
	%IACS	Hv	MPa	MPa	%
0	27.54	160.25	520.3	373.4	23.04
1	28.6	167.75	539.2	412.5	26.69
2	28.86	169	537.5	413.5	19.82
3	29.61	173	544.2	435.2	18.53
4	29.95	177.5	548.8	450.3	17.99
5	30.17	181.75	563.5	467.6	19.64
6	30.34	184	562.7	465.3	16.8
7	30.46	185.75	566.1	474.9	16.55
8	30.6	185.75	574.8	487.2	16.89
9	31.48	183	561.1	485.2	15.73
10	32	186.5	563.1	496.2	15.59
11	32.3	185.25	564.9	504.6	11.78
12	32.75	189.5	575.8	524.2	13.7
13	32.98	192	576	527.3	12.06
14	33.48	193	583.9	543.9	11.23
15	34.59	193.25	585.4	548.5	12.14
16	35.4	194	593.1	554.8	11.54
17	36.11	192	579.2	538.9	11.84
18	36.43	189.5	574.3	532.6	12.58
19	37.22	185.8	570.9	526	12.38
20	37.76	184.75	567.7	519.6	9.8
21	38.57	178.25	555.5	504	12.53
22	39.18	175.25	551	495.4	11.08
23	39.67	173	538.2	478.9	12.63
24	39.95	167.8	530.4	467.8	12.63
25	40.36	164.75	519.7	452.5	16.82
26	40.8	159	513.5	442	14.6
27	41.18	158.75	508.5	436.9	15.02
28	42.21	148.25	470.7	379.2	15.68
29	43.62	126.5	420	316.2	12.03
30	43.99	122.5	409.1	300.8	13.35
31	44.29	118.5	391.8	282.7	17.23

Table 5.5 Properties for test pieces with a quench delay of 113 seconds, measured nine months after the artificial ageing treatment

Set	EC	Hardness	UTS	0.2 % PS	Elongation
	%IACS	Hv	MPa	MPa	%
0					
1	29.46	168.60	535.6	421.7	19.97
2	29.67	170.60	542.2	408.9	18.66
3	30.40	169.80	539.5	418.5	16.38
4	30.84	171.90	542.3	433.1	15.12
5	31.15	175.00	552.3	446.8	15.71
6	31.16	177.00	556.5	455.7	15.89
7	31.32	181.30	556.3	459.8	15.52
8	31.32	182.10	561.3	470	15.97
9	32.34	180.40	549.8	473	16.18
10	32.75	183.50	556.7	487.5	13.07
11	33.17	184.60	559.1	495.4	13.02
12	33.80	186.00	561.5	503.3	13.04
13	33.91	188.00	562.1	507.3	13.2
14	34.61	189.50	566.2	515.7	12.79
15	35.57	189.50	566.5	520.2	10.83
16	36.33	188.50	574.7	533.2	12.41
17	37.24	186.00	562.2	511.5	12.9
18	37.44	185.80	561.8	512.8	14.09
19	38.17	182.30	552.8	499	9.65
20	38.69	179.50	543.2	486.7	10.99
21	39.32	173.80	534.2	474.4	12.16
22	40.01	171.30	522.7	459	11.86
23	40.25	170.30	522.6	456.9	13.04
24	40.64	164.80	510.9	441.8	12.99
25	41.09	161.80	501	427.6	11.42
26	41.30	158.80	494.6	418.5	10.81
27	41.72	157.80	490.9	414.3	14.37
28	42.44	142.50	453.4	361.1	13.15
29	43.76	125.00	400.9	297.2	14.91
30	44.18	119.50	388.7	285.3	14.06
31	44.33	115.50	380.1	273.1	15.32

Table 5.6 Properties for test pieces with a quench delay of 198 seconds, measured nine months after the artificial ageing treatment

Set	EC	Hardness	UTS	0.2 % PS	Elongation
	%IACS	Hv	MPa	MPa	%
0	30.06	153.5	496.8	437.9	11.79
1	30.54	156	507.5	370.5	10.66
2	30.9	155	510.5	376.8	14.07
3	31.62	156	504.1	385.2	10.55
4	31.87	160	512.7	400.4	11.11
5	32.12	162	513.4	407.9	11.45
6	32.33	163	515.5	415.9	9.53
7	32.55	167	524.6	428.2	9.02
8	32.67	169	531	442.4	6.84
9	33.54	163	504	421.9	5.7
10	34.46	164	513.6	432.3	6.23
11	34.91	165.5	517.5	440.3	6.63
12	35.39	168	520.2	448.9	5.1
13	35.7	169	528.3	465.2	6.2
14	36.02	167	518.3	448.5	6.21
15	37.01	169	527	460.9	5.51
16	37.87	172	533.6	469.9	6.9
17	38.21	171.5	532.8	472.2	7.48
18	38.5	171	531.9	471.3	7.88
19	39.15	168	521.1	457.1	6.6
20	39.51	166	515.7	449	7.35
21	39.9	164	516.7	449.6	8.39
22	40.13	163.5	521.1	456	8.15
23	40.59	159.5	514.5	446.7	7.9
24	40.95	159	501.7	429.8	8.39
25	41.41	154	492.9	413.7	10.74
26	41.89	149.5	480.6	397.4	10.2
27	42.1	149	480.4	397.3	10.6
28	42.76	135	445	348.2	12.07
29	43.86	117.5	390.1	279	13.49
30	44.14	112.5	379.5	266.6	13.89
31	44.43	110	371.6	256.6	13.53

Table 5.7 Properties for test pieces with a quench delay of 474 seconds, measured nine months after the artificial ageing treatment

Set	EC	Hardness	UTS	0.2 % PS	Elongation
	%IACS	Hv	MPa	MPa	%
0	31.92	140.9	464	317.6	7.315
1	32.28	144.5	480	337.8	7.403
2	32.64	147	474.3	337.3	7.188
3	33.23	148.5	475.7	346.6	8.308
4	33.68	147.25	477.3	353.8	7.273
5	34.07	146.5	477.2	360.6	8.094
6	34.21	150	478.6	366.4	8.202
7	34.53	152.25	479.8	371.4	6.784
8	34.64	153	481.2	372.1	6.69
9	35.33	150.5	477.9	377.4	6.969
10	35.77	149	469	376.1	4.348
11	36.15	150.6	479.7	383	7.197
12	36.55	152	477.2	384.6	5.872
13	36.71	152.5	479.7	389.9	6.402
14	37.44	151.8	476.3	385.2	6.209
15	38.12	153.25	482.9	395.4	5.68
16	38.89	152.8	482	388.7	6.996
17	39.37	149.25	474.4	384.1	7.097
18	39.67	147.5	480.2	388.7	7.651
19	40.11	147	477.8	386.2	6.861
20	40.61	146.5	473.7	383.4	7.661
21	40.97	145.5	469.9	380.3	7.645
22	41.2	144.2	467.4	376.1	6.92
23	41.72	141.25	460.4	367.6	9.767
24	41.82	139.5	459.4	366.3	8.971
25	42.33	134.8	446.6	352.6	9.51
26	42.62	132.8	442	346	10.06
27	42.93	131.25	438.5	340.7	9.742
28	43.47	119.5	408.9	305	10.72
29	44.23	109.5	372.6	260	12.38
30	44.4	106	364.2	250.1	12.91
31	44.67	102.25	358.6	242.8	13.66

Table 5.8 Properties for test pieces with a quench delay of 813 seconds, measured nine months after the artificial ageing treatment

Set	EC	Hardness	UTS	0.2 % PS	Elongation
	%IACS	Hv	MPa	MPa	%
0	33.18	133.25	481.3	319.8	9.49
1	33.74	134.25	480.3	331.9	8.88
2	34.00	134.00	472	327.4	9.93
3	34.60	133.50	470.8	328	10.31
4	35.10	135.75	466.3	330.2	11.09
5	35.40	136.00	471.2	342.9	10.85
6	35.55	136.25	469	342	11.6
7	35.79	137.75	460.6	341.7	9.95
8	35.94	139.00	461.2	344.7	9.99
9	36.61	136.75	456.5	340.4	11.3
10	36.94	138.75	457.9	348.2	9.78
11	37.22	137.75	456.5	350.4	10.77
12	37.49	137.00	458.3	351.6	10.56
13	37.69	135.50	459.5	355.7	9.82
14	38.08	136.00	454.2	357	9.91
15	38.78	135.25	456.7	353.4	8.451
16	39.59	133.25	452.4	353.6	8.224
17	39.99	132.00	454	354.2	7.07
18	40.36	131.75	446.8	353.6	5.53
19	40.67	132.75	454.2	356.6	5.31
20	41.03	131.00	441.4	348.4	5.634
21	41.50	129.50	436.8	344.9	6.816
22	41.94	130.00	443.8	350.4	5.934
23	42.31	127.75	433.7	340.5	9.907
24	42.55	127.25	427.7	329.1	8.352
25	42.68	125.25	424	326.4	9.909
26	43.03	124.00	420	323.4	10.3
27	43.38	121.25	416.7	319.3	10.96
28	43.84	112.25	390.8	286.5	13.3
29	44.42	100.75	357	244.5	13.42
30	44.69	98.08	346.5	236.9	14.69
31	45.00	96.58	341.9	230.1	15.38

Table 5.9 Properties for test pieces air cooled to room temperature, measured nine months after the artificial ageing treatment

Set	EC	Hardness	UTS	0.2 % PS	Elongation
	%IACS	Hv	MPa	MPa	%
0	32.87	140.25	497.7	350.3	8.26
1	32.97	139.75	495	352.5	9.83
2	33.15	138.5	492.2	350.3	9.24
3	33.85	138	483.4	350.4	10.18
4	34.2	140.75	488.4	362.4	10.5
5	34.3	144.75	487	376.7	8.24
6	34.51	145.75	494.7	383.2	8.93
7	34.54	146	498.9	391.2	7.67
8	34.77	148.5	498.4	401.3	6.69
9	35.28	146.5	484.9	387.2	4.76
10	35.6	147	489.1	392.3	7.95
11	36.06	147.5	492.2	401.1	8.31
12	36.4	146.5	484.8	402.8	6.7
13	36.64	146.5	491.1	408.4	6.98
14	37.07	147	494.5	411.7	7.44
15	37.87	149.25	488.6	414.7	7.28
16	38.55	147.25	494.8	413.8	7.89
17	39.28	148.25	485.4	405.9	6.85
18	39.5	146	488.5	410.1	8.97
19	39.97	143.75	485.8	405.9	7.51
20	40.52	142	476.4	397.6	7.21
21	40.91	140	469.4	388.4	8.03
22	41.3	137	460.7	379.9	8.81
23	41.74	136.5	455.1	371.5	7.53
24	41.99	133.25	451.5	368	8.98
25	42.14	132.25	448.1	361.5	10.07
26	42.47	130	443.1	356.3	10.76
27	42.79	129	435.9	347.1	9.83
28	43.6	118.5	402.3	303.1	10.67
29	44.17	107.25	368.8	262.1	12.7
30	44.39	102.75	357.5	250.2	15.67
31	44.67	99.25	349.2	240.3	14.53

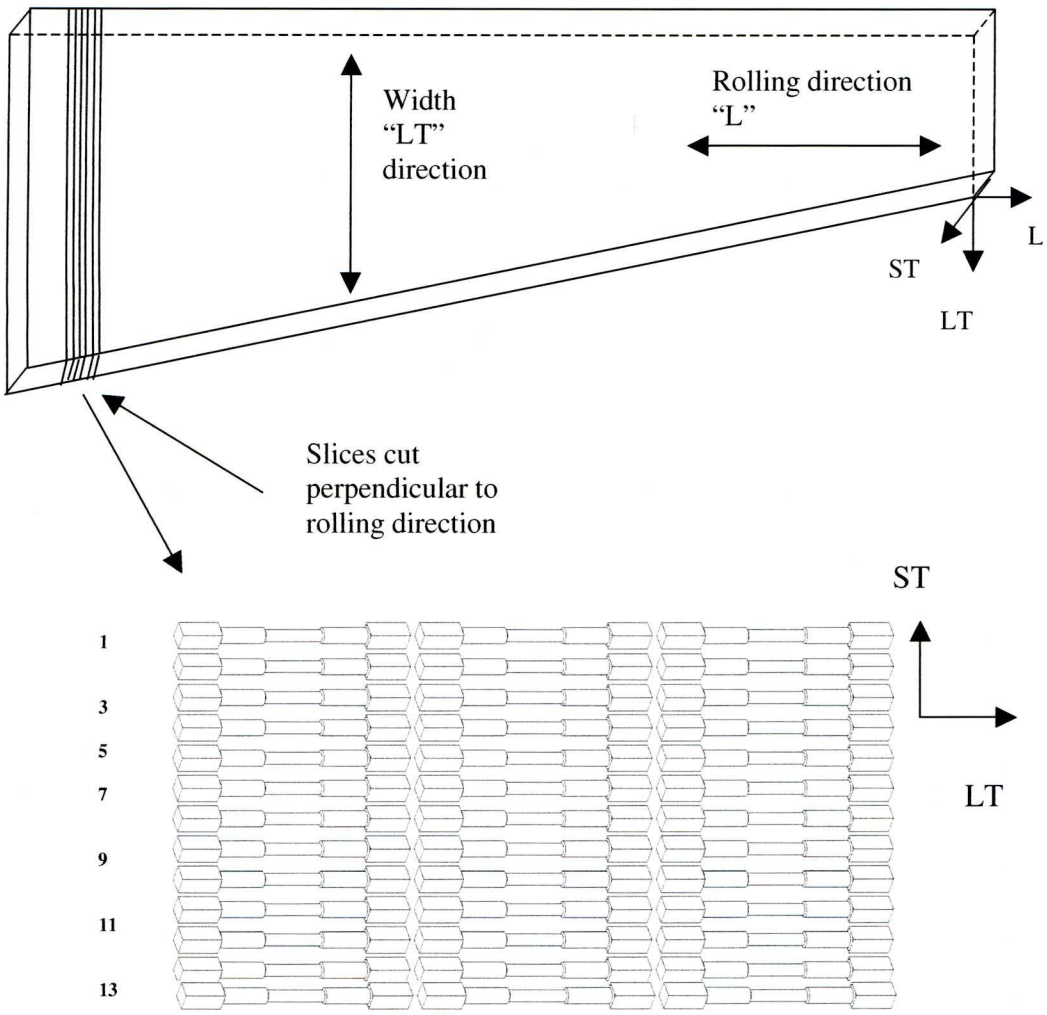

Fig. 5.1 Schematic diagram indicating the locations of the slices in the plate from which tensile test pieces were machined.

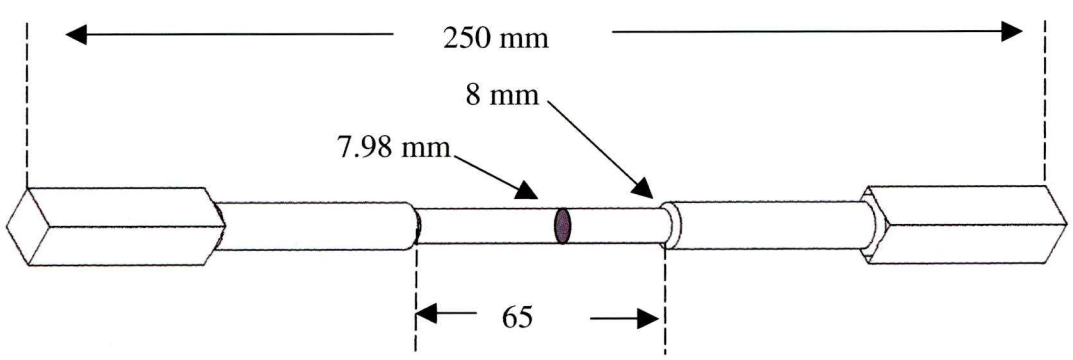

Fig. 5.2 Geometry of the tensile test pieces with cylindrical gauge length and square ends

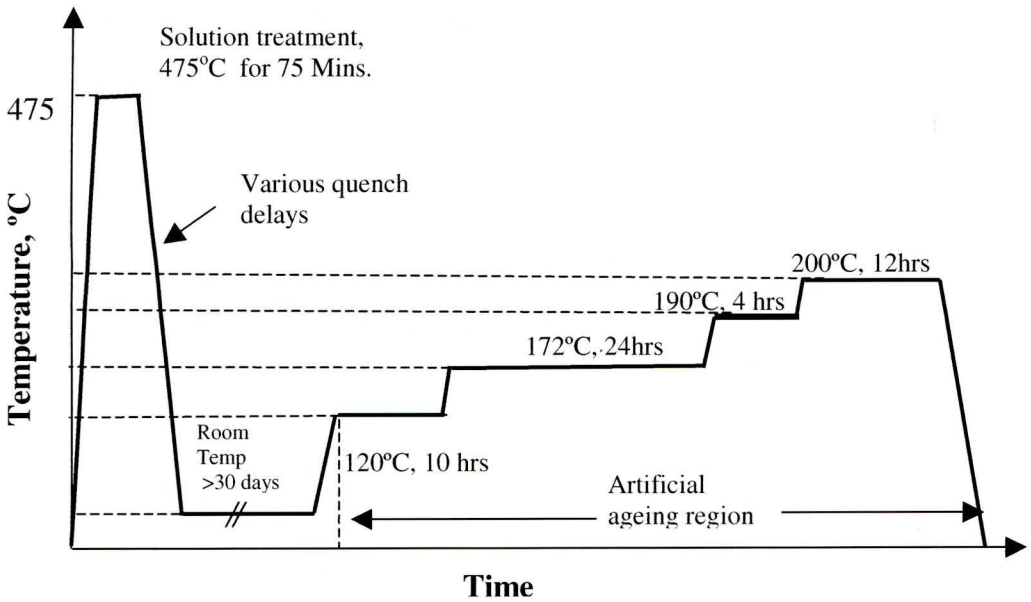

Fig. 5.3 Overall thermal cycle for the test pieces

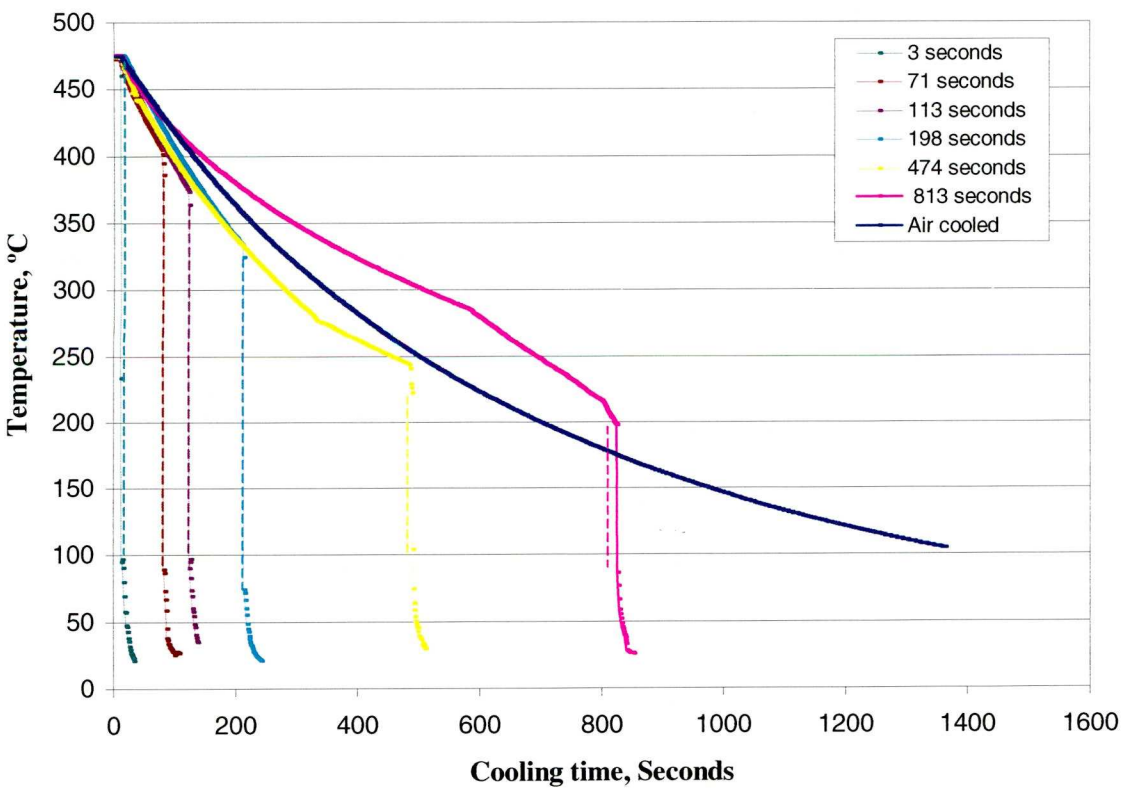

Fig. 5.4 Cooling curves of the seven groups

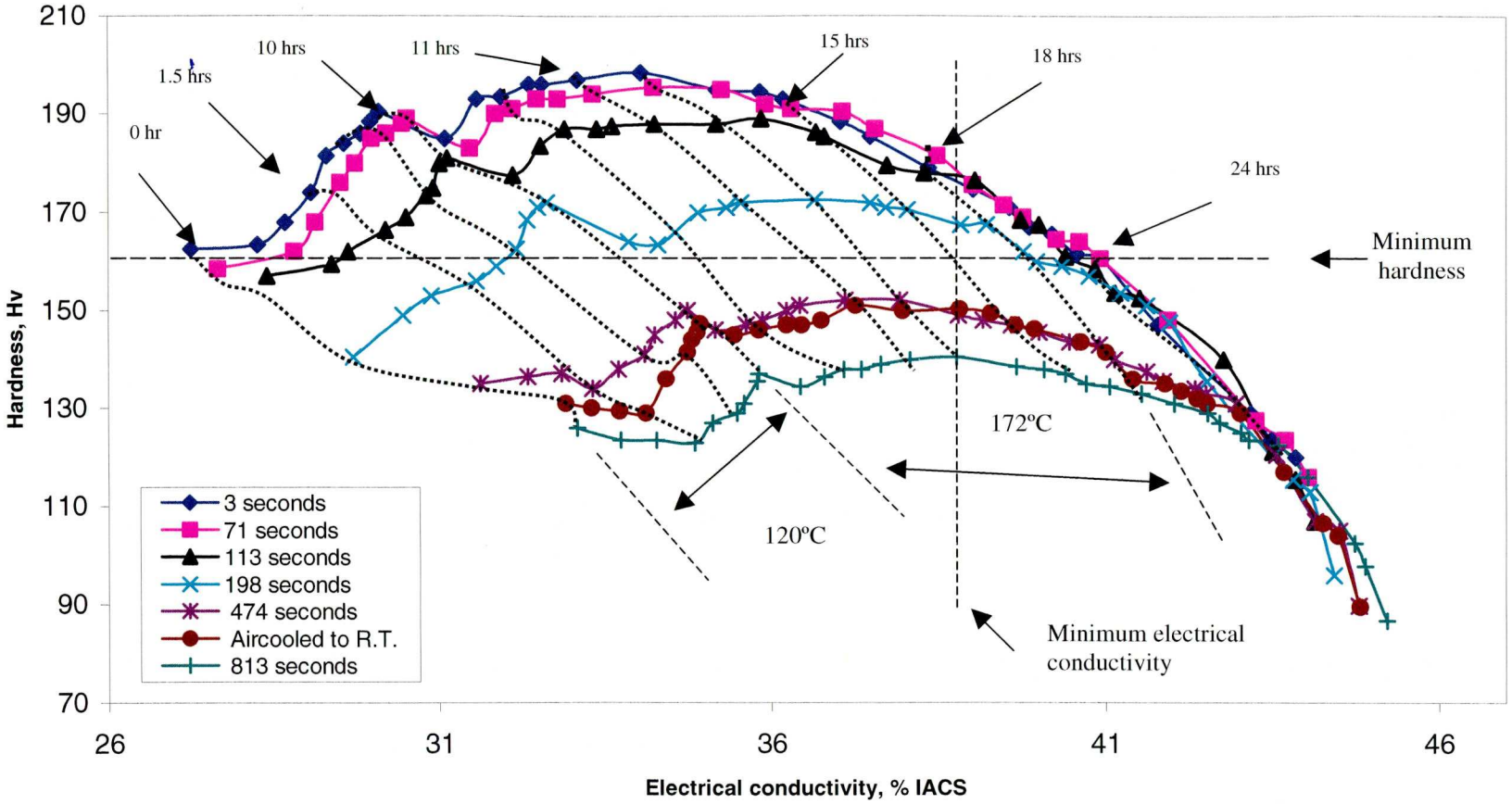

Fig. 5.5 Responses of hardness and electrical conductivity to artificial age hardening on seven different quench delays.

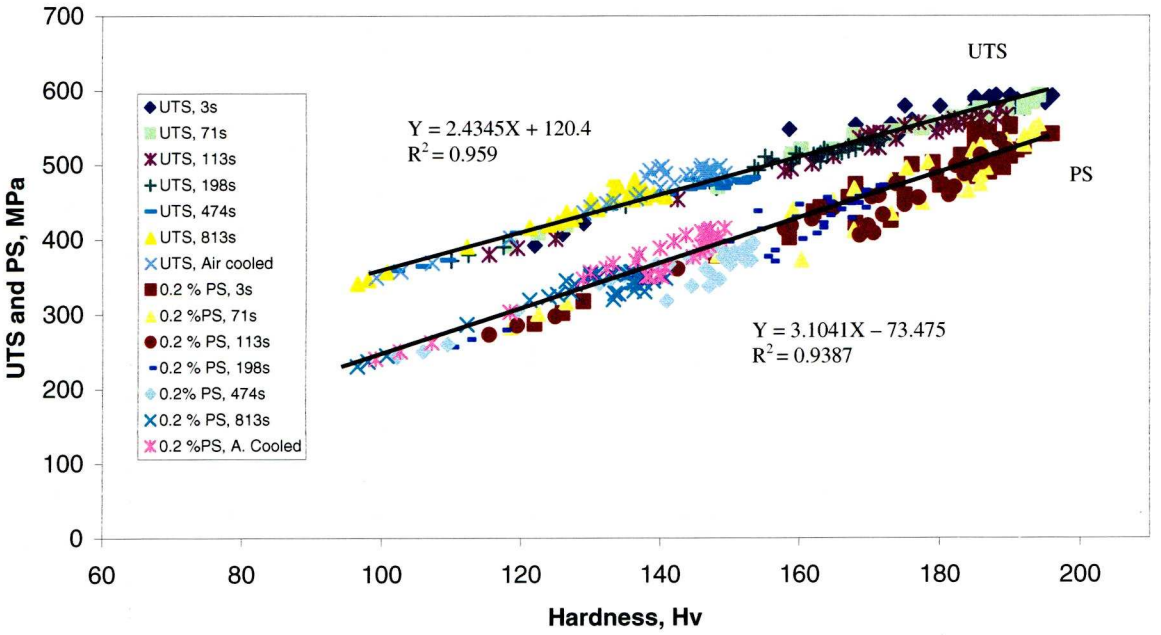

Fig. 5.6 Relationships of UTS and 0.2% PS with hardness for different quench delays

Chapter 6

Conclusions and Recommendations

6.1 Conclusions

6.1.1 Electrical conductivity and hardness

The electrical conductivity and hardness values are sensitive to the changes of processing parameters such as temperature and ageing time. When ageing conditions are changed, the variations of electrical conductivity and hardness are a direct cause of the formation of precipitates and the continuous change of their size and volume fraction. Therefore, the combination of electrical conductivity and hardness tests is a reliable quality indicator to assess the ageing process of AA 7010 and can be used in non-destructive assessment of property homogeneity of thick products.

In the full range of age hardening conditions, a unique correlation between electrical conductivity and hardness or between electrical conductivity and strength does not exist. It is possible to have two different hardness and strength values for the same electrical conductivity value, or vice versa. Therefore, it is not possible to predict hardness or strength from electrical conductivity values alone. However, in the natural ageing and over ageing regions, there exists a nearly linear correlation of electrical conductivity with hardness or strength, in agreement with the previous work in the literature.

In the over ageing region, the hardness and strength of AA 7010 decrease nearly linearly with increasing electrical conductivity, due to direct correlation between the precipitate particle spacing and electrical conductivity, hardness or strength.

Hardness and strength can be determined from the electrical conductivity values with a reasonable accuracy for any electrical conductivity values above 35.9% IACS.

In the peak ageing condition, namely 120°C for 10 hours followed by 172°C for 8 hours, the maximum attained hardness and strength can be found within a wide range of electrical conductivity values between 32 and 36.5% IACS. This clearly suggests that, if this alloy is to be age hardened to peak hardness or strength, the ageing time for the last ageing temperature (172°C) could be selected from a wide tolerance range.

6.1.2 Strength prediction

When AA 7010 was solution heat treated to standard conditions, a linear correlation between hardness and UTS was obtained with a high regression correlation coefficient value, R^2, of 0.98 for the full range of age hardening conditions, i.e. natural ageing, artificial ageing and over ageing. For heat treatments including non-standard conditions, with varying quench delays and age hardening temperature above the design requirement up to 200°C, a liner relationship resulted between hardness and UTS with a high R^2 value of 0.96. The UTS can be predicted from a given hardness value with a reasonable degree of accuracy for AA 7010, regardless of its thermal history.

On the other hand, the prediction of PS from hardness values is less accurate. The reason of the lower accuracy appears to be due to its different responses to under-ageing and over-ageing conditions. The accuracy of this prediction can be improved using its correlation with electrical conductivity for any electrical conductivity values

greater than 35.9% IACS.

6.1.3 Property homogeneity

There is evident inhomogeneity of properties across the plate thickness of AA 7010, specifically, low hardness and high electrical conductivity at the centre and the high hardness and low electrical conductivity at a depth of 32 mm from the surface. The variations in electrical conductivity and hardness through the plate thickness, perpendicular and parallel to the rolling direction, are very similar. In the artificially age hardened conditions, they showed consistent flattened "W" and "M" shaped profiles respectively. In the re-solution heat-treated and artificially aged condition, the variations were more pronounced.

The lack of property homogeneity across the plate thickness appears to be inherent from the ingot casting and thermo-mechanical operations, which induced some degree of segregation of the alloying elements and created different thermal histories at different locations across the plate thickness.

Chemical analysis showed some degree of segregating of alloying elements Zn, Cu and Mg at a plate depth of 32 mm from the surface and segregating of Zr and Ti at the plate centre. The high hardness and low electrical conductivity at the location of 32 mm from the surface are considered to be primarily due to the segregation of Zn, Cu and Mg at this location during solidification.

The test pieces in the as received condition showed that the electrical conductivity values were within the material specification requirements; however, the hardness at

the centre of the plate was marginally below the minimum (160 Hv) on six test pieces out of eight. There appears to be a macro-segregation of peritectic and eutectic precipitates or dispersoids at the centre of the plate, which are inherited from the solidification and high temperature rolling operations. The precipitation of the equilibrium phases reduced the concentrations of the strengthening alloying elements in the solid solution. This was believed to be the dominant cause for low hardness and high electrical conductivity at the plate centre. The gradient of quenching rate from the surface to the centre of the plate during the quench operation after the solution heat treatment was not the main contributor.

The anisotropy of strength through the plate thickness is mainly due to the crystallographic texture formed during fabrication, the effect of precipitates directionality and the different thermal histories through the thickness.

6.1.4 Effect of quench delays

The electrical conductivity, hardness and strength were found to be sensitive to the quench paths. In general, short quench delays led to higher hardness, higher strength and lower electrical conductivity. Long quench delays led to high temperature diffusion of alloying elements from the solid solution and subsequent heterogeneous precipitation of the equilibrium phases, depleting the alloying elements available for subsequent age hardening. Therefore, long quench delays resulted in low hardness, low strength and high electrical conductivity.

For AA 7010 test pieces of 11×11 mm^2, a cooling path with quench delays up to 198 seconds, followed by a final fast quench into water at room temperature and

subsequent standard artificial ageing, produced satisfactory electrical conductivity, hardness and strength values. Cooling paths with quench delays longer than 198 seconds resulted in properties below the material specification requirement.

A network of hardness versus electrical conductivity curves under a wide range of age conditions was obtained. From this network of curves, the age condition for an unknown AA 7010 material could be estimated from a known set of values of hardness and electrical conductivity.

6.2 Recommendations for future work

The findings from the correlations of electrical conductivity with hardness and hardness with strength for AA 7010 provided a basis as a general tool for non-destructive inspections. However, they should not be extrapolated directly to other aluminium alloys, as non-consistency between different alloys may be possible. Each alloy should be assessed on its own merit.

In addition to UTS and PS, fatigue limit, fracture toughness and resistance to stress corrosion cracking are also important properties of aluminium alloys for aeroplane applications. The effects of varying electrical conductivity and hardness on these properties are recommended for further studies.

The nature of texture variation and its through thickness effect on the strength along the longitudinal, long transverse and short transverse directions are recommended for future investigations.

The effect of retrogression on the strengthening precipitates when they are exposed to temperatures above artificial age hardening treatments needs to be characterised. This will help to understand the effect of high temperature and time on strength of over heated AA7010.

Although bulk chemical analysis can help to formulate explanations for the changes of electrical conductivity, hardness and strength through the plate thickness to some degree, it is unable to explain the property change at the plate centre. This shortfall could be overcome by analysing the quantities and chemical compositions of the dispersoids and the quench induced precipitates formed heterogeneously at grains and sub-grain boundaries. The analysis can help to establish the amounts of strengthening alloying elements associated with these non-strengthening precipitates, which are not available for the precipitation hardening. This study will be able to elucidate the effects of the casting, thermo-mechanical operations and the solution treatment on chemical homogeneity.

References

Airbus UK (2003), Airbus Material Specification: Aluminium Alloy 7010 – T7651 Plate, ABM 3-1030, Issue 5.

Airbus UK (2004a), Airbus Process Specification: Hardness Testing of Metallic Materials, ABP 6-5226, Issue 2.

Airbus UK (2004b), Airbus Process Specification: Refrigerated Storage of Aluminium After Heat Treatment, ABP 3-1120, Issue1.

Airbus UK (2005), Airbus Process Specification: Testing of Aluminium Alloys by Electrical Conductivity, ABP 6-5224, Issue 2.

Airbus UK (2006a), Airbus Process Specification: Heat Treatment of Aluminium Alloys, ABP 3-1119, Issue 6.

Airbus UK (2006b), Airbus Process Specification: Testing by Penetrant Flaw Detection, ABP 6-5230, Issue 8.

Airbus UK (2008), Airbus Process Specification: Chromic acid Anodising of Aluminium, ABP 1-1023, Issue 5.

AMS Handbook (1991), "Heat Treating of Aluminium Alloys" in *AMS Handbook – Heat Treating,* Institute of Metals, Metals Park, Ohio, USA, pp.841-879.

Askeland, D.R. (1992), *The Science and Engineering of Materials* (2nd edition), Boston: Chapman.

Avner, S.H. (1974), *Introduction to Physical Metallurgy* (2nd edition), London: McGraw – Hill.

Bate, P., Roberts, W.T., & Wilson, D.V. (1981), "The Plastic Anisotropy of Two-Phase Aluminium Alloys - I. Anisotropy in Unidirectional Deformation", *Acta Metallurgica* Vol. **29**, 1797-1814.

Bartŭska, P., Kroggel, R., Löffler, H., Minerská, M., Synecek, V. & Wendrok, G. (1979), "On the Room Temperature Stability of Meta-Stable Phases Formed at 200°C in Al-Zn Alloys", *Physica status solidi: Applied research,* Vol. **A55**, 673-679.

Bergner, D., Freiberg & Löffler, H. (1995), "General Aspects of Binary Aluminium Alloys", in Löffler, H. (ed), *Structure and Structure Development of Al-Zn Alloys* (1st edition), Berlin: VCH Publisher, Inc., pp.19 – 23.

Bigot, A., Danoix, F., Auger, P., Blavette, D., & Revees, A. (1976), *Materials Science Forum,* Vol. **217-222**, 695-700.

Brasche, L.J.H., Bracci, D.J., Jiles, D.C. & Buck, D. (1989), "Correlation of Mechanical Properties With Non-Destructive Evaluation Measurements in Al-Li Alloys", *Materials Science and Engineering* Vol. **A119**, 7-15.

British Standard (1966), "Test Pieces and Test Methods for Metallic Materials", *B.S. 4A –4,* Issue 4, pp.4-7.

British Standard (2001), "Tensile Testing", *B.S. EN10002-1,* pp.4-13.

British Standard (2005), "Metallic Materials – Vickers Hardness Test", *B.S. EN ISO 6507-1*, pp.1-7.

Brown, D. & Heaton, H.B. (1984), "An Investigation into the Machining Damage in Airbus Wing Ribs", Met. Tech. Report YMM131, British Aerospace Public Ltd, Kingston - Borough Division, UK.

Buha, J., Lumley, R.N. & Croskey, A.G. (2008), "Secondary Ageing in an Aluminium Alloy 7050", *Material Science and Engineering* Vol. **A492**, 1-10.

Chakrabarti, D. J., Weiland H., Cheney, B. A., & Staley, J. T. (1996), "Through Thickness Property Variation in 7050 Plate", *Materials Science Forum* Vol. **217-222,** 1085-1090.

Chakraborty, J. & Chakrabarty, J. (2000,) Applied Plasticity. Springer, 3873.

Chen, J.Z., Zhen, L., Shao, W.Z., Dai, S.L. & Cui, Y.X. (2008), "Through Thickness Texture Gradient in AA 7055 Aluminum Alloy", *Materials Letters* Vol. **62**, 88-90.

Csontos, A.A., Gable, B.M., Gaber, A., & Starke, Jr. (2000), "Effect of Quench Rate on the Microstructure and Properties of AF/C-458 and AF/C-489 Al-Li-Cu-X alloys", Materials *Science Forum,* Vols. **331-337**, 133-1340.

Deschamps, A. & Brechét, Y. (1998), "Nature and Distribution of Quenched Induced Precipitation in an Al-Zn-Mg-Cu Alloy", *Scripta Materilia,* Vol. **39**, (11), 1517-1522.

Dixit, M., Mishra, R.S., Sankaran, K.K. (2008), "Structure-Property Correlations in Al 7050 and 7055 High - Strength Aluminium Alloys", *Material Science and Engineering A* **478,** 163-172.

Dunn, E.M., Davison, A.P., Faunce, J.P., Maitra, S., Mehrabian, R. (1984), "Constitution of Alloys", in Hatch, J.E. (ed), *In Aluminium: Properties and Physical Metallurgy* (1st edition), Ohio, Metal Park, pp.25-57.

Engler, O., Sachot, E., Ehrström, J.C., Reeves, A., Shahani, R. (1996), "Recrystallisation and Texture in Hot Deformed Aluminium Alloy 7010 Thick Plates", *Materials Science and Technology* Vol. **12,** 717-729.

Esmaeili, S., Poole, W.J. & Lloyd, D.J. (2000a), "The Role of Natural Ageing on Subsequent Precipitation During the Artificial Ageing of AA6111 Aluminium Alloy", In: Das, S.K. (ed) *Proceedings of Automotive Alloys 1999*, The Minerals Metals & Materials Society, Warrendale, pp.143-52.

Esmaeili, S., Poole, W.J. & Lloyd, D.J. (2000b), "Electrical Resistivity Studies on the Precipitation Behaviour of AA6111", *Material Science Forum,* Vol. **333-337**, 995.

Esmaeili, S., Poole, W.J. & Lloyd, D.J. (2005), "Effect of Natural Ageing on the Resistivity Evolution During Artificial Ageing of the Aluminium Alloy AA6111", *Materials Letters* Vol. **59**, 575-577.

Esmaeili, D., Vaumousse, M., Zandbergen, Poole, W.J., Cerezo, A. & Lloyd, D.J. (2007), "A Study on the Early - Stage Decomposition in the Al-Mg-Si-Cu Alloy AA6111 by Electrical Resistivity and Three-Dimensional Atom Probe", *Philosophical Magazine,* Vol.**87,** (25), 3797-3816.

Evancho, J.W. & Staley, J.T. (1974), " Kinetics of Precipitation in Aluminium Alloys During Continuous Cooling", *Metallurgical Transactions* Vol. **5A**, 43-47.

Federighi, T. & Thomas, G. (1962), *Philosophical Magazine Vol.* **7,** 127-131.

Ferragut, R., Somoza, A., & Dupasquier, A. (1996), "On two-Step Ageing of a Commercial Al-Zn-Mg alloys; A Study by Positron Lifetime Spectroscopy", *Journal of Physics:* Condensed Matter 8, 8945-8952.

Ferragut, R., Somoza, A., & Dupasquier, A. (1998), "Positron Lifetime Spectroscopy and Decomposition Processes in Commercial Al-Zn-Mg Based Alloys", *Journal of Physics:* Condensed Matter 10, 3903-3918.

Fink, W.L. & Willey, L.A (1947), "Quenching of 75S Aluminium alloys", *Transactions - American Institute of Mining and Metallurgical Engineering,* Vol. **175,** 1-13.

Flynn, R.J. & Robinson, J.S. (2004), "The Application of Advances in Quench Factor Analysis Property Prediction to the Heat Treatment of 7010 Aluminium Alloy", *Journal of Materials Processing Technology* Vol. **153-154**, 674-680.

Frank, W.B., Koch, G.P., Mills, J.J. (1984), "Microstructure of Alloys", in Hatch, J.E. (ed), *In Aluminium: Properties and Physical Metallurgy* (1st edition), Ohio, Metal Park, pp.58-104.

Gable, B.M., Csontos, A.A. & Starker, Jr. E.A. (2000), "The Role of Mechanical Stretch on Processing- Microstructure-Property Relationship of AF/C 548", *Materials Science Forum* Vols. **331-337**, 1341-1346.

Godard, D., Archambault, P., Aeby-Gautier, E., Lapasset G. (2002), "Precipitation Sequence During Quenching of the AA 7010", *Acta Materialia* Vol. **50**, 2319-2329.

Gottstein, G., Buescher, M. & Hirsch, J., (2007), "Anisotropy", *AluMatter,* Online at http:// aluminium.matter.org.uk/content/html eng/default.asp?catid=101&pageid=1039626806 [accessed on 28/04/2007]

Hagemaier, D., & Kleint, R. (1964), "Evaluating Aluminium Alloys by Nondestructive Tests" *Metal Progress Vol.* ?, 115-118.

Hagemaier, D., & Basl, G. J. (1967), "Evaluation of Mechanical Properties of 2014-T6 Weldments by Nondestructive (Eddy Current) Methods," *Materials Evaluation* Vol. **January 1967**, 1-6.

Hamerton, R.G., Cama, H., & Meredith, M.W. (2000), "Development of the Coarse Intermetallic Particle Population in Wrought Aluminium Alloys During Ingot Casting and Thermo-Mechanical Processing", *Materials Science Forum,* Vols. **331-337,** 143-154.

Higgins, R.A. (1970), *Engineering Metallurgy-Metallurgical Process and Technology* (2nd edition), London: Edward Arnold.

Higgins, R.A. (1983), *Engineering Metallurgy-Part I Applied Physical Metallurgy* (5th edition), London: Hodder and Stoughton.

Higgins, R.A. (1993), *Engineering Metallurgy-Applied Physical Metallurgy* (6th edition), London: Edward Arnold.

Hillel, A.J., Edwards, J.T., & Wilkes, P. (1975), "Theory of Resistivity and Hall Effect in Alloys During Guinier-Preston Zone Formation", *Philosophical Magazine* Vol. **31,** 189-208.

Hillel, A. J. & Rossiter, P. L. (1981), "Resistivity Mechanisms During Clustering in Alloys", *Philosophical Magazine B,* Vol. **4** (3) 383-388.

Hirsch, P. B., Silcox, J., Smallman, R. E. & Westmacott, K. H., (1958), "Dislocation Loops in Quenched Aluminium", *Philosophical Magazine Vol.* **3,** 897-908.

Hughes, R.E., Levy, S.A., Ball, M.D., Sperry, P.R., Miller, A.G. & Graham, H.G. (1984), "Microstructure of Alloys", in Hatch, J.E. (ed), *In Aluminium: Properties and Physical Metallurgy* (1st edition), Ohio, Metal Park, pp.58-104.

Jolley, G. (1992), "Effect of Abusive Machining on Alloys ABM 3-1031 and B.S. 2L97". Report Prepared by Salford University for BAe Airbus UK, Manufacturing Systems Engineering, p4-5.

Kelly, A., & Nicholson, R.N. (1963), "Precipitation Hardening", *Progress in Material Science,* Vol. **10**, (3), 149-391.

Koch, G.H. & Kolijn, D.T., (1979) "The Heat Treatment of Commercial Aluminium Alloy 7075", *Journal of HeatTtreating,* Vol.**1** (2), 3-14.

Krol, J., Cravov and Löffler, H., Halle. (1995), "Texture in Al and its Alloys", in Löffler, H. (ed), *Structure and Structure Development of Al-Zn Alloys* (1st edition), Berlin: VCH Publisher, Inc., pp.445-448.

Löffler H. (1995), *Structure and Structure Development of Al-Zn Alloys* (1st edition), Berlin: VCH Publisher, Inc.

Ma, X., & Peyton A. J. (2004), "Eddy Current Measurement of the Electrical Conductivity and Porosity of Metal Foams", *Instrumentation and Measurement Technology Conference,* Como, Italy, 18-20.

Martin, J.W. (1998), *Precipitation Hardening* (2nd edition), Oxford: Butterworth - Heinemann.

Marshall, G., Evans, P., Ricks, R. & Green, A.(2007), "Strain Hardening Processes", *AluMatter,* Online at http:// aluminium.matter.org.uk/content/html eng/default.asp?catid=71&pageid=17125, 4215 & 1534 [accessed on 28/04/2007]

Matthew, B., M. B., & Martin, J.W.(1994), "Effect of Retrogression Temperatures on Properties of an RRA 7150 Aluminium Alloy", *Journal Engineering-Zeirschnft fűr Metall Kunde,* Vol. **85**, 134-139.

Milek, J. R. & Wells, S.J. (1969), "Chemical Composition and Electrical Resistivity of Aluminium", *Report AD-687-145, National Bureau of Standards,* Hughes Aircraft Company Culver City, California, pp.1-30.

Military Hand Book – 5G. (1994), "Metallic Materials and Elements for Aerospace Vehicle Structures", *Department of Defense USA* Vol. **2,** pp.3273.

Mil-STD-1537B (1988), "Test Methods Standard for Electrical Conductivity Tests for Measurement of Heat Treatment of Alloys, Eddy Current Method." *Department of Defence,* Washington, USA, DC20301, pp.3659.

Morere, B., Maurice, C.L., Driver, J., Shahani, R.(1996), "Microstructural Characterisation of A7010 Alloy After Hot Deformation and Solution Treatment" *Materials Science Forum* Vols. **217-222**, 517-522.

Morris, A.J., Robey, R.F., Couch, P.D., and De los Rios, E. (1997), "A Comparison of Damage Tolerance of 7010 T7451 and 7050 7451", *Materials Science Forum* Vol. **242**, 181-186.

Morris, L., Marchand, G., Sanders, Jr R.E., Kelsy, R.A., & Hatch, J.E. (1984), "Effects of Alloying Elements and Impurities on Properties", in Hatch, J.E (ed), *Aluminium: Properties and Physical Metallurgy* (1 st edition), Ohio: Metal Park, pp.200-240.

Mott, N.F. & Nabarro, F.R.N. (1948), "An Attempt to Estimate the Degree of Precipitation Hardening, With a Simple Model" *Proceedings of Physical Society*, pp.541.

Natan, M. & Chihoski, R.A. (1983), "Relationship Between Microstructure, Hardness & E.C. of 2219 Aluminium", *Journal of Material Science* Vol.**18**, 3288-3298.

Naumov, N.M., Zueva N.M. & Krastilevskii A.A. (1976), "Relationship Between Depth of Intercrysllite Corrosion and Specific Electrical Conductivity in Aluminium alloy D 16", *Soviet Journal of Non Destructive Testing,* Vol.**12** (3) 323-325.

Nes, E. (1972), "Precipitation of the Metal Stable Cubic Al3Zr-Phase in Subperitectic Al-Zr Alloys", *Acta Metall,* Vol. **20,** 499-506.

Nielson, N.W., Peak, B.N., Yerger, Jr., J.D., Faunce, J., Gayle, F.W., Thompson, D.S., Kulp, D.B., (1984), "Constitution of Alloys", in Hatch, J.E. (ed), *In Aluminium: Properties and Physical Metallurgy* (1st edition), Ohio, Metal Park, pp.25-57.

Olafson, P., Sandstroenm, R. & Karlsson, A. (1996), "Electrical Conductivity of Aluminium Alloys", *Materials Science Forum* Vol. **217-222**, 981.

Orowan, E. (1948), "Symposium of Internal Stresses in Metals and Alloy", *Institute of Metals, London,* Vol. **5**, 451-453.

Panseri, C. & Federighi, T. (1966), "A Resistometric Study of Precipitation in an Aluminium – 1.4% Mg_2Si Alloy", *Journal Institute of Metals* **Vol. 94,** 99-107.

Park, J.K. & Ardell, A.J. (1986), "Microstructures of the Commercial 7075 Al Alloy in the T651 and T7 Tempers", *Metallurgical Transaction A* Vol. **14A**, 1957-1965.

Polmear, I. J. (1981), *Light Alloys, Metallurgy of Light alloys* (1st edition), London: Edward Arnold.

Polmear, I.J. (1995), *Light Alloys, Metallurgy of Light alloys* (3 rd edition), London: Edward Arnold.

Poole, W.J. & Shercliff, H.R. (1996), "The Effect of Deformation Prior to Artificial Ageing on the Ageing Characteristics of A 7475 Aluminium Alloys", *Materials Science Forum,* Vols. **217-222**, 1287-1292.

Raeisinia, B., Poole, W.J. & Lloyd, D.J. (2006), "Examination of Precipitation in the AA6111 Using Electrical Resistivity Measurements", *Materials Science and Engineering* Vol. **A420**, 245 -249.

Reed-Hill, R.E. (1973), *Physical Metallurgy Principles* (2nd edition), Boston: D.Van Nostrand Company.

Reed-Hill, R.E. (1991), *Physical Metallurgy Principles* (3rd edition), Boston: D.Van Nostrand Company.

Reynolds, M.A., Fitzsimmons, P.E., & Harris, J.G. (1976), "Presentation of Properties of a New High Strength Aluminium Alloy Designated 7010", *Proceedings of the Symposium on Aluminium in the Aircraft Industry,* pp.115-130.

Riggs, B.A., Berkey, W.W., Kulp, D.B., McBride, J.k., Sperry. P.R. (1984), "Work Hardening, Recovery, Recrystallization, and Grain Growth", in Hatch, J.E. (ed), *In Aluminium: Properties and Physical Metallurgy* (1st edition), Ohio, Metal Park, pp. 105-133.

Riontino, G. & Abis, S. (1991), "A Scanning Electrical Resistivity Study of Phase Transformation in an Al-Cu Alloy", *Philosophical Mangazine B-Physics of Condensed Matter Structural Electronic Optical & Magnetic Properties,* Vol. **64**, (No 4), p447.

Rollason, E.C. (1973), *Metallurgy for Engineers* (4th edition), Norwich: Edward Arnold.

Rosen, M. Horowitz, E. Swartzedruber, L., Fick, S. & Mehrabian, R., (1982), "The Ageing Process in Aluminium Alloy 2024 Studied by Means of Eddy Currents", *Material Science and Engineering* Vol. **53**, 191-198.

Rosen, M. (1989), "Eddy Current Analysis on Precipitation Kinetics in Aluminium Alloy", *Metallurgical Transaction A*, Vol. **20A**, 605-609.

Rossiter, P.L. & Wells, P. (1971), "The Dependence of the Electrical Resistivity on the Short-Range Order", *Journal Physics C: Solid state* Vol. **4,** 354-363.

Rossiter, P. L. (1976), "A Comment on the Electrical Resistivity During GP Zone Formation", *Philosophical Magazine*, Vol. **33** (6) 1015 –1020.

Rummel, W. D. and Arbegast, W. J. (1981), "Characterization of 2014, 2219, 6061 and 7075 Aluminium Alloy Heat Treat Response by Eddy Current, Conductivity, Hardness, and Mechanical Properties," *Paper Summaries, National Spring Conference of the ASNT, March,* Philadelphia, pp.201-208.

Sanders, Jr., R.E., Sanders, Jr., T.H. & Staley, J.T. (1983), "Relationships Between Microstructure, Conductivity and Mechanical Properties of Alloy 2024.T4", *Communication From Alcoa Technical Centre Vol.* **59,** 13 –17.

Sato, T. (2000), "Early Stage Phenomena and Role of Micro-alloying Elements in Phase Decomposition of Aluminium alloys", *Materials Science Forum,* Vols. **331-337,** 85-96.

Shimizu, H. & Kimura, H. (1969), "Mechanism of Reversion in an Aluminium 4% Copper Alloy", *Materials Science and Engineering,* American Society for Metals, Metals Park, Ohio, pp.127-134.

Sigli, C., Terryn, H., De Grave, I., Shercliff, H. & Tyckerboer, M. (2007), "Electrical Resistivity", *AluMatter,* Online at http:// aluminium.matter.org.uk/content/html eng/default.asp?catid=158&pageid=2144416488-2144416491 [accessed on 20/08/2007]

Solas, D., Canova, G., Brechét, Y., Saintfort, P. (1996), "Anisotropy of Mechanical Properties in 7010 Aluminium Thick Plate". *Materials Science Forum* Vols. **217-222** 1533-1538.

Smallman, R.E. (1970), *Modern Physical Metallurgy* (3 rd edition), London: Butterworths.

Staley, J.T., Ashton, R.F., Broverman, I., & Sperry, P.R. (1984), "Metallurgy of Heat Treatment and General Principles of Precipitation Hardening", in Hatch, J.E. (ed), *In Aluminium: Properties and Physical Metallurgy* (1st edition), Ohio, Metal Park, pp.134-199.

Staley, J.T. (1992), "Metallurgical Aspects Affecting Strength of Heat Treatable Alloy Products used in the Aerospace Industry" *The 3rd International Conference on Aluminium Alloys,* Alcoa Technical Centre, Alcoa Centre, PA 15069, USA. pp.107-122.

Starink, M.J. & Wang, S.C. (2003), "A Model for Yield Strength of Over Aged Al-Zn-Mg-Cu Alloys, *Acta Materialia* Vol. **51**, 5131-5150.

Suhr, H & Gűttinger, T.H. (1993), "Error Reduction in Eddy Current Conductivity", *Institut DR Förster,* Report No 313, pp.1-12, Foerster UK, Ltd, Wrens Court, 50 Victoria Road, B72 1SY.

Sundberg, R. (1989), "Eddy Current Testing to Detect Property Change Caused by the Heat Treatment of 2024 Aluminium", *Materials Evaluation,* Vol. **47**, (No 9), pp.1062-1064.

Tanner, D.A. & Robinson, J.S. (2004), "Effect of Precipitation During Quenching on the Mechanical Properties of the Aluminium Alloy 7010 in the W-Temper", *Journal of Materials Processing Technology* Vol. **153-154**, pp.998

The Aluminium Association Inc. (1982), "Report on Electrical Conductivity in Heat Treated Aluminium Alloy Plate", *The Aluminium Association, Inc.* 818 Connecticut Ave, N.W., Washington, DC 2006, 1-6.

Tiryakioglu, M., Cambell, J. & Staley, J.T. (2000), "Hardness – Strength Relationship in Cast Al-Si-Mg alloys", *Material Science Forum* Vols. **331-337**, 295-300.

Vietz, J. T. (1968), "The Use of Eddy Current Conductivity Measurements for Checking and Predicting the Strength of Heat-Treated Aluminium Alloys," *Journal of the Australian Institute of Metals* Vol. **13** (4) 211-217.

Yan, J., Starink, J.M., & Gao, N. (2004), "Modelling of Precipitation Hardening of Al-Cu-Mg alloys" *Proceedings of the 9th International Conference on Aluminium Alloys,* Institute of Materials Engineering Australia Ltd, pp.926-932.